Princeton University

Final Report

NASA RESEARCH PROGRAM

The Fluid Mechanics of Continuous Flow Electrophoresis

Contract NAG 8-597

September 1986 - July 1990

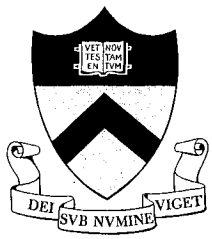

TABLE OF CONTENTS

ABSTRACT

This work is a logical continuation of an earlier study (NAS 8-32614) on electrophoresis technology and forms part of a two-pronged effort involving research at Princeton University and the Marshall Space Flight Center (MSFC). The overall objective is to establish theoretically and confirm experimentally the ultimate capabilities of continuous flow electrophoresis chambers operating in an environment essentially free of particle sedimentation and buoyancy. The efforts at Princeton are devoted to:

(i) Studying the effects of particle concentration on sample conductivity and dielectric constant. The dielectric constant and conductivity have been identified as playing crucial roles in the behavior of the sample and, thus, on the resolving power and throughput of continuous flow devices.

(ii) Improving the extant mathematical models to predict flow fields and particle trajectories in continuous flow electrophoresis.

A dielectric spectrometer was designed and built to measure the complex dielectric constant of a colloidal dispersion as a function of frequency between 500 Hz and 200 kHz. The real part of the signal can be related to the sample's conductivity and the imaginary part to its dielectric constant. Measurements of the dielectric constants of several different dispersions disclosed that the dielectric constants of dilute systems of the sort encountered in particle electrophoresis are much larger ($\epsilon \approx 1000$) than would be expected based on the extant theory. Experiments were carried out to show that, in many cases, this behavior is due to the presence of a filamentary structure of small "hairs" on the particle surface.

A technique for producing "electrokinetically ideal" synthetic latex particles by heat-treating was developed. Here the term "electrokinetically ideal" means that the particles conform to the tenets of the classical theory.

Given the ubiquitous nature of "hairy" surfaces with both cells and synthetic particles, it was deemed necessary to develop a theory to explain their behavior. A theory for electrophoretic mobility of hairy particles was developed; an extension to include conductivity and dielectric behavior is underway.

Finally, the extant computer programs for predicting the structure of electro-osmotically driven flows were extended to encompass flow channels with variable wall mobilities.

SUMMARY AND CONCLUSIONS

Earlier work at Princeton (under contract NAS 8-32614) showed that particle concentration has a strong influence on sample conductivity (more specifically, on the "real" or "DC" conductivity). Concurrently, experimental studies by P. H. Rhodes at MSFC showed that sample and buffer conductivities profoundly influence spreading of the sample. A large conductivity mis-match between sample and buffer causes sample to spread rapidly from the front to rear walls of the channel. Rhodes developed an electrohydrodynamic theory of this spreading which shows that in addition to the conductivity, the dielectric constant should also affect spreading behavior. Therefore, to optimize performance of a continuous flow device it will be necessary to understand the spreading process and how it is influenced by the conductivity and dielectric constant of the sample. Accordingly, one needs to be able to measure the dielectric behavior of particulate samples as well as their DC conductivity.

Much of the work accomplished under the present contract has been published in the refereed literature; copies of the papers that have appeared or are "in the press" are attached and copies of the two PhD theses are available from the principal investigator. Accordingly, only a brief synopsis of the results is given here.

The dielectric spectrometer designed and built at Princeton measures the properties of a given suspension at frequencies between 500 Hz and 200 KHz[1,11]. A complete frequency scan takes about 25 minutes. The instrument has been used to measure the dielectric constant and conductivity of latex suspensions[2,3], similar to those used in Rhodes' experiments, and colloidal silica particles[4]. The results are linear in the volume fraction of particles for dilute systems (< 8 vol%) as they should be. One surprising result is that the low frequency limit of the dielectric constant is much larger (over 1000 for some suspensions) than the extant theory predicts. In addition, the relaxation frequency is lower than predicted by the theory.

It follows from these results that the effect of the dielectric constant on the sample's configuration in an electrophoresis machine may be even larger than anticipated. Clearly, it is of crucial importance to understand these phenomena if electrophoresis is to be used to fractionate cells or cell fragment populations.

Inasmuch as the dielectric constants of a number of suspensions were found to exceed those predicted by the classical theory, it is natural to inquire as to why. According to the classical theory the particle surfaces are smooth and the charge is immobile. Thus, one ought to be able to measure the particle mobility, deduce the charge from the classical theory, and use it to predict the dielectric response. This turns out not to be the case is most situations. The weak point in the theory appears to be in the notion of an immobile charge. For example, if the interfacial region is somewhat thick, as it would be if the shear surface is displaced a small

---

1. Numerals refer to the papers in the bibliography.

distance from the particle surface, then ions might migrate laterally within this region. Moreover, it is believed that many synthetic latex particles are hairy due to the presence of (i) oligomeric chains adsorbed or otherwise attached to the surface or (ii) polymer filaments protruding from the surface. Hairiness provides a means for moving the shear plane out away from the particle and furnishes a relatively thick region in which ions might move across the surface in response to lateral forces.

We sought to test the hairy layer hypothesis by suppressing or removing the layer. This was done with two sorts of particles: native surfaces with naturally occurring hairiness and with particles to which covalently bound polymer filaments are attached[3,12]. A mild heat treatment was used wherein particles were heated to 120°C for 1 to 12 hours. We were able to follow the collapse of the hairy layer using measurements of electrophoretic mobility and dielectric behavior. It should be noted that the dielectric measurements were much more sensitive to changes in the surface morphology than measurements of particle mobility. With some particles, our annealing procedure produced "electrokinetically ideal" particles where the dielectric response could be predicted accurately from the surface charge inferred from the mobility measurements. Moreover, the dielectric constants of such suspensions are an order of magnitude smaller than those comprised of native particles. It would be interesting to carry out some of Rhodes' electrohydrodynamic experiments with such particles.

As matters now stand, it appears that the dielectric constants and conductivities of most synthetic particle dispersions are heavily influenced by the presence of a hairy surface texture. This may also be the case with many biological cells and their dielectric properties should be measured with the new spectrometer. Clearly, surface texture affects the electrokinetic response of any dispersion.

There is, at present, no theory which encompasses the behavior noted above. As part of the current effort, a theory for the electrophoretic mobility was developed[7,8]. Work on the corresponding theory for dielectric behavior is underway[9].

Under the auspices of the previous contract some work was done on the mobilities of particles in concentrated suspensions. Two papers were completed during the present contract dealing with that subject[5,6].

Finally, we also updated our program for predicting the flow structure in continuous flow devices to encompass non-uniform electro-osmosis along the boundary of the flow channel.

BIBLIOGRAPHY OF PUBLICATIONS, THESES, AND SCIENTIFIC PAPERS
FROM NAG 8-597

Publications in referred journals.

1. "Dielectric spectroscopy of colloidal suspensions I:The dielectric spectrometer."
J. Colloid Interface Science 313 448-460 1989.
[with D. F. Myers].

2. "Dielectric spectroscopy of colloidal suspensions II: Comparisons between theory and experiment."
J. Colloid Interface Science 313 461-470 1989.
[with D. F. Myers].

3. "The Dielectric Response of Polystyrene Lattices: Effects of Alterations in the Structure of the Particle Surface."
J. Colloid & Interface Science (in the press)
[with L. A. Rosen]

4. "Dielectric Spectroscopy of Colloidal Dispersions: Comparisons Between Theory and Experiment."
Langmuir (in the press)
[with L. A. Rosen]

5. "Electrokinetic properties of particles in concentrated suspensions: Heterogeneous suspensions."
Journal of Colloid & Interface Science 132 220-229 (1989)
[with C. F. Zukoski].

6. "Particle Migration in Suspensions by Thermocapillary or Electrophoretic Motion."
J. Fluid Mech. 212 95-110 (1990).
[with A. Acrivos and D. J. Jeffrey]

**********In Preparation*********

7. "Electrokinetic properties of hairy particles"

8. "Electrophoretic mobility of hairy particles with thin double-layers."

9. "Dielectric spectroscopy in dispersions of colloidal particles with dynamic Stern Layers."

PhD Theses

11. "Dielectric Spectroscopy of Colloidal Suspensions."
D. F. Myers (1988).

12. "Dielectric Spectroscopy as a Probe of Colloidal Surface Structure."
L. A. Rosen (1990)

Papers at technical meetings

13. "Electrokinetic Phenomena" (Invited Review)
The 1987 Conference on Physico-chemical Hydrodynamics, Oxford, England, April 1987.

14. "An Instrument for Measuring the Dielectric Properties of Suspensions"
Annual Meeting of the American Chemical Society, New Orleans, September 1987.
[with D. F. Myers]

15. "Dielectric Spectroscopy of Colloidal Suspensions"
Colloid & Surface Science Meeting of the American Chemical Society, Penn State University, June 1988.
[with D. F. Myers]

16. "Dielectric Spectroscopy of Colloidal Suspensions - Design and Construction of a New Dielectric Spectrometer"
The International Fine Particle Society, Santa Clara, CA, July 1988
[with D. F. Myers]

17. "Dielectric Spectroscopy of Latex Suspensions"
AICHE Annual Meeting, Washington D.C., December 1988
[with L. A. Rosen]

18. "Dielectric Spectroscopy of Colloidal Dispersions: The Effect of Heat-Treatment on Latex Particles."
ACS Colloid Meeting, Seattle, Washington June 1989.
[with L. A. Rosen]

19. "Electrokinetic Phenomena in the Fractionation of Biological Materials." [Invited paper]
Gordon Research Conference on Materials Processing, August 1989.

20. "Electrokinetic and Electrohydrodynamics in the separation of biological materials." [Invited review]
AIAA Annual Meeting, Reno, Nevada January 1990.

21. "Dielectric Spectroscopy of Colloidal Dispersions: Effects of Surface Structure on the Electrokinetic Response."
ACS 64th Colloid & Surface Science Symposium, Lehigh University, June 1990.
[with L. A. Rosen]

22. "Heat Treatment of Polystyrene: One Step Towards the Preparation of Ideal Colloid Particles."
IUPAC Symposium on Polymer Colloids - Montreal, Canada, July 1990.
[with R. Chow, K. Takamura, & L. A. Rosen]

23. "Dielectric Spectroscopy of Colloidal Dispersions: The Effects of Surface Treatment on the Electrokinetic Response."
Discussions of the Faraday Society - Bristol, UK, September 1990.
[with L. A. Rosen]

24. "The Electrophoretic Mobility of a Fuzzy Particle"
Annual Meeting of the American Institute of Chemical Engineers, Chicago, Illinois, November 1990.

APPENDIX

1. "Dielectric spectroscopy of colloidal suspensions I:The dielectric spectrometer."
J. Colloid Interface Science 313 448-460 1989.
[with D. F. Myers].

2. "Dielectric spectroscopy of colloidal suspensions II: Comparisons between theory and experiment."
J. Colloid Interface Science 313 461-470 1989.
[with D. F. Myers].

3. "The Dielectric Response of Polystyrene Lattices: Effects of Alterations in the Structure of the Particle Surface."
J. Colloid & Interface Science (in the press)
[with L. A. Rosen]

4. "Dielectric Spectroscopy of Colloidal Dispersions: Comparisons Between Theory and Experiment."
Langmuir (in the press)
[with L. A. Rosen]

5. "Electrokinetic properties of particles in concentrated suspensions: Heterogeneous suspensions."
Journal of Colloid & Interface Science 132 220-229 (1989)
[with C. F. Zukoski].

6. "Particle Migration in Suspensions by Thermocapillary or Electrophoretic Motion."
J. Fluid Mech. 212 95-110 (1990).
[with A. Acrivos and D. J. Jeffrey]

Dielectric Spectroscopy of Colloidal Suspensions

I. The Dielectric Spectrometer

D. F. MYERS AND D. A. SAVILLE[1]

Department of Chemical Engineering, Princeton University, Princeton, New Jersey 08544

Received July 11, 1988; accepted November 7, 1988

Four-electrode signal-processing techniques have a number of advantages over conventional bridge techniques in dielectric spectroscopy, but are not widely used because complex electronic circuits are required. A new design for a dielectric spectrometer of this type which circumvents these problems is described here. The device has been tested using electrical networks, pure electrolytes, and dilute colloidal suspensions. In experiments with a dilute, amphoteric latex, large suspension dielectric constants are found.

I. INTRODUCTION

Dielectric spectroscopy offers certain advantages over the static techniques customarily used to study the electrokinetic properties of colloidal particles. Measuring the dielectric constant and conductivity over a range of frequencies provides information on temporal processes in the Stern and diffuse layers associated with the particles. In addition, the low frequency limits of the measurement can be related to static measurements. Unfortunately, it is difficult to measure the dielectric behavior of dilute, conducting suspensions, and no "off-the-shelf" instrument for this purpose exists. The most serious experimental problem is electrode polarization, which arises whenever current passes through an electrode–electrolyte interface. In the simplest measurement configuration, current passes through a sample placed between two electrodes and the voltage drop divided by the applied current yields the complex impedance. However, electrode polarization creates an additional voltage drop at the electrode–electrolyte interface which is difficult to measure or predict. This clouds interpretation of the results.

Another problem stems from the need to study dilute suspensions so that the experimental data can be interpreted using rigorous theories. Since the contribution of the particles to the suspension's electrical properties is proportional to the volume fraction of particles, the signal-to-noise ratio is low in dilute suspensions. Also, small temperature fluctuations in the electrolyte produce changes in the electrolyte conductivity larger than the change due to the particles, creating a stringent temperature control requirement.

Nevertheless, dielectric spectroscopy has been used successfully with colloidal dispersions. Schwan *et al.* (1) used apparatus consisting of an AC Wheatstone bridge and a variable electrode-gap cell, the latter to minimize errors due to electrode polarization. Dielectric constants as large as 2500 were observed with 30 vol% suspensions of 0.188-μm polystyrene particles. Springer *et al.* (2) and Lim and Franses (3) employed cells similar to those of Schwan *et al.*, with a transformer ratio-arm bridge in place of the Wheatstone bridge. Large dielectric constants were measured although the suspensions were much more dilute than those used by Schwan *et al.* Recently, Midmore *et al.* (4) used a system much like Schwan's to measure electrical

[1] To whom correspondence should be addressed.

0021-9797/89 $3.00

conductivities at low frequency. Midmore and O'Brien (5) measured high-frequency dielectric spectra of concentrated suspensions with a fixed-electrode cell and a bridge circuit.

Despite its record of success, Schwan's two-electrode technique (6) has a number of drawbacks. First, the method requires several measurements at every frequency, each requiring manual adjustment of the electrode spacing. This limits the degree to which the measurement can be automated and increases the measurement time substantially. Second, the signal-to-noise ratio is poor when dilute suspensions are involved. To eliminate errors due to electrode polarization and avoid manual adjustments or multiple measurements at each frequency, Hayakawa *et al.* (7) used a four-electrode cell design originally proposed by Schwan (6). An analog and digital signal-processing scheme improved the signal-to-noise ratio of the measurement and an electronic compensation circuit removed the need for precise temperature control. However, the technique is difficult to implement due to the complexity of the circuitry and the need for very precise electronic components.

II. THE NEW INSTRUMENT

We set out to develop a device which would incorporate the advantages of the Hayakawa instrument (7) in a simpler design. A four-electrode cell geometry was chosen, with a detector patterned after those used by Hayakawa *et al.* (7) and Nakamura *et al.* (8). The signal generator and signal processing circuits were based on a new design which allows the use of off-the-shelf equipment and facilitates computerized control and data acquisition.

Our instrument employs a four-electrode sample cell (Fig. 1). The total volume of the sample contained in the cell is approximately 2 cm^3. In Fig. 2, current (I) enters the cylindrical cell through the source electrode and exits at the sink electrode, each having large, disk-shaped surfaces. Two needle-shaped sensing electrodes measure the voltage drop across the middle of the cell. Platinum foil was

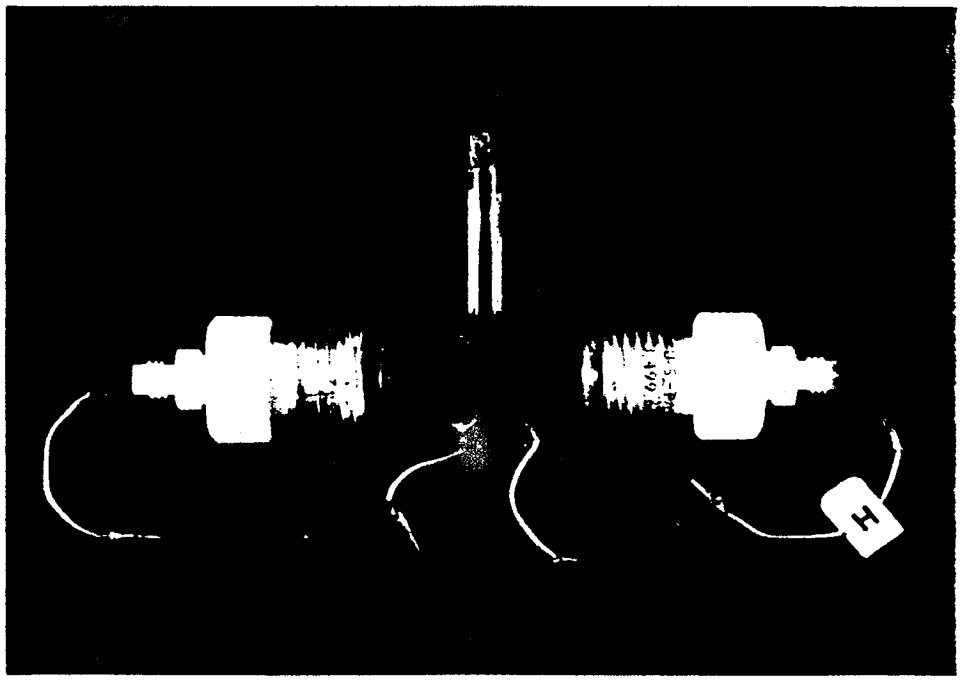

FIG. 1. A photograph of the four-electrode sample cell.

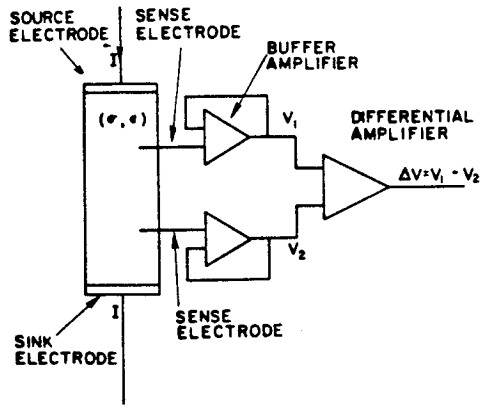

FIG. 2. A diagram of the four-electrode cell configuration.

used for the source–sink electrodes and platinum wire for the sense electrodes. All electrodes were platinum blacked using Schwan's procedure (6). Electrode polarization influences the sense electrode voltage only to the extent that the voltage measurement causes a current flow. Current flow is minimized by connecting each sense electrode to a high-impedance, unity-gain buffer amplifier. A differential amplifier subtracts the "negative" sense voltage V_2 from the "positive" sense voltage V_1 to yield the voltage drop ΔV. Thus, if the magnitude of the current (I) passing through the cell via the source electrode is known, the impedance in the region between the two sense electrodes can be computed by simply dividing the voltage drop by the current, $Z = \Delta V/I$. Alternatively, the admittance is given by $Y = I/\Delta V$.

This technique is insensitive to the effects of electrode polarization because the four-electrode configuration separates electrode functions. No single electrode is required to pass current and measure voltage simultaneously. Electrode polarization at the source and sink electrodes affects the voltage drop across the entire cell, but not the current, keeping I unchanged. Although electrode polarization at the sense electrodes is large, the high impedance of each buffer amplifier minimizes current flow through the electrodes so the voltage drop is negligible compared to ΔV.

The complete instrument consists of the four-electrode cell, signal generator, detector, and automatic balancing circuit sections, along with two lock-in amplifiers (Fig. 3). The signal generator section provides an alternating current to the source electrode using sine-wave generators, a summing amplifier, and a voltage-to-current (V/I) converter. Two sine waves are produced by the generators, one at a measuring frequency ω and the second at the reference frequency ω_r. The summing amplifier combines the two signals to produce a composite waveform, and the V/I converter circuit changes the constant-amplitude voltage signal to a constant current

$$I = I(\omega) + I(\omega_r) \qquad [1]$$

independent of the impedance presented by the cell. This ensures that the current in the cell and ΔV will be independent of fluctuations in the source electrode impedances.

Buffer amplifiers, a differential amplifier, a summing amplifier, and a current-to-voltage converter form the detector. It was noted earlier that simply measuring the differential voltage and the cell current is sufficient for a determination of the complex admittance. However, instead of measuring the current through the cell directly, it is useful to produce a voltage proportional to the current. This is the function of the current-to-voltage (I/V) converter. The output of this circuit is

$$V_F = -IZ_F, \qquad [2]$$

where Z_F is the impedance of the feedback network consisting of a resistor R_F in parallel with a capacitor C_F. Note that the "+" and "−" terminals of the op-amp draw no current, so the current passing through the feedback network (R_F, C_F) is I, the current which passes through the sample.

The summing amplifier combines the outputs of the I/V converter and the differential amplifier to form the inverted sum

$$V_0 = -(\Delta V + V_F), \qquad [3]$$

representing the balance voltage. If Z_C rep-

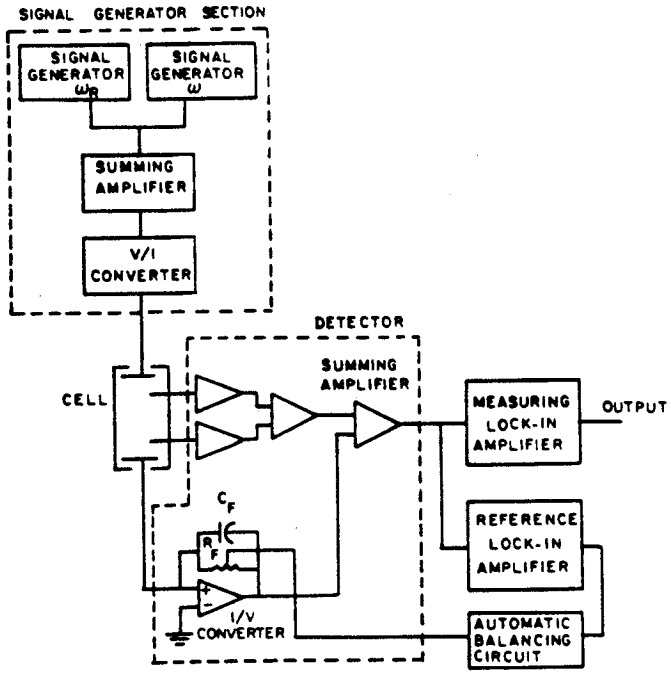

FIG. 3. Block diagram of the four-electrode frequency-difference dielectric spectrometer.

resents the impedance of the region of the cell between the sense electrodes, then

$$\Delta V = IZ_C \qquad [4]$$

and

$$V_0 = -I(Z_C - Z_F). \qquad [5]$$

This is the final output from the device: a voltage proportional to the difference between the sample impedance and the impedance of the reference network. A lock-in amplifier measures the in-phase and out-of-phase components of this signal.

The reason this approach increases the signal-to-noise ratio of the experiment can be seen from the following argument. Recall, first, that the signal applied to the celi is composed of sine waves at the reference frequency ω_r and the measuring frequency ω. Suppose, now, that the measuring lock-in amplifier is tuned to ω_r. Then, R_F and C_F can be adjusted until both the in-phase and the out-of-phase components of the output signal at ω_r are nulled. From Eq. [5] we see that a null output at ω_r means that $Z_C(\omega_r)$ is equal to $Z_F(\omega_r)$.

Next note that the admittance of a material in a cell with cell constant G is

$$Y = G(\sigma + i\omega\epsilon\epsilon_0). \qquad [6]$$

In the case of a pure electrolyte, σ and ϵ can be considered frequency-independent constants, σ_∞ and ϵ_∞ at the frequencies employed here; ϵ_0 is the permittivity of the vacuum. Thus, the admittance

$$Y = G(\sigma_\infty + i\omega\epsilon_\infty\epsilon_0) \qquad [7]$$

has a real part which is constant, and an imaginary part linear in the frequency ω. In a similar manner, the admittance of an electrical network consisting of a resistor and a capacitor in parallel can be written

$$Y = \frac{1}{R} + i\omega C, \qquad [8]$$

where R is the resistance and C is the capacitance. Note the similarity between the RC

parallel circuit admittance and the electrolyte admittance. The RC parallel circuit models the behavior of the pure electrolyte if component values are chosen such that

$$\frac{1}{R} = G\sigma_\infty \qquad [9]$$

and

$$C = G\epsilon_\infty \epsilon_0, \qquad [10]$$

At null, Eqs. [9] and [10] yield $C = C_F$ and $R = R_F$.

Now consider the output when the lock-in amplifier is tuned to the measuring frequency ω under two experimental conditions: first, when the sample consists of a pure electrolyte, and, second, when the sample is a suspension. With pure electrolyte the sample impedance can be accurately modeled as a resistor and capacitor in parallel, as shown above. Since the reference network is also an RC parallel network, the null condition $Z_C(\omega_r) = Z_F(\omega_r)$ implies that R_F equals the equivalent resistance of the sample, and C_F equals the equivalent capacitance of the sample. Because the frequency dependences of the electrolyte and the RC circuit are the same, $Z_F(\omega) = Z_C(\omega)$, and the output will remain zero at all frequencies. The reference network models the frequency response of the sample. When the model is accurate, as it is when the sample is a homogeneous electrolyte, the output remains null at frequencies below 1 GHz.

With suspension in the cell $Z_F(\omega)$ will differ from $Z_C(\omega)$ and the output signal will be nonzero. The amplitude and phase shift of the output reflect the presence of the particles in the suspension and will be proportional to their volume fraction. Accordingly, the influence of the impedance of the background electrolyte has been eliminated and a signal sensitive to the properties of the particles obtained.

The four-electrode cell supresses electrode polarization effects and the detector increases the signal-to-noise ratio. A third problem which must be addressed is the error caused by small temperature changes during a frequency scan. Assume, for the moment, that the cell is filled with a pure electrolyte. To maintain zero output voltage, the impedance Z_F must mimic the electrical behavior of the pure electrolyte. Temperature changes in the electrolyte cause the resistance of the sample, R_C, to change so R_F will not match the sample resistance. A mismatch between R_F and R_C produces an output proportional to the difference and reduces the resolution of the instrument. If the resistance R_F could track changes in the electrolyte conductivity, the system output would remain null despite thermal drift and the error would be eliminated. Tracking is performed by the automatic balancing circuit (Fig. 4). A second lock-in amplifier, the "reference" lock-in, is tuned to the reference frequency ω_r and monitors system output. The lock-in output is a dc signal, proportional to the ac amplitude of the in-phase output voltage at ω_r. This amplitude reflects the amount of mismatch between R_F and the resistance of the sample at the reference frequency and can be used to decrease the mismatch by compensating R_F for changes in R_C. The dc output from the lock-in is applied to an interface circuit which controls the current through a light-emitting diode (LED). The LED is placed in close proximity to a cadmium sulfide (CdS) photoconductive cell, a device which has a resistance dependent upon the light intensity at its surface. Together, the LED and the CdS cell form a voltage controlled resistor. The LED/CdS combination is placed in series with a conventional resistor to form the feedback

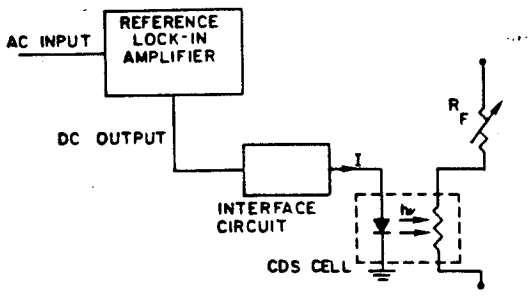

FIG. 4. The automatic balancing circuit.

resistance R_F. R_F can then be varied automatically by controlling the current flow to the LED.

Suppose $Z_C(\omega_r) = Z_F(\omega_r)$ at the outset of an experiment, and that an increase in the sample temperature has caused $Z_C(\omega_r)$ to decrease. Whenever the in-phase output becomes nonzero, the current through the LED is changed so that the difference between R_F and R_C decreases in magnitude to renull the in-phase output. Here, since $V_0(\omega_r)$ is positive, current flow through the LED increases. This reduces the resistance of the CdS cell, thereby reducing R_F until it is again equal to $R_C(\omega_r)$, and $V_0(\omega_r)$ vanishes. In this way R_F is compensated for the change in the sample resistance. Typically, the "effective" level of temperature variation is less than 0.0001°C during the 20- to 30-min period required to obtain a spectrum when this circuit is used.

The instrument described here is different from that designed by Hayakawa *et al.* (7) in some important ways. First, custom circuits in the signal generator and demodulator sections of Hayakawa's device were replaced by commercially available equipment in order to facilitate implementation of the technique. However, a simple substitution of standard equipment for custom made components was not possible, so significant design changes were required.

In Hayakawa's system, the digital signals used to create sine waves in the signal generator section function as syncronization signals in the demodulators, thereby defining the point of zero phase shift in an unambiguous way. However, phase shifts in the bandpass filters of the signal generator create very large phase errors which are eliminated by manually adjusting the phase characteristics of the filters. In our system the function of the demodulators is performed by the Princeton Applied Research (PAR) 124 lock-in amplifier. Instead of relying on a fixed phase reference, the phase of the system output V_0 is measured relative to the phase of ΔV, the differential amplifier output. This is a convenient choice since the ratio $V_0/\Delta V$ is the quantity used in data analysis, and no manual nulling of phase errors is required.

A second difference between our approach and Hayakawa's is the addition of the balance capacitance C_F in the detector circuit. The addition of this capacitance stabilizes the I/V converter circuit without changing the frequency response of the operational amplifier used in the circuit. Also, C_F can be adjusted so that the in-phase and out-of-phase components of V_0 are similar in magnitude, thus minimizing errors which would occur if the phase shift of the signal was near 0° or 90°.

III. DATA ANALYSIS

The output voltage of the experiment is related to the electrical properties of the sample through Eq. [5] but the electrical properties of the sample are buried in the complex quantity Z_C so V_0, I, and Z_F must be measured. Since the sample current (I) is difficult to measure directly, it is useful to measure a voltage proportional to it. A particularly convenient voltage is ΔV, which was shown to be related to I through Eq. [4]. Combining this with Eq. [5] we obtain

$$\frac{V_0}{\Delta V} = -\left[1 - \frac{Z_F}{Z_C}\right]; \qquad [11]$$

V_0 and ΔV are both measurable quantities.

The complex impedances Z_F and Z_C can be written in terms of real quantities,

$$\frac{1}{Z_F} = \frac{1}{R_F} + i\omega C_F \qquad [12]$$

$$\frac{1}{Z_C} = G(\sigma + i\omega\epsilon\epsilon_0), \qquad [13]$$

where G is the cell constant. Substituting these expressions into the equations above yields

$$\sigma + i\omega\epsilon\epsilon_0 = \left[1 + \frac{V_0}{\Delta V}\right] \times \left[\frac{1}{R_F} + i\omega C_F\right]\frac{1}{G}. \qquad [14]$$

Equating the real and imaginary parts of the equation shows that

$$\sigma = \frac{1}{G}\,\mathrm{Re}\left\{\left[1 + \frac{V_0}{\Delta V}\right]\left[\frac{1}{R_F} + i\omega C_F\right]\right\} \quad [15]$$

and

$$\epsilon = \frac{1}{G\omega\epsilon_0}\,\mathrm{Im}\left\{\left[1 + \frac{V_0}{\Delta V}\right] \times \left[\frac{1}{R_F} + i\omega C_F\right]\right\}. \quad [16]$$

To determine σ and ϵ, values for V_0, ΔV, R_F, C_F, and ω are needed. V_0 and ΔV are measured directly with the measuring lock-in amplifier (Fig. 3), a PAR 124. The measuring frequency ω is obtained from the front panel dial settings of the PAR 124, which have been checked against calibrated frequency meters. The reference frequency ω_r is measured with a digital counter in a Stanford Research Systems SR530 lock-in amplifier, which is used in the automatic balancing circuit.

To calculate R_F and C_F, two additional measurements or assumptions are required. Two quantities are measurable: σ_r, the conductivity at the reference frequency, and C_F, the reference capacitance. The conductivity of the sample at balance is measured using the four-electrode cell and a low-frequency conductivity bridge. Here, the four-electrode cell is used in a two-electrode configuration, with the source electrodes connected to a bridge circuit and the sense electrodes disconnected. The cell constant for the chamber used in this work is approximately 0.250 cm. An Altex (Beckman, Inc.) conductivity bridge is used to obtain measurements of the cell conductance at 85 Hz and 1 kHz. Since the balance frequency is usually in the range 100 Hz to 1 kHz, these are very convenient frequencies to use. Although the conductivity is not measured at exactly the balance frequency, measurements show that the conductivity is not a strong function of frequency in this range. Thus, the error incurred by the small frequency mismatch is negligible.

The reference capacitance, C_F, is determined as follows. First the capacitors used to balance the system are measured with a capacitance bridge (General Radio 1620-A) using a very accurate three-terminal measurement at 1 kHz. These capacitances are independent of frequency below 1 MHz. The primary error in the measurement of C_F is that not all of the balance capacitance is directly attributable to the measured capacitors. For example, stray capacitance to ground at the negative sensing lead appears as "extra" balance capacitance and is not measurable. There are certainly other sources of stray capacitance and they cause errors in the determination of the effective C_F and the absolute dielectric constant, ϵ. The way we deal with these errors will be explained shortly.

Given measured values of σ_r and C_F, σ and ϵ can be computed at any frequency, provided that R_F can be computed. This is accomplished by applying Eq. [15] at the reference frequency ω_r. The output ratio $V_0/\Delta V$ is written in the form

$$\frac{V_0}{\Delta V} = r' + ir'', \quad [17]$$

where r' and r'' are both real. At the reference frequency they are denoted as r_r' and r_r'' so R_F is

$$R_F = \frac{1 + r_r'}{G\sigma_r + \omega_r C_F r_r''}. \quad [18]$$

Thus, the measurement of σ_r and C_F allows R_F to be calculated. Given R_F and C_F, $\sigma(\omega)$ and $\epsilon(\omega)$ can be calculated using Eqs. [15] and [16].

A second approach involves making two assumptions instead of two measurements. If the conductivity and the dielectric constant of the material are known at the reference frequency, then R_F and C_F can be computed by solving

$$\frac{1}{R_F} + i\omega_r C_F = \frac{G(\sigma_r + i\omega_r\epsilon_r\epsilon_0)}{(1 + r_r' + ir_r'')} \quad [19]$$

for R_F and C_F. This approach is possible with pure electrolytes, where σ_r and ϵ_r are known.

In the first method σ_r and C_F are measured, but errors implicit in C_F are present. In the second approach, the effective value of C_F is computed exactly, but only for an electrolyte where ϵ is known. A hybrid approach can be used to take advantage of the favorable attributes of the two approaches. Before an experiment with a dilute suspension, measurements are made with the pure suspending electrolyte and the electrical properties computed by the second technique; σ_r and ϵ_r take on their "textbook" values at the balance frequency. The balance capacitance is then calculated and compared to the measured value. A value for ΔC_F, the difference between the capacitance needed for balance and the measured C_F, is obtained. Then, in experiments with the suspension, the first approach is used, but ΔC_F is added to the measured balance capacitance to compensate for stray capacitance. This procedure, which is analogous to the substitution method (6) used with conventional bridges, reduces the error in the measured values.

Nevertheless, it should be understood that the experiment is not optimized to obtain values for σ and ϵ. Instead, it is designed to measure the frequency-difference spectra, i.e., $\sigma(\omega) - \sigma(\omega_r)$ and $\epsilon(\omega) - \epsilon(\omega_r)$. The instrument errors for these quantities are much smaller than those for σ and ϵ alone. Expressions for the difference quantities are

$$\sigma(\omega) - \sigma(\omega_r) = \frac{1}{GR_F}\left\{(r' - r'_r) - \omega_r R_F C_F\left[\frac{\omega}{\omega_r} r'' - r''_r\right]\right\} \quad [20]$$

and

$$\epsilon(\omega) - \epsilon(\omega_r) = \frac{1}{G\epsilon_0}\left\{\frac{1}{\omega_r R_F}\left[\frac{\omega_r}{\omega} r'' - r''_r\right] + C_F(r' - r'_r)\right\}. \quad [21]$$

Consider, first, the expression for $\sigma(\omega) - \sigma(\omega_r)$. The most important component on the right of Eq. [20] is the first term in the brackets, the difference in the in-phase output as the frequency is varied between ω_r and ω. The second term contains the out-of-phase output ratio r''. Instead of appearing as a simple frequency difference $r'' - r''_r$, r'' is multiplied by the frequency ratio ω/ω_r. Since $r''(\omega)$ is roughly linear in frequency, this term increases as ω^2. However, it is multiplied by $\omega_r R_F C_F$, which is quite small in most circumstances. This prevents the second term from being important except at high frequencies. Note that only the second term in Eq. [20] contains C_F so errors in C_F do not show up until the high-frequency part of the spectrum is reached. Tests show that $\sigma(\omega) - \sigma(\omega_r)$ at high frequencies is indeed sensitive to the value of C_F.

The difference spectrum for the dielectric constant is much less sensitive to errors in C_F. According to Eq. [21], the out-of-phase response dominates since the second quantity in brackets is multiplied by the small quantity C_F. The second term contains the frequency difference of the in-phase output, which is small under most conditions. Thus, errors in C_F have a small effect on the dielectric constant difference and experiments show that $\epsilon(\omega) - \epsilon(\omega_r)$ is insensitive to the exact value of C_F. On the other hand, the absolute magnitude of ϵ is sensitive to C_F.

IV. INSTRUMENT CALIBRATION

In a measurement as complicated as this, it is important to provide proof that the results are accurate. This is difficult in the range of sample conductivities and relaxation frequencies of interest here since no standards exist for a thorough calibration. Nevertheless, our testing of the apparatus provides evidence that the technique is accurate.

Two sorts of tests were performed. First, RC circuits having a known frequency response were substituted for the four-electrode cell. The ability of the instrument to duplicate the

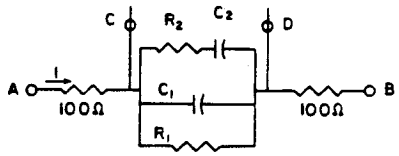

FIG. 5. The networks used in dummy load tests.

known response shows that the electronic design is sound. Second, "wet" experiments were conducted with pure electrolytes of known conductivity and dielectric constant, each independent of frequency, and with dilute suspensions. These tests showed that the cell performed as expected.

The first electrical tests were designed to show that the electronics could reproduce the frequency response curve for a "dummy load." Each load was of the general form shown in Fig. 5. Terminals "A" and "B"' represent the source electrodes and two 100-Ω resistors represent, in an approximate manner, the impedance which exists in the regions separating the source electrodes from the sense electrodes. Terminals "C" and "D" represent the sense electrodes. The network between the sense electrodes simulates the electrical behavior of a material in the cell.

All of the components used in the test network were carefully measured: resistances with a Data Precision (Analogic Corp.) DVM, and capacitances with a capacitance bridge at 1 kHz. Tests were carried out with five different loads to cover the range of responses expected with the cell. In each test an experiment was conducted with a given dummy load in place, and the in-phase and out-of-phase components of the ratio $V_0/\Delta V$ were measured. Then the predicted frequency response was compared with the experimental results. Figure 6 shows results from one such test. Agreement between the prediction and the experiment was always excellent.

Tests were also carried out with aqueous electrolytes. Since the conductivity and dielectric constants of these materials are independent of frequency over the frequency range of interest, the measured frequency-difference spectrum should be flat. Electrical tests showed that despite the good agreement between measured and predicted output voltages, there is an electronic limitation to the accuracy of the dielectric constant measurement at low frequencies. Electrolyte tests show whether electrochemical problems cause additional errors.

Results from one set of tests are shown in Fig. 7. In the upper panel the absolute conductivity is plotted against frequency. Note that the scale is expanded considerably; the conductivity is essentially constant to 20 kHz, and the error at 200 kHz is less than 2%. The second panel shows the dielectric constant. The percentage error shown for this test is about 20%. In most cases the error in the dielectric constant is much smaller, as will be shown shortly. Furthermore, the error decreases as the dielectric constant of the ma-

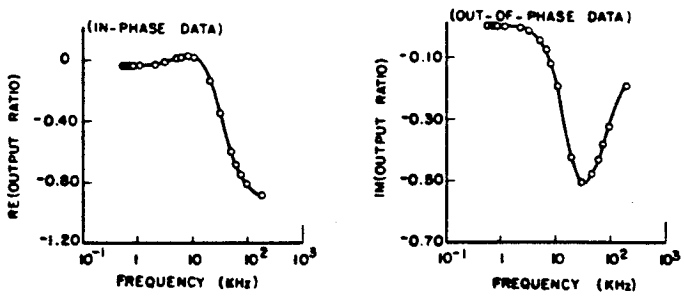

FIG. 6. Comparison between measured and predicted output ratios for a dummy load test showing the in-phase (left) and out-of-phase (right) data; theory, —; experiment, O.

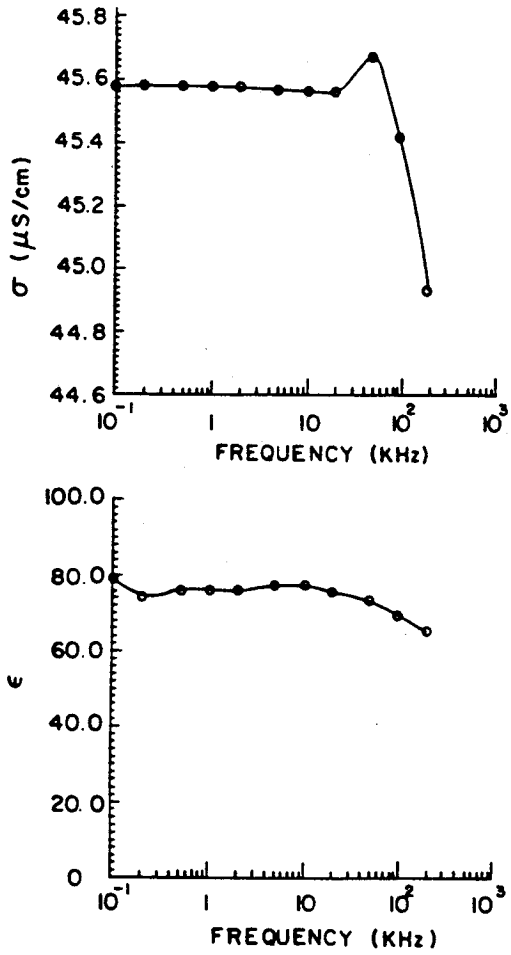

FIG. 7. Measured conductivities and dielectric constants for a 10^{-4} M HCl solution.

terial in the cell increases so that the errors in the dielectric behavior of suspensions are much less [6].

V. TESTS WITH SUSPENSIONS

Extensive tests were carried out to establish the characteristics of the instrument with suspensions in the measuring cell. The suspensions consisted of 0.191-μm amphoteric latex particles in 10^{-4} M HCl. Detailed information on these particles is given in a companion paper (9). For the present it suffices to note that the ζ-potential of these particles in 10^{-4} M HCl is roughly 80 mV. To obtain frequency-difference spectra, six separate experiments were conducted, two with the pure electrolyte and four with suspensions. The volume fraction ϕ varied between 0.024 and 0.041 in the experiments with suspensions. The reference frequency used in every case was 500 Hz and the measuring frequencies, eight in all, followed a logarithmic sequence from 1 to 200 kHz.

Figure 8 shows the variation of the absolute dielectric constant with frequency at different particle concentrations. Results of the baseline measurements before and after the tests with suspension are almost identical, and flat. The repeatability, and the minimal frequency dependence of the measured dielectric constant of the pure electrolyte, indicates that no unusual electrochemical effects influenced the experiment. Note also that the accuracy here is better than that found in the earlier tests.

The remaining curves show results for experiments with suspensions. As expected, there is a tremendous change in the dielectric constant due to the addition of relatively small amounts of colloidal material; a dielectric constant of 800 with a volume fraction of only 0.041 is 10 times the value for pure water. Suspensions with successively smaller particle volume fractions yield smaller values for the low-frequency dielectric constant. In each case the dielectric constant decreases as the frequency is increased. At 50 kHz, the dielectric constant of the suspension is very close to that of pure water.

To further check the instrument, the frequency difference spectra measured with suspensions of various particle concentrations were normalized by the volume fraction of particles and plotted together (Figs. 9 and 10). For dilute suspensions the spectra should be linear in the volume fraction and the fact that the data superimpose shows that the cell and electronics are free of errors due to the electrical or chemical properties of the suspension. If such errors did exist, they would need to be

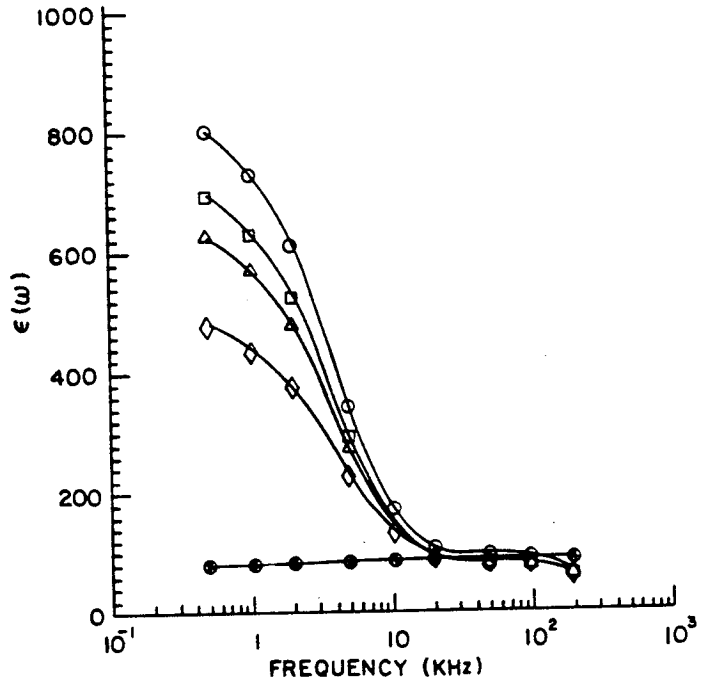

FIG. 8. The dielectric constant for suspensions of (0.191-μm) latex particles in 10^{-4} M HCl; volume fractions: ○, 0.041; □, 0.035; △, 0.032; ◇, 0.024; ⊛, 0.000.

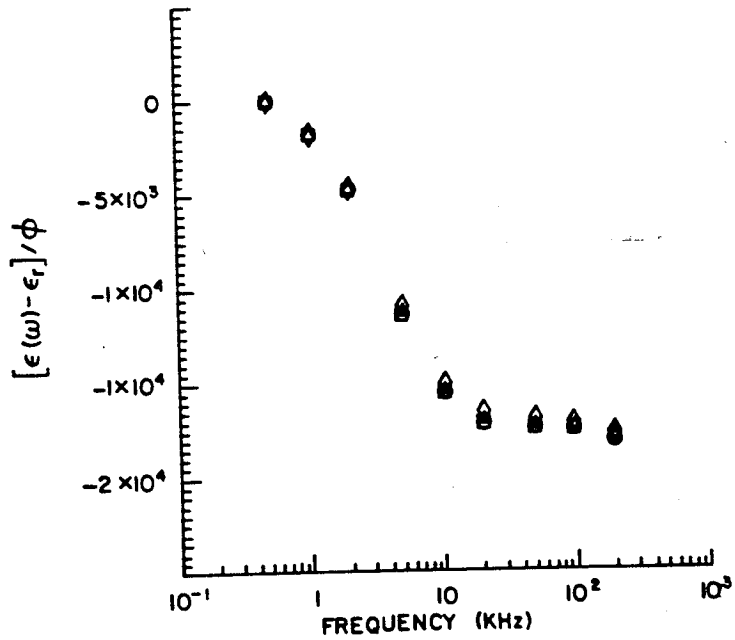

FIG. 9. Normalized frequency-difference spectra for the dielectric constant of suspensions of (0.191-μm) latex particles in 10^{-4} M HCl; volume fractions as noted on Fig. 8.

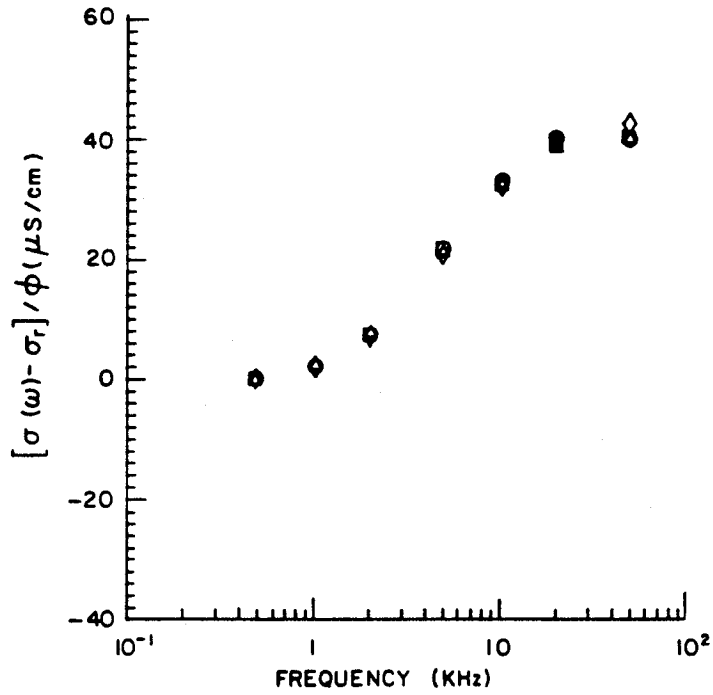

FIG. 10. Normalized frequency-difference spectra for the conductivity of suspensions of (0.191-μm) latex particles in 10^{-4} M HCl; volume fractions as noted on Fig. 8.

linear in the volume fraction of particles to avoid detection, which is unlikely.

The linearity of the frequency-difference spectra with respect to particle volume fraction was also checked at every frequency using linear regression. The linear correlation coefficient for the experiments was in excess of 0.998 except for the conductivity measurements at 100 and 200 kHz.

The change in the conductivity caused by the addition of particles to the electrolyte is markedly less than the change in the dielectric constant. The conductivity of 10^{-4} M HCl is about 45 μS/cm, and a 4.1% by volume addition of particles increases this by about 2 μS/cm. Instead of an order of magnitude change, this is a modest 4.4% increase. This makes the conductivity frequency-difference spectrum more difficult to measure than the dielectric constant difference spectrum.

The experiments described were repeated using a fresh suspension as a check on the reproducibility of the results. The differences in the frequency-difference quantities were less than 5%.

VI. DISCUSSION

The instrument described here employs a four-electrode frequency-difference technique adapted for colloidal suspensions. Dielectric spectrometers of this type are an improvement over the traditional Wheatstone bridge devices, offering shorter measurement times, improved signal-to-noise ratios, and elimination of the thermal drift problem without precise temperature control. The dielectric constants and conductivities of colloidal dispersions measured with this instrument are linear in the volume fraction of particles at low volume

fractions and quite reproducible. In the subsequent paper (9) we discuss extensive measurements covering a range of ionic strengths.

ACKNOWLEDGMENTS

This work was supported by NASA's Microgravity Science and Applications Division, the Xerox Corp., and an equipment grant from the Shell Foundation.

REFERENCES

1. Schwan, H. P., Schwartz, G., Maczuk, J., and Pauly, H., *J. Phys. Chem.* **66,** 2626 (1962).
2. Springer, M. M., Korteweg, A., and Lyklema, J., *J. Electroanal. Chem.* **153,** 55 (1983).
3. Lim, K.-H., and Franses, E. I., *J. Colloid Interface Sci.* **110,** 201 (1986).
4. Midmore, B. R., Hunter, R. J., and O'Brien, R. W., *J. Colloid Interface Sci.* **120,** 210 (1987).
5. Midmore, B. R., and O'Brien, R. W., *J. Colloid Interface Sci.*, in press.
6. Schwan, H. P., "Physical Methods in Biological Research" (W. L. Nastuk, Ed.), Vol. VI. Academic Press, New York, 1963.
7. Hayakawa, R., Kanda, H., Sakamoto, M., and Wada, Y., *Japan. J. Appl. Phys.* **14,** 12 (1975).
8. Nakamura, H., Husimi, Y., and Wada, A., *J. Appl. Phys.* **52,** 4 (1981).
9. Myers, D. F., and Saville, D. A., *J. Colloid Interface Sci.* **131,** 461 (1989).

Dielectric Spectroscopy of Colloidal Suspensions

II. Comparisons between Experiment and Theory

D. F. MYERS AND D. A. SAVILLE[1]

Department of Chemical Engineering, Princeton University, Princeton, New Jersey 08544

Received July 11, 1988; accepted November 7, 1988

A four-electrode frequency-difference dielectric spectrometer is used to study the dielectric response of suspensions of amphoteric polystyrene particles in dilute HCl solutions. Results are given for one set of particles with relatively thick diffuse layers, i.e., $3 < a\kappa < 10$. When the dielectric spectra are compared to those predicted by classical electrokinetic theory, large discrepancies are found. The measured dielectric constant is an order of magnitude larger than the theoretical value. The limited body of experimental data extant in the literature confirms these results, suggesting that the standard electrokinetic model is somehow deficient when applied to dispersions of this sort.

I. INTRODUCTION

A growing body of evidence suggests that the electrokinetic behavior of some colloidal particles cannot be characterized by a single parameter such as the ζ-potential (1–4). However, much of the experimental evidence is based on static measurements, such as the electrophoretic mobility of individual particles, or low-frequency measurements (<100 Hz), such as the electrical conductivity of suspensions. Thus, to some extent, the evidence is inconclusive. Part of the difficulty stems from the low information content of these measurements, essentially one data point per experiment. Furthermore, since the anomalous behavior appears connected with processes on the particle surface, it is important to be able to study this region and its interaction with the diffuse layer experimentally. Dielectric spectroscopy offers a means of studying relaxation behavior because the properties of a suspension can be measured over a range of frequencies. In the first paper of this series a new instrument was described (5). Here we report measurements on dispersions made at several salt strengths.

II. EXPERIMENTAL PROTOCOLS

Suspensions of polystyrene particles are popular model colloidal systems because standard synthesis techniques produce nearly spherical and monodisperse particles. An additional advantage is that surface properties and the particle diameter can be varied by modifying the synthesis procedure. An amphoteric polystyrene latex served as the model system for this work. It was synthesized according to the procedure developed by Homola and James (6), with the modification suggested by Harding and Healy (7). Particle surfaces contained both amine and carboxyl groups. The former are positively charged at low pH and neutral under other conditions; the latter are negatively charged at high pH. On the basis of the synthesis used for our latex, the isoelectric pH should be approximately 5.4 (7). In our experiments the particles were in the cationic form.

Particle size and monodispersity were determined by transmission electron microscopy, which gave an average particle diameter

[1] To whom correspondence should be addressed.

0021-9797/89 $3.00

of 0.191 μm, with a standard deviation less than 0.003 μm. Particles in the TEM images appeared to be perfectly spherical.

The particles were cleaned using a sedimentation–decantation procedure (4) that employed a Beckman Model L5 ultracentrifuge with the Model 21 rotor running at 8000 rpm (9000 g). A run of 90 min was sufficient to achieve complete separation and produced a pellet which was easily redispersed without sonication. Particles were spun down in electrolyte at the ionic strength used in the experiment. The cleaning process continued over several sedimentation–decantation cycles until the supernatant conductivity was within 1% of the conductivity of the pure suspending electrolyte. The spectroscopy experiment was completed within 48 h of cleaning.

Particle mobilities were measured by microelectrophoresis, using a Rank Brothers Mark II device. Potentials were computed from the measured electrophoretic mobilities with the computer program of O'Brien and White (8); results are shown in Fig. 1. These data represent two series of experiments, conducted approximately 30 days apart with the error bars reflecting two standard deviations about the mean of 20 measurements at each salt strength. The large error bars near 0.001 M reflect the flat nature of the ζ-potential–mobility relation at this double-layer thickness; the scatter in the mobility measurement is much less.

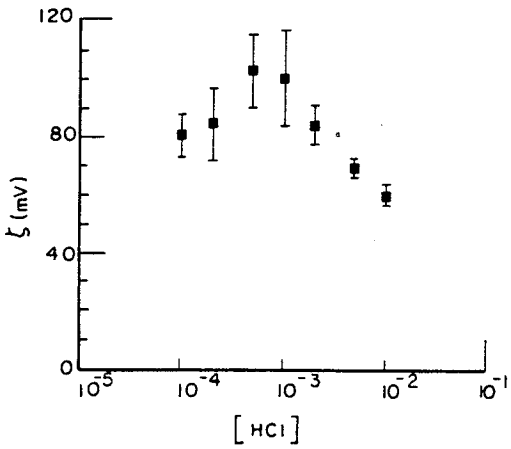

FIG. 1. The ζ-potentials of 0.191-μm particles in HCl solutions.

Prior to each experiment involving a suspension, the cell used in the dielectric spectroscopy experiment was filled with the suspending electrolyte and allowed to stand overnight. Then, immediately before the experiment, the cell was emptied and refilled with electrolyte approximately five times. A sequence of six experiments was performed for each ionic strength. First, an experiment with the pure suspending electrolyte was done to establish the experimental baseline. Next, the cell was filled with suspension and four experiments were conducted, each at a different particle volume fraction. Finally, the cell was emptied of suspension and thoroughly cleaned with the pure electrolyte, and the baseline measurement was repeated.

The experiment sequence proceeded toward successively less concentrated suspensions, each obtained by withdrawing a small volume of suspension with a pipet and replacing it with the same volume of the pure electrolyte. Then, the contents of the cell were mixed by redispersing with a pipet. The small volume (<1 cc) of suspension removed during each dilution was saved for the volume fraction determination. Each sample was saved in a plastic vial and refrigerated until the entire set of experiments was complete. The volume fraction was measured by drying a known mass of suspension, assuming the specific gravity of polystyrene to be 1.057.

Several sets of experiments were done with particles suspended in HCl at increasing salt strengths. The particles for the first experiment (10^{-4} M HCl) were cleaned starting from raw latex. Subsequent experiments used the same latex cleaned in the more concentrated salt solution, with a small quantity of the raw latex stock added to make up for the sample used in the volume fraction determination.

III. EXPERIMENTAL RESULTS

The experimental results were analyzed using procedures described by Myers and Saville

(5). Experiments on suspensions with different particle concentrations were checked to ensure that the response was linear in the volume fraction of particles. Only data for which the correlation coefficient was better than 0.99 are reported; in most cases the correlation coefficient exceeded 0.999. The results are reported as "difference spectra," i.e., the difference between the value at the measuring frequency and the reference frequency (500 Hz) normalized by the volume fraction of particles, ϕ, i.e.,

$$\text{conductivity spectrum: } [\sigma(\omega) - \sigma_r]/\phi$$

$$\text{dielectric constant spectrum: } [\epsilon(\omega) - \epsilon_r]/\phi.$$

Note that this procedure eliminates effects due to nonspecific adsorption and added counterions (9).

Figure 2 shows the normalized frequency-difference spectrum for the conductivity at several ionic strengths. The most striking feature is the increase in the magnitude of the conductivity difference with increasing salt strength. Increasing the HCl concentration by a factor of 10 brings a factor of 4 increase in the conductivity difference at 50 kHz. The full behavior of the relaxation frequency is not readily apparent here. The data at 10^{-4} M reach the high-frequency plateau at 50 kHz, but at the other ionic strengths there is still a substantial frequency dependence at the highest frequencies measured.

The normalized frequency-difference spectra for the dielectric constant are shown in Fig. 3. Here again, the magnitude of each spectrum increases with increasing salt strength. The dielectric constant difference has clearly reached a high-frequency plateau by 20 kHz in 10^{-4} M HCl, but not with 10^{-3} M HCl. At intermediate salt strengths the same trend is apparent, leading to the conclusion that the characteristic frequency increases monotonically with salt strength.

The experiments described in this section were repeated with fresh latex as a check on

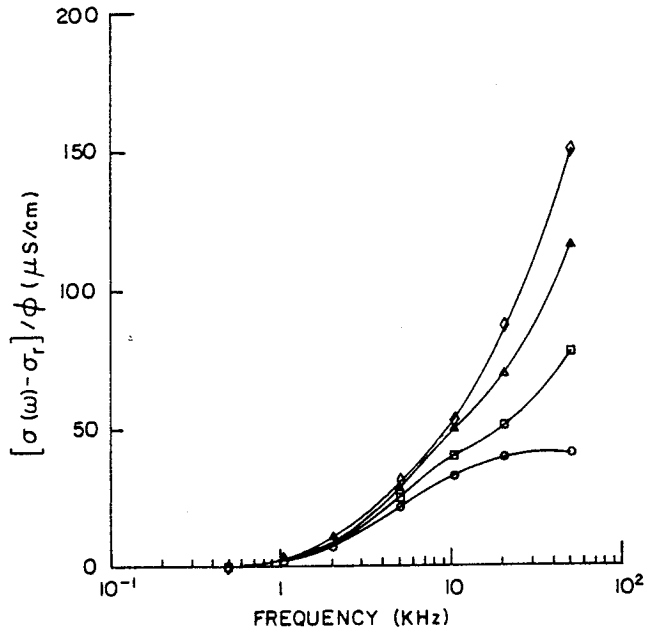

FIG. 2. Frequency difference spectra for the conductivity of suspensions of 0.191-μm particles at different salt strengths; ○, 10^{-4} M, $a\kappa$ = 3.1; □, 2×10^{-4} M, $a\kappa$ = 4.4; △, 5×10^{-4} M, $a\kappa$ = 7.0; ◇, 10^{-3} M, $a\kappa$ = 9.9. Note that the frequencies quoted here and elsewhere in the figures are the *linear* frequencies, $\omega/2\pi$.

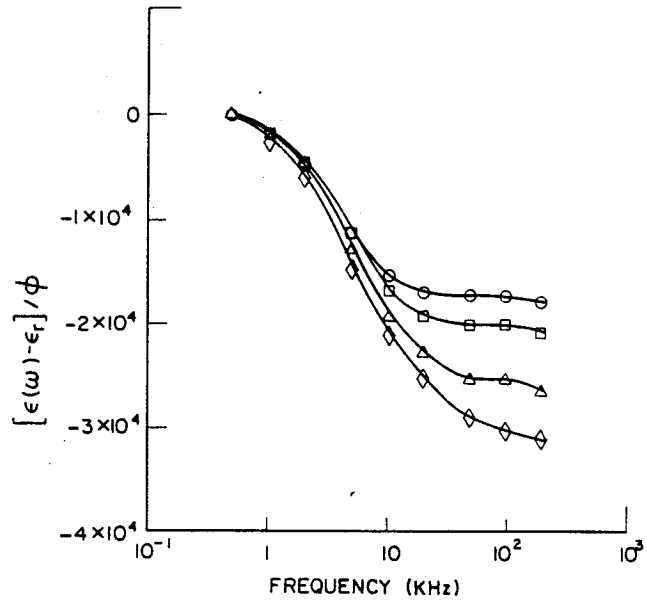

FIG. 3. Frequency difference spectra for the dielectric constant of suspensions of 0.191-μm particles at different salt strengths: ○, 10^{-4} M, $a\kappa = 3.1$; □, 2×10^{-4} M, $a\kappa = 4.4$; △, 5×10^{-4} M, $a\kappa = 7.0$; ◇, 10^{-3} M, $a\kappa = 9.9$.

reproducibility. The average deviation for the conductivity was 7%; for the dielectric constant it was 4.6%.

These data show that the conductivity and dielectric constant frequency-difference spectra are strong functions of ionic strength, in terms of both the magnitude of the effect and the relaxation frequency of the dielectric constant. The spectra are linear in the particle volume fraction and reproducible. In the next section these results are compared with a theory of dielectric relaxation based on the classical electrokinetic model.

IV. A COMPARISON BETWEEN EXPERIMENTAL DATA AND THEORY

Since bulk suspension properties alone are accessible to our experimental technique, a mathematical model must be used to relate the relevant physical processes to the surface properties of the particles. Here, the experimental data are compared to predictions from the standard electrokinetic model, using the solution of DeLacey and White (10). Although a number of dielectric relaxation models for colloidal suspensions have been proposed in the literature (11–16), only the work of DeLacey and White (10) treats the problem without any mathematical approximations. Theirs is a thorough treatment of the problem using the standard model. To avoid ambiguities, the equations making up the standard model will be reviewed briefly.

In the classical theory of electrokinetics, particles of radius a and dielectric constant ϵ_p are immersed in an electrolyte containing N distinct ion types. Each ion is characterized by its volume density n_j, mobility m_j, and valence z_j. The electrolyte is assumed to act as a Newtonian fluid with viscosity μ, density ρ, and dielectric constant ϵ_∞. $N + 3$ coupled differential equations and $N + 1$ constitutive relations are available to solve for the independent variables: the fluid velocity $\mathbf{u}$; the fluid pressure P; the electric potential ψ; and the ion densities n_j, $j = 1, 2, \ldots, N$. For oscillatory fields, the time-dependent nature is assumed to be $\exp(i\omega t)$; ω is the angular frequency of the applied field and i stands for $\sqrt{-1}$. The differential equations are

$$\epsilon_0\epsilon_\infty \nabla^2\psi = -\rho_e \quad [1]$$

$$\mu\nabla^2\mathbf{u} - \nabla P = -\rho_e\mathbf{E} \quad [2]$$

$$\nabla\cdot\mathbf{u} = 0 \quad [3]$$

$$\nabla\cdot\mathbf{f}_j = \frac{\partial}{\partial t} n_j, \quad j = 1, 2, \ldots, N \quad [4]$$

$$\rho_e = \sum_{j=1}^{N} ez_j n_j \quad [5]$$

$$f_j = n_j\mathbf{u} - m_j ez_j n_j \nabla\psi - m_j kT\nabla n_j. \quad [6]$$

Equation [1] is Poisson's equation, with ρ_e representing the volume charge density in the electrolyte. Equations [2] and [3] are the Stokes equations where viscous and pressure forces are balanced against the electrical body force term; $\mathbf{E}$ is the electric field vector. Equation [4] relates the divergence of the flux of the jth ion to the time rate of change of its volume density. The constitutive relation for charge density is given by Eq. [5], where e is the fundamental electric charge. Equation [6] gives the ion fluxes in terms of components due to convection, electromigration, and diffusion. Here k is Boltzmann's constant and T is absolute temperature. The boundary conditions will be discussed shortly.

It is desirable to separate this problem into two simpler problems by assuming that the dependent variables can be written as a perturbation expansion in the dimensionless electric field strength $\beta \equiv aeE_0/kT$, where E_0 represents the imposed field. Thus, for $\beta \ll 1$,

$$\psi = \psi^0 + \beta\delta\psi + O(\beta^2)$$
$$n_j = n_j^0 + \beta\delta n_j + O(\beta^2). \quad [7]$$

First, the $O(1)$ problem, which represents the equilibrium situation, is solved with the Poisson–Boltzmann equation used to relate ψ^0 to n_j^0. The boundary conditions on the electric potential are

$$\psi^0(\mathbf{r}) \to 0 \quad \text{as} \quad |\mathbf{r}| \to \infty \quad [8]$$

$$\psi^0(a) = \zeta. \quad [9]$$

The $O(\beta)$ problem is more complicated. Fluid flow must be considered and, due to the oscillatory nature of the problem, all the terms in the perturbation equations are complex-valued. Boundary conditions must be applied to $\delta\psi$, $\delta\mathbf{u}$, and all of the δn_j in the $O(\beta)$ problem. Far from the particle,

$$\delta\psi \to -\mathbf{E}_0\cdot\mathbf{r} \quad [10]$$

$$\delta\mathbf{u} \to -\mu_e\mathbf{E}_0 \quad [11]$$

$$\delta n_j \to 0, \quad [12]$$

where μ_e stands for the electrophoretic mobility of the particle.

At the particle surface,

$$\delta\psi(a) - \delta\psi_1(a) = 0 \quad [13]$$

$$[\epsilon\nabla\delta\psi(a) - \epsilon_p\nabla\delta\psi_1(a)]\cdot\mathbf{n} = 0 \quad [14]$$

$$\mathbf{f}_j(a)\cdot\mathbf{n} = 0 \quad [15]$$

$$\mathbf{u}(a) = 0. \quad [16]$$

Equation [13] ensures that the electric potential is continuous across the particle surface ($\delta\psi_1$ is the electric potential inside the particle). The next expression represents the charge induced at the particle, which is proportional to the jump in the electrical displacement; $\mathbf{n}$ is a unit vector pointing out from the surface. Since the jump is set equal to zero, the particles have a constant charge. The other equations specify that the ion fluxes normal to the particle surface vanish and that the no-slip condition prevails.

These model equations constitute what is called the standard model of electrokinetics: the Gouy–Chapman model of the diffuse layer coupled with conservation equations and boundary conditions where the equilibrium interface is unaffected by dynamic processes. DeLacey and White (10) solved these equations numerically to obtain the dipole coefficient from the far-field form of the electric potential and this was used to compute the complex conductivity, i.e., the conductivity and dielectric constant of the suspension. Their results are presented in a normalized form which is independent of the volume fraction of particles using two functions; $\Delta\epsilon'$ and ΔK^{eff}. These are defined by

$$\epsilon = \epsilon_\infty + \phi\Delta\epsilon' \qquad [17]$$

$$\sigma = \sigma_\infty + \phi\Delta K^{\text{eff}}, \qquad [18]$$

where ϵ_∞ and σ_∞ are the dielectric constant and conductivity of the electrolyte in the absence of particles, and ϕ is the particle volume fraction.

The frequency-difference spectra from our dielectric spectroscopy measurement can be related to DeLacey and White's (10) functions in a straightforward way using Eqs. [17] and [18]. Thus

$$\frac{\sigma(\omega) - \sigma_r}{\phi} = \Delta K^{\text{eff}}(\omega) - \Delta K^{\text{eff}}(\omega_r) \qquad [19]$$

$$\frac{\epsilon(\omega) - \epsilon_r}{\phi} = \Delta\epsilon(\omega) - \Delta\epsilon(\omega_r). \qquad [20]$$

Accordingly, the normalized frequency-difference spectrum from the measurement is equal to the frequency-difference spectrum of DeLacey and White's functions.

DeLacey and White's published results (10) have been checked for low ζ-potentials by O'Brien (17), who found good agreement with dimensionless ζ-potentials as high as 2. The DeLacey–White algorithm is available as a FORTRAN program, which we have implemented and checked by computing the results shown in three figures in DeLacey and White's paper (Figs. 1, 4, and 7, each at ζ = 100 mV). We also checked the zero-frequency limits of the conductivity and mobility against the results of Zukoski and Saville (18).

The first comparison with experimental data will be for dispersions in 10^{-4} M HCl. The measured ζ-potentials are given in Fig. 1. Figure 4 shows the measured and theoretical frequency-difference spectra for the conductivity. The theoretical spectrum is about 50% larger than the measured magnitude but the characteristic relaxation frequencies differ by over an order of magnitude.

The comparison between measured and theoretical spectra for the dielectric constant shows even larger discrepancies (Fig. 5). Here the predicted magnitude of the relaxation is more than an order of magnitude smaller than

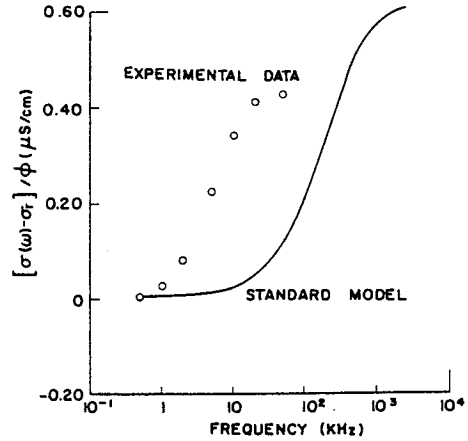

FIG. 4. Comparison between the measured frequency-difference spectrum for the conductivity and that predicted by the standard model for 0.191-μm particles in 10^{-4} M HCl.

that measured. The difference between the relaxation frequencies is similar to that observed in the conductivity-difference spectrum. Similar differences were found at the other salt concentrations (Figs. 6 and 7).

Needless to say, these are very striking comparisons. The discrepancy between theory and experiment seen in the conductivity spectrum magnitude is relatively small and might be brought into agreement by adjusting the ζ-potential, but the predicted relaxation frequency is far too large. However, both the magnitude and the characteristic frequency of the theoretical dielectric constant spectrum disagree considerably with the experimental results. These discrepancies cannot be removed by adjusting ζ-potentials.

Several factors were investigated to see if they would account for the discrepancies: errors in the ζ-potential and the formation of permanent or temporary aggregates. In the experiments at 10^{-4} M HCl the measured ζ-potential was 100 mV. To test the sensitivity of the theory to changes in the ζ-potential, results were calculated for ζ-potentials of 100 and 200 mV. Figure 8 shows that this effect is too small to account for the discrepancy.

Another possibility is the presence of agglomerates. The predicted dielectric constant

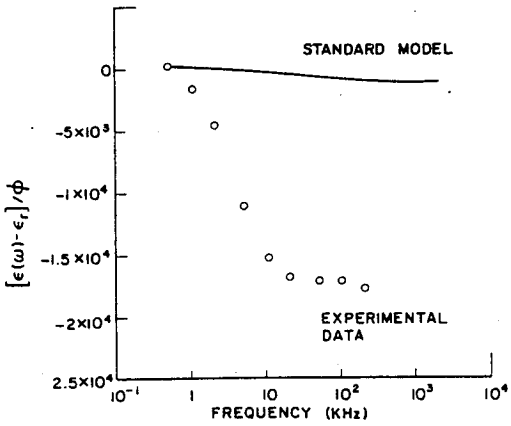

FIG. 5. Comparison between the measured frequency-difference spectrum for the dielectric constant and that predicted by the standard model for 0.191-μm particles in 10^{-4} M HCl.

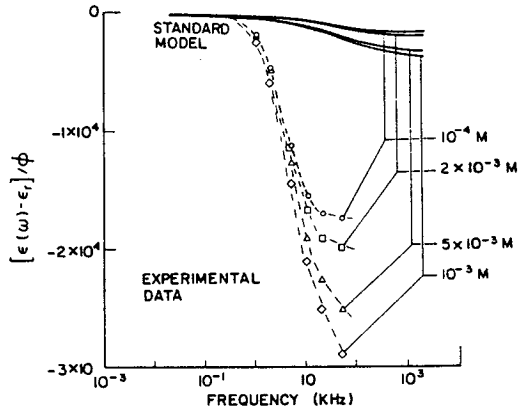

FIG. 7. Comparison between the measured frequency-difference spectrum for the dielectric constant and that predicted by the standard model for 0.191-μm particles at four salt strengths: ○, 10^{-4} M, $a\kappa = 3.1$; □, 2×10^{-4} M, $a\kappa = 4.4$; △, 5×10^{-4} M, $a\kappa = 7.0$; ◇, 10^{-3} M, $a\kappa = 9.9$.

increases with particle size and Lyklema *et al.* (19) suggested that this could lead to discrepancies. Increasing the value of $a\kappa$ by as much as a factor of 16, however, fails to bring theory and experiment into agreement and it is unlikely that agglomerates of this size or larger existed in our suspensions. No agglomerates of any size were seen in the TEM images, so the agglomeration would have to take place in the cleaning procedure or during the experiment. Furthermore, agglomerates of this size would have settling properties different from those of individual particles. No sediment was ever observed in the bottom of the sample cell, nor was any coagulum ever observed floating on the surface of the sample. It can be stated with some confidence that agglomerates of this size did not exist before or after our experiments.

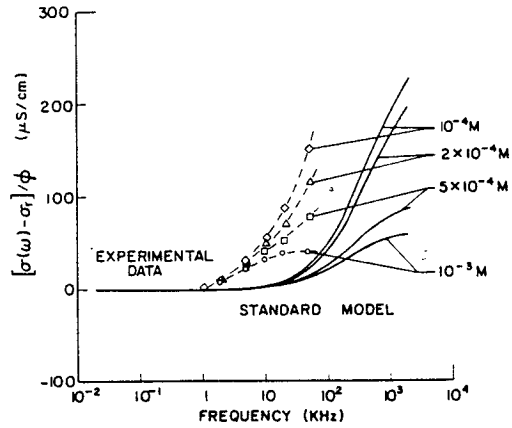

FIG. 6. Comparison between the measured frequency-difference spectrum for the conductivity and that predicted by the standard model for 0.191-μm particles at four salt strengths: ○, 10^{-4} M, $a\kappa = 3.1$; □, 2×10^{-4} M, $a\kappa = 4.4$; △, 5×10^{-4} M, $a\kappa = 7.0$; ◇, 10^{-3} M, $a\kappa = 9.9$.

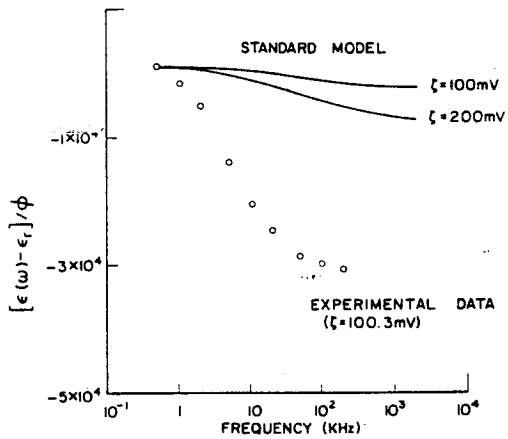

FIG. 8. Comparison between the measured frequency-difference spectrum for the dielectric constant and that predicted by the standard model for 0.191-μm particles in 10^{-4} M HCl at two ζ-potentials.

A third possibility is that temporary aggregates were formed. If dipole–dipole interactions between particles induced doublets or larger chains to form, this would increase the dielectric constant and the doublets would disappear after the field was removed. However, this mechanism can be discounted on the grounds of a scaling argument and experimental evidence. The interaction energy between two dipoles separated by a distance r is given by Israelachvili (20) as

$$\text{Interaction Energy} = \frac{2u_1u_2}{4\pi\epsilon\epsilon_0 r^3}, \quad [21]$$

where u_1 and u_2 are the dipole moments of the interacting particles. If doublets are formed, the interaction energy must exceed the energy of thermal motion, kT. Thus, for identical particles dipole–dipole interactions will be negligible when

$$\frac{2u^2}{4\pi\epsilon\epsilon_0 r^3 kT} \ll 1. \quad [22]$$

To compute this ratio, an estimate for the dipole moment is needed. This is related to the particle dipole coefficient, i.e.,

$$u = 4\pi\epsilon\epsilon_0 a^3 E_0 C_0, \quad [23]$$

with C_0 representing the dipole coefficient of a particle. Thus,

$$\frac{64\pi\epsilon\epsilon_0 C_0 E_0^2 a^3}{kT} \ll 1 \quad [24]$$

if dipole–dipole interactions are negligible. Here, the interaction distance r has been assumed to equal to twice the particle radius a. Taking $C_0 = 1.0$ (a large value), an electric field strength of 10 V/m (typical of those used in our experiments), and a particle radius of 0.1 μm, yields a value of 3.6×10^{-6}. This is sufficiently small to justify neglecting dipole interactions.

Finally, to see if the field strength in our apparatus had any effect, frequency scans were done with field strengths of roughly 10, 20, and 40 V/m. Since the scaling argument indicates that the dipole–dipole interaction increases with the square of the electric field strength, doubling the field should increase the dipole interaction by factors of 4 and 16. Little or no effect was observed and we conclude that effects due to induced dipoles are negligible.

At this point we are forced to conclude that the standard model fails to describe our experimental results. Next, other experimental studies were scrutinized to see whether similarly large deviations between experiment and theory had been observed previously. The work of Springer *et al.* (21) and Lim and Franses (22) was used although precise ζ-potential data were not available. Springer *et al.* do not report ζ-potentials, but do give titratable charge from which we have estimated the ζ-potentials. Lim and Franses report ζ-potentials, but they have an unexplained dependence on the particle volume fraction and may be inaccurate. Although the ζ-potentials may be in error, the influence of the errors can be estimated. It should also be noted that neither of these reports included a direct comparison of experimental data with the standard model in a detailed form. However, Springer *et al.* did compare their results with a theory for thin double layers and found substantial disagreement (19).

For the purposes of comparison, a measure of the magnitude of the change in the dielectric constant is needed. We used the "static specific dielectric increment" (SSDI) defined by Lim and Franses (22), viz.,

$$\text{SSDI} = \frac{\epsilon(0) - \epsilon(\infty)}{\phi}, \quad [25]$$

where

$$\epsilon(0) \equiv \lim_{\omega \to 0} \epsilon(\omega) \quad \text{and}$$

$$\epsilon(\infty) \equiv \lim_{\omega \to \infty} \epsilon(\omega). \quad [26]$$

In each case studied, the dielectric constants in the two limits and the particle volume fraction were obtained from the published experimental data and computed with DeLacey and White's computer program (10). For com-

parison with Lim and Franses' work the measured ζ-potentials were used; for Springer *et al.* (21), ζ-potentials were estimated.

It should be pointed out that there is some ambiguity in the choice of $\epsilon(0)$ and $\epsilon(\infty)$ in each data set. For Lim and Franses' data (22), the published values based on a Cole–Cole extrapolation were used. For Springer *et al.* (21), as well as our own data, the lowest frequency and highest frequency data points were used. Although these procedures are imprecise, we are looking for order-of-magnitude effects so the approximation is useful. The SSDIs from the experiments will be underestimated, in any event.

The results of the comparison are given in Table I. To test the sensitivity to changes in the ζ-potential, different values were chosen. Nevertheless, the differences cannot be explained by low ζ-potentials. The tabulated data show that at least three different experimental studies yield dielectric constants substantially larger than predicted by the standard model. Moreover, a large number of experimental parameters have been varied in the studies. Both Springer *et al.* (21) and Lim and Franses (22) used two-electrode bridge methods, while a four-electrode frequency-differencing technique was used in our work. It seems unlikely that experimental errors would consistently give inflated values for the dielectric constant using such different techniques.

V. CONCLUSIONS

A comparison between the experimental results and the predictions of the standard model has identified several discrepancies. The difference between theory and experiment in the measurement of the electrical conductivity is relatively small, consistent with the earlier results of Van der Put and Bijsterbosch (1, 2), O'Brien and Perrins (3), and Zukoski and Saville (4). However, the characteristic relaxation frequency of the suspension and the magnitude of the dielectric constant, two measurements unique to dielectric spectroscopy, show substantial differences between theory and experiment. Studies with other instruments show similar behavior.

Our work and the work of other investigators involve a variety of configurations and conditions: two- and four-electrode cells, two types of particles (polyvinyltoluene and polystyrene), three different salts (NaCl, KCl, and HCl), and a range of salt strengths and particle

TABLE I

Comparison between Theoretical and Measured SSDI Values

Case	Author[a]	Salt	a (μm)	$a\kappa$	ζ (mV)	SSDI $\times 10^{-2}$ (experimental)	SSDI $\times 10^{-2}$ (theoretical)
1	L&F	NaCl	1.0	120	−37	1300	4 (307)[b]
2	L&F	NaCl	0.6	80	−33	2000	3 (630)
3[c]	L&F	NaCl	0.6	80	−132	2000	250 (8)
4	S	KCl	0.2	15	−50[d]	170	7 (23)
5	S	KCl	0.2	15	−75[d]	170	20 (9)
6	S	HCl	0.2	12	−50[d]	140	8 (18)
7	S	HCl	0.2	12	−100[d]	140	41 (3)
8	M&S	HCl	0.1	3	81	170	15 (11)
9	M&S	HCl	0.1	4	84	200	18 (11)
10	M&S	HCl	0.1	7	103	250	32 (8)

[a] L&F, Lim and Franses (22); S, Springer *et al.* (21); M&S, this work.

[b] Numbers in parentheses are the ratios of the experimental to theoretical SSDIs.

[c] Conditions the same as for case 2 except that the ζ-potential has been quadrupled.

[d] Estimated ζ-potentials for each case.

sizes ($a\kappa$ varied from 3 to 120). In every case the experimental data on the dielectric constant exceeded the theoretical values obtained from the standard model. This suggests that the discrepancies encountered with synthetic latex particles result from a general phenomenon somehow absent from the standard model.

ACKNOWLEDGMENTS

This work was supported by NASA's Microgravity Science and Applications Division, the Xerox Corp., and a grant from the Shell Foundation. We are indebted to L. A. Rosen and A. B. Eidsath for their assistance with the experiments.

REFERENCES

1. Van der Put, A. G., and Bijsterbosch, B. H., *J. Colloid Interface Sci.* **75,** 512 (1980).
2. Van der Put, A. G., and Bijsterbosch, B. H., *J. Colloid Interface Sci.* **92,** 499 (1983).
3. O'Brien, R. W., and Perrins, W. T., *J. Colloid Interface Sci.* **99,** 20 (1984).
4. Zukoski, C. F., IV, and Saville, D. A., *J. Colloid Interface Sci.* **107,** 322 (1985).
5. Myers, D. F., and Saville, D. A., *J. Colloid Interface Sci.* **131,** 448 (1989).
6. Homola, J., and James, R. O., *J. Colloid Interface Sci.* **59,** 123 (1977).
7. Harding, I. H., and Healy, T. W., *J. Colloid Interface Sci.* **89,** 185 (1982).
8. O'Brien, R. W., and White, L. R., *J. Chem. Soc. Faraday Trans. 2* **74,** 1607 (1978).
9. Saville, D. A., *J. Colloid Interface Sci.* **91,** 34 (1983).
10. DeLacey, E. H. B., and White, L. R., *J. Chem. Soc. Faraday Trans. 2* **77,** 2007 (1981).
11. Maxwell, J. C., "A Treatise on Electricity and Magnetism." Oxford Univ. Press, London/New York, 1873.
12. Wagner, K. W., *Arch. Electrotech.* **3,** 83 (1914).
13. O'Konski, C. T., *J. Phys. Chem.* **64,** 605 (1960).
14. Schwartz, G. J., *Phys. Chem.* **66,** 2636 (1962).
15. Schurr, J. M., *J. Phys. Chem.* **68,** 2407 (1964).
16. Dukhin, S. S., and Shilov, V. N., "Dielectric Phenomena and the Double-Layer in Disperse Systems and Electrolytes." Wiley, New York, 1974.
17. O'Brien, R. W., *Adv. Colloid Interface Sci.* **16,** 281 (1982).
18. Zukoski, C. F., IV, and Saville, D. A., *J. Colloid Interface Sci.* **114,** 32 (1986).
19. Lyklema, J., Springer, M. M., Shilov, V. N., and Dukhin, S. S., *J. Electroanal. Chem.* **198,** 19 (1986).
20. Israelachvili, J. N., "Intermolecular and Surface Forces." Academic Press, New York, 1985.
21. Springer, M. M., Korteweg, A., and Lyklema, J., *J. Electroanal. Chem.* **153,** 53 (1983).
22. Lim, K.-H., and Franses, E. I., *J. Colloid Interface Sci.* **110,** 201 (1986).

DIELECTRIC SPECTROSCOPY OF COLLOIDAL DISPERSIONS:

COMPARISONS BETWEEN EXPERIMENT AND THEORY

L. A. Rosen and D. A. Saville

Department of Chemical Engineering

Princeton University

Princeton NJ 08544

February 7, 1990

ABSTRACT

Recent developments in theory and instrumentation have contributed to renewed interest in the dielectric properties of colloidal dispersions. One reason for the renewed interest is that dielectric measurements appear to be more sensitive to characteristics of the particle surface than conventional electrophoretic mobility measurements. However, the amount of data on well-characterized systems is small and it is premature to generalize. To broaden the data base, two different types of colloidal particles were studied: an amphoteric polystyrene latex and colloidal silica. In both cases, the dielectric response was found to differ from that predicted with the standard electrokinetic theory using ζ–potentials measured electrophoretically. The dielectric constant of the latex suspensions exceeded the theoretical prediction by an order of magnitude or more. At the same time, the characteristic relaxation frequencies were consistently lower than the theoretical. Experiments with silica dispersions yielded smaller dielectric constants than those found with the latex and the disagreements between theory and experiment were less. The results also indicate that dielectric spectroscopy is sensitive to characteristics of the dispersion other than the particle size and the ionic composition of the suspending electrolyte.

INTRODUCTION

The electrostatic state of colloidal particles is often characterized by a single quantity, the ζ–potential. However, for polystyrene latices this parameterization can be ambiguous since ζ–potentials measured by different techniques often disagree[1-3]. This is indicative of a fundamental problem since the classical electrokinetic theory[4–6] is used to interpret the measurement in each study. It has been suggested that the inconsistency in the ζ–potential results from disregarding processes occurring on the particle surface[7]. Before this hypothesis can be tested comprehensively, techniques need to be developed which yield more information per experiment than mobility or static conductivity measurements. Dielectric spectroscopy offers an intriguing possibility, but our experience with well-characterized suspensions is small. The purpose of this work is to increase our understanding of the dielectric behavior of model dispersions.

Dielectric spectroscopy yields much more information than static measurements of mobility or conductivity due to the presence of dielectric relaxation at frequencies below 100 kHz[8,9]. This relaxation is of particular interest since it arises from the temporal behavior of transport processes which polarize the electrical double layer[10]. The effects due to diffuse layer transport are included in the classical electrokinetic theory[4,11], and predictions for the dielectric constant and the conductivity are available as a function of frequency. Thus, given the particle size, the ζ–potential, and the electrolyte composition, experimental results can be compared with the theory.

Previous measurements of dielectric spectra for anionic latices[9,12] and an amphoteric latex in the cationic form[13] reveal that the low-frequency dielectric constant is substantially larger than the classical theory predicts. Furthermore, increasing the ζ–potential to values much greater than those inferred from the electrophoretic mobility does little to improve matters[13]. Evidently, the small, systematic discrepancies in the static-field experiments[1-3] are greatly amplified in measurements of the low-frequency electrical response. In this paper, we present results for positively-charged polystyrene particles and negatively-charged silica spheres. The objectives are to examine the effect of the counterion on the suspension's electrical response, and to expand the experimental database in anticipation of future modelling work. Measurements of the normalized frequency-difference spectra are

reported for latex in two different electrolytes (HCl, HNO_3) with $4 < a\kappa < 12$. Electrophoretic mobilities were measured to facilitate a comparison of the dielectric data with the classical electrokinetic theory. It is found, once again, that the magnitude of the relaxation is much larger than expected by the theory, and that the characteristic relaxation frequency is lower than the theory predicts. The dielectric response for the silica systems differs markedly from that of the latex, suggesting that the electrical properties of colloidal suspensions are sensitive to the specific nature of the particle surface.

EXPERIMENTAL

Amphoteric Latex

An amphoteric polystyrene latex was synthesized according to the procedure of Homola and James[14], using the modification discussed by Harding and Healy[15]. The amphoteric (or zwitterionic) latex possesses amidine and carboxyl groups which give rise to a pH-dependent surface charge. Based on the synthesis recipe, the predicted isoelectric pH of the latex is approximately 5.4. For our experiments, the latex was in the cationic form.

The latex was cleaned by sedimentation/decantation in a Beckman Model L5-65 ultracentrifuge with a Type 21 rotor. Dilute hydrochloric acid was used initially as the suspension medium, followed by the electrolyte to be employed in the electrokinetic experiments. Approximately twelve cycles were required to remove residual ionic impurities. The cleanliness of the latex was assured by requiring that the decanted supernatant conductivity be constant to within 1% of the conductivity of the wash electrolyte. Experiments were carried out in sequences of increasing ionic strength, beginning with 0.1mM HCl and culminating with 1mM HCl. Latex equilibrated in 0.1mM HCl was used as the starting point for the nitric acid experiments, beginning with 0.1mM HNO_3.

Particle size and monodispersity were determined by transmission electron microscopy. The magnification was calibrated with latex standards of known diameter (Interfacial Dynamics, Portland OR). The latex had a mean diameter of 226 nm with a coefficient of variation of 3.0%.

Electrophoretic mobilities were measured with a PenKem 3000 Instrument. The HCl samples inexplicably showed two peaks corresponding to small positive and negative mobilities (< 1 μm-cm/volt-sec in absolute magnitude), suggesting that those samples were somehow contaminated. The HNO_3 samples had uniformly large positive mobilities (> 4 μm-cm/volt-sec) which were comparable to those measured previously for a similar latex[13]. Accordingly, we used the HNO_3 mobility data in the comparisons with theory. Mobilities for the HNO_3 samples (Table I) were converted into ζ–potentials using the computer program of O'Brien and White[4].

Silica

Colloidal silica furnished by E. Matijevic was prepared according to the method of Stober et al.[16] with a proprietary modification used to synthesize large quantities of material[17]. The particles were aged in dilute electrolyte for approximately two months, whereupon the pH was adjusted to 4.0 with 0.1M HCl. The dispersion was equilibrated at the desired pH and ionic strength by sedimentation/decantation, using six wash cycles over roughly a two week period until the conductivity and pH of the supernatant were constant. Once again, dielectric spectroscopy measurements were made in an order of increasing ionic strength.

The mean particle diameter was 330 nm with a coefficient of variation of 7.2% according to transmission electron microscopy. Zero-field electrophoretic light scattering with the Coulter DELSA 440 instrument provided a rough estimate of the mean diameter, 300 nm < $\bar{d}$ < 350 nm.

Electrophoretic mobilities were measured with the Coulter DELSA 440 (Table I). ζ–potentials were obtained from the measured mobilities using the computer program of O'Brien and White[4].

Dielectric Spectroscopy

The dielectric and conductivity spectra were measured with the dielectric spectrometer of Myers and Saville[18] operated at a reference frequency of 500 Hz. The instrument calibration and operating procedures are described in previous publications[18,19]. Note that the use of a four-electrode cell eliminates complications due to electrode polarization[20]. The spectrometer's electronic drift

compensation system effectively controls the temperature to within $0.0001^{o}C$[18]. The absolute temperature inside the cell was maintained at $25.0 \pm 0.1^{o}C$ by a control system which employs thin film heaters (Minco, Minneapolis, MN) and a refrigerated air stream[21]. The low-frequency conductivity, which is needed in the data analysis[18], was measured using an Altex conductivity bridge (Beckman) operated at 85 Hz.

Dielectric constant and conductivity spectra for each suspension were determined at three volume fractions for the latex and four volume fractions in the silica experiments. After measuring the electrical response at a given volume fraction, a small amount of suspension was withdrawn from the cell and saved for a gravimetric determination. The colloidal material removed was replaced with the same volume of pure electrolyte yielding a suspension of lower particle concentration. Densities for polystyrene and silica were taken to be 1.057 and 1.8, respectively. Typical particle concentrations were 2-6% by volume. The reproducibility of the gravimetric determination was $\pm 1.0 \times 10^{-4}$ volume fraction units.

RESULTS AND DISCUSSION

Dielectric Spectroscopy

The dielectric constant ε and the specific conductivity σ were measured over the frequency range 0.5-200 kHz. The dielectric spectrometer is designed to measure the electrical properties as normalized frequency-difference functions, or

$$[\varepsilon(f,\phi) - \varepsilon_r]/\phi \ , [\sigma(f,\phi) - \sigma_r]/\phi \ . \qquad (1)$$

Here f is the linear frequency in Hz, ϕ is the particle volume fraction, and the subscript r identifies quantities measured at the reference frequency, i.e. $\sigma_r = \sigma(f_r,\phi)$. The frequency-difference functions represent the change in the electrical properties relative to their values at the reference frequency, divided by the particle volume fraction. By subtracting the signals at the reference frequency, the frequency-difference functions eliminate the frequency-independent contribution of the background electrolyte, thereby increasing the signal-to-noise ratio of the measurement[18]. For dilute suspensions,

the normalized frequency-difference functions are independent of ϕ to the extent that particle-particle interactions are negligible.

We begin by describing the behavior of a representative system in detail, to illustrate the relationship between the specific electrical properties and the related normalized frequency-difference functions. Figure 1a shows the dielectric constant (or relative permittivity) for the amphoteric latex in 0.2mM HNO_3 at three volume fractions, along with the pure electrolyte ($\phi = 0$) spectrum. At frequencies below 2kHz, ε varies slowly with frequency, as the field-induced polarization remains in phase with the oscillating electric field. In the frequency range 2-20 kHz, ε drops sharply, a phenomenon known as dielectric relaxation. This behavior is due to the relaxation time associated with the polarization response, which is comparable to the period of oscillation in this intermediate frequency range. At high frequencies, the polarization is unable to keep pace with the applied field, so the suspension dielectric constant approaches the value characteristic of the pure electrolyte (about 78 at 25°C).

The normalized frequency-difference of the dielectric constant is displayed in Fig. 1b. The normalized difference spectra superimpose, indicating that the change in the dielectric constant relative to the reference frequency is a linear function of particle volume fraction[18,19]. This implies that particle-particle interactions do not significantly influence the dielectric response, so the results can be interpreted using the existing dilute suspension theory.

The behavior of the suspension conductivity is shown in Fig. 2a. Since all experiments were performed at 25°C, the separation between the data at different volume fractions is due to the electrical characteristics of the particles, rather than changes in the absolute temperature of the suspensions. It is clear from the data that the conductivity, in contrast to the dielectric constant, is a relatively weak function of frequency. Figure 2b shows the normalized conductivity difference spectra. Once again the data sets superimpose, with the exception of the results at 200 kHz. The deviations observed at high frequencies are systematic and appear to reflect an electronic limitation of the current spectrometer configuration. Consequently, in the results for latex which follow we report the conductivity spectra only up to 50 kHz.

Figures 3 and 4 summarize the electrical response for the amphoteric latex in HCl and HNO_3 solutions. The spectra are averages of measurements made at three volume fractions as described above and the standard deviation associated with each data point is typically 1-5%. Here, the dominant feature is the sensitivity to changes in the electrolyte concentration. The normalized frequency-difference spectra increase by nearly an order of magnitude as the ionic strength is elevated from 0.1mM to 1mM. The data for HCl and HNO_3 suspensions are remarkably similar, especially at the lower ionic strengths. Only at 1mM ionic strength are significant differences in the relaxation magnitude evident. Calculation of the dielectric loss from the measured conductivity differences[11,12] shows that the relaxation is centered between 5-7 kHz, and that the central frequency is essentially independent of electrolyte concentration.

Figures 5 and 6 are the normalized frequency-difference spectra for the silica/HCl dispersions. The relaxation is much smaller than that observed in the latex experiments. For example, the magnitude of the normalized dielectric difference at 200 kHz is only 600 for silica in 0.2mM HCl, compared to 11,000 for the latex under the same conditions. This means that the dielectric constant of a 1% silica dispersion changes by only 6 units over the entire frequency range. This decrease in relaxation magnitude increases the relative error in the frequency-difference functions, making it more difficult to measure the response accurately. The standard deviation of the frequency-difference data is 4-15% of the reported averages. Errors in the conductivity were larger at frequencies above 20 kHz. The signal-to-noise problem was especially severe in the dielectric measurements for 0.5mM HCl/silica at low frequencies. The small change in the dielectric constant below 7 kHz for this sample could not be resolved with sufficient accuracy; hence the data in Fig. 5 spans the frequency range 7-200 kHz.

These results show that particles of comparable size in the same suspension medium can exhibit completely different electrical behavior. According to the classical electrokinetic theory, measurements of the ζ–potential should specify the electrical response of a dispersion given the particle size and the ionic composition of the bathing electrolyte. In the next section, the relationship between the dielectric relaxation data and the measured mobilities (and ζ–potentials) is discussed.

Electrophoresis

Since the surface charge of amphoteric particles depends on $[H^+]$, it is possible that part of the ionic strength sensitivity revealed in the dielectric measurements results from an increase in the surface charge. Unfortunately, it is difficult to deduce the behavior of the surface charge from the electrophoretic mobility data (Table I). The mobility in 0.1mM HNO_3 slightly exceeds the theoretical mobility maximum[4], so the potential at that maximum was used to estimate ζ. The measured mobilities at higher ionic strength fall short of the maxima, however the mobility-ζ function is quite flat for these systems[4] so there is considerable uncertainty (*ca.* 15%) in the value of ζ. Even if ζ were known unambiguously, the relationship between ζ and the surface charge needs to be specified. In general the electrokinetic charge differs from the surface charge due to ion localization inside the shear surface[22]. The structure of the region inside the shear surface is not well understood, and in fact it has been suggested that the location of the shear surface in latex systems may depend on the ionic strength[23,24]. In view of these difficulties, it is not possible to state whether the surface charge is constant over the pH range of the measurements. Nevertheless, the contrast between the relatively constant ζ–potentials and the large increases in the frequency-difference spectra with ionic strength is quite striking.

Silica is negatively charged for $3.3 < pH < 4$; the point of zero charge is nominally at pH ~ 2.5[22]. Both the decrease in charge and the compression of the double layer as the pH is lowered tend to suppress the mobility, as demonstrated by the data in Table I. Here, in contrast to the latex experiments, the behavior of the ζ–potential appears to be consistent with the behavior of the specific electrical properties: both ζ and the frequency-difference spectra decrease as the pH is lowered.

In the following section, the measured ζ–potentials will be used to compare the dielectric relaxation data with predictions from the classical electrokinetic theory.

COMPARISON BETWEEN THEORY AND EXPERIMENT

Information obtained from electrokinetic experiments is generally interpreted using a model which specifies the relationship between a measurable quantity and an intrinsic property of the colloidal dispersion. For example, measurements of the electrophoretic mobility are used to estimate the

electrokinetic charge or ζ–potential derived from the classical electrokinetic theory. The interpretation of bulk measurements is more complicated since the behavior results from the influence of a large number of particles and their associated double layers. If the suspension is not too concentrated and the ionic strength is not too low, then the double layers of neighboring particles will not interact significantly and the suspension can be treated as an ensemble of isolated particles. The model used in the electrophoretic mobility problem can be adapted to calculate the bulk suspension electrical properties given a suitable procedure for averaging local current densities and electric fields.

Here, we summarize the model used to describe the response of an isolated spherical particle immersed in a dilute electrolyte in the presence of an externally applied electric field[4-6,11,25]. For alternating applied currents, it is assumed that the time dependence can be represented by sinusoidal functions. The essential problem is to compute the field-induced perturbations in the equilibrium potential and ion distributions. If the external field is small in comparison to the electric field present in the equilibrium double layer, the problem can be attacked by constructing perturbation expansions in the dimensionless applied field. The basic equations are Poisson's equation for the distribution of electrical potential, the Stokes equations with an electrical body force for the low Reynolds number incompressible fluid motion, and conservation equations for the transport of mass and ionic species. The constitutive relations for the ion fluxes include the effects of convection, diffusion, and electromigration. The specification of boundary conditions completes the mathematical description of the problem. Far away from the charged surface, the fluid velocity tends to zero, the electric field is uniform and equal to the applied field, and the ion concentrations approach their bulk values. At the surface, the no-slip condition is assumed, the charge is taken to be constant, and the normal flux of ions into the particle is identically zero.

The electrokinetic equations have been solved numerically by O'Brien and White[4] for the single particle electrophoretic mobility and by DeLacey and White[11] to predict the electrical response of a dilute suspension. These are the most comprehensive treatments of the classical theory available, and are not limited to thin double layers or small surface potentials. Accordingly, results from the O'Brien-

White and DeLacey-White methodologies will be used in the comparisons between theory and experiment.

The procedure for comparing the experimental data to the theoretical predictions is as follows. The measured electrophoretic mobility is converted into its equivalent ζ–potential using the computer program of O'Brien and White. Using this ζ–potential in the DeLacey and White computer program yields predictions for the bulk suspension electrical properties as a function of frequency. The results of the computation are the coefficients in the density expansions

$$\varepsilon(f,\phi) = \varepsilon(f,0) + \Delta\varepsilon'(f)\,\phi + \ldots$$
$$\sigma(f,\phi) = \sigma(f,0) + \Delta K^{eff}(f)\,\phi + \ldots \quad , \tag{2}$$

correct to $O(\phi)$. Here, $\varepsilon(f,0)$ and $\sigma(f,0)$ are the specific electrical properties of the pure electrolyte. The functions $\Delta\varepsilon'$and ΔK^{eff} represent the increment in the electrical properties due to the particles and are directly related to the measured frequency-difference functions:

$$[\varepsilon(f,\phi) - \varepsilon_r]/\phi = \Delta\varepsilon'(f) - \Delta\varepsilon'(f_r)$$
$$[\sigma(f,\phi) - \sigma_r]/\phi = \Delta K^{eff}(f) - \Delta K^{eff}(f_r)\ . \tag{3}$$

The normalized frequency-difference functions are equal to the frequency-difference of DeLacey and White's Δ-functions. Thus, measurements of the normalized frequency-difference spectra are referenced to calculated frequency-difference functions based on ζ–potentials obtained from electrophoresis. This procedure provides a critical test of the electrokinetic theory, since the theories for the mobility and the electrical response are self-consistent.

Figure 7 illustrates the comparison for amphoteric latex/HNO_3 dispersions at two ionic strengths. Theoretical predictions using ζ = 111 mV for 0.2mM HNO_3 and ζ = 98 mV for 1 mM HNO_3 are displayed

with data taken from Fig. 3. It is obvious that there is a substantial disagreement between the measured and calculated dielectric difference spectra. The magnitude of the relaxation response is much larger than predicted, especially at the highest ionic strength. Moreover, the relaxation is centered at frequencies well below the 30-40 kHz range predicted by the theory. The conductivity-difference data exhibits similar discrepancies between theory and experiment.

It may be shown that these discrepancies cannot be eliminated by increasing the value of the ζ-potential or the effective particle size[13]. For example, increasing the ζ-potential to a value of 250 mV for latex in 1 mM HNO_3 yields an estimate of 9,000 for the magnitude of the normalized dielectric difference at 200 kHz, far less than the value of 44,000 observed experimentally. Such a large value for ζ is exceedingly improbable. Furthermore, treating ζ as an adjustable parameter does not address the discrepancy in the relaxation frequency, which is another distinct feature of the experimental data.

Similar discrepancies have been observed in previous studies with latices[9,12,13] synthesized by a variety of surfactant-free emulsion polymerization recipes. Several carefully calibrated measurement techniques have been applied, and it is unlikely that all of these approaches could contain systematic errors large enough to explain the discrepancies. Moreover, the theory has been checked by an approximate analytical solution valid in the limit of small ζ-potentials (< 50 mV), and the agreement is satisfactory[25]. In the absence of an obvious problem with either the experiments or the theory, the results rekindle questions about the suitability of polymer colloids as model systems for studies of electrokinetic phenomena. Given the dearth of published data on the dielectric relaxation of inorganic colloids, it seemed prudent to begin to investigate whether the discrepancies observed with latices occur with other colloidal systems as well.

The comparison for the silica dispersions is shown in Fig. 8. The relatively small relaxation noted in Figs. 5 and 6 results in much improved agreement between the measured values and the theoretical predictions. For the 0.5mM HCl/silica data set, agreement between experiment and theory is rather good at high frequencies. Discrepancies become apparent as the ionic strength is lowered, coincident with increases in the measured ζ-potentials. Still, the experiment and theory are of the same order of magnitude, so that relatively small increases in the ζ-potentials will improve the agreement. Analysis

of the conductivity-difference data shows that there remains a discrepancy in the characteristic frequency, which is centered at ~5 kHz in the experiments, and between 10-20 kHz according to the theory. The origin of this discrepancy is not understood, and remains a subject for future study.

CONCLUSIONS

The results of this investigation confirm earlier studies[9,12,13] which identified large discrepancies between theory and experiment for polymer latices. The electrical response of amphoteric latex is shown to be a sensitive function of the electrolyte concentration, and is virtually independent of the counterion for HCl and HNO_3. The strong concentration dependence of ϵ is not reflected in the electrophoretic mobilities, which depend only moderately on the ionic strength. Furthermore, dielectric spectra calculated using ζ–potentials inferred from electrophoretic mobility disagree with the measured frequency-difference spectra. The theory does better with silica, which exhibits only a small enhancement in the electrical properties for the dilute dispersions at low pH. More experiments at higher pH and in different electrolytes are needed to ascertain whether this behavior is typical for silica. Dielectric spectroscopy appears to be sensitive to factors other than the particle size and the ionic strength, as demonstrated by the disparate behavior of latex and silica under the same conditions.

ACKNOWLEDGEMENTS

We are indebted A. B. Eidsath for synthesizing the amphoteric latex, and to F. J. Micale for allowing us to use the PenKem 3000 instrument in his laboratory. E. Matijevic kindly supplied the silica and measured electrophoretic mobilities for the three silica/HCl dispersions. This work was supported by NASA's Microgravity Science and Applications Division, the Xerox Corp., and a grant from the Shell Foundation.

REFERENCES

1. Van der Put, A. G., and Bijsterbosch, B. H., *J. Colloid Interface Sci.* **75**, 512 (1980).
2. O'Brien, R. W., and Perrins, W. T., *J. Colloid Interface Sci.* **99**, 20 (1984).
3. Zukoski, C. F., IV, and Saville, D. A., *J. Colloid Interface Sci.* **107**, 322 (1985).
4. O'Brien, R. W., and White, L. R., *J. Chem. Soc. Faraday Trans.* 2 **74**, 1607 (1978).
5. O'Brien, R. W., *J. Colloid Interface Sci.* **81**, 234 (1981).
6. Saville, D. A., *J. Colloid Interface Sci.* **91**, 34 (1983).
7. Zukoski, C. F., IV, and Saville, D. A., *J. Colloid Interface Sci.* **114**, 32 and 45 (1986).
8. Schwan, H. P., Schwarz, G., Maczuk, J., and Pauly, H., *J. Phys. Chem.* **66**, 2626 (1962).
9. Springer, M. M., Korteweg, A., and Lyklema, J., *J. Electroanal. Chem.* **153**, 55 (1983).
10. Dukhin, S. S., and Shilov, V. N., "Dielectric Phenomena and the Double Layer in Disperse Systems and Polyelectrolytes." Wiley, New York, 1974.
11. DeLacey, E. H. B., and White, L. R., *J. Chem. Soc. Faraday Trans.* 2 **77**, 2007 (1981).
12. Lim, K-H., and Franses, E. I., *J. Colloid Interface Sci.* **110**, 201 (1986).
13. Myers, D. F., and Saville, D. A., *J. Colloid Interface Sci.* **131**, 461 (1989).
14. Homola, A., and James, R. O., *J. Colloid Interface Sci.* **59**, 123 (1977).
15. Harding, I. H., and Healy, T. W., *J. Colloid Interface Sci.* **89**, 185 (1982).
16. Stober, W., Fink, A., and Bohn, E., *J. Colloid Interface Sci.* **26**, 62 (1968).
17. Matijevic, E., private communication.
18. Myers, D. F., and Saville, D. A., *J. Colloid Interface Sci.* **131**, 448 (1989).
19. Myers, D. F., "Dielectric Spectroscopy of Colloidal Suspensions", Ph.D. Thesis, Princeton U., 1988.
20. Schwan, H. P., in "Physical Techniques in Biological Research", ed. W. L. Nastuk, Vol. VI. Academic Press, New York, 1963.
21. Rosen, L. A., Ph. D. Thesis, in preparation.
22. Hunter, R. J., "Zeta Potential in Colloid Science", Academic Press, New York, 1981.
23. Van der Put, A. G., and Bijsterbosch, B. H., *J. Colloid Interface Sci.* **92**, 499 (1983).
24. Van den Hoven, Th. J. J., and Bijsterbosch, B. H., *Colloids and Surfaces* **22**, 187 (1987).
25. O'Brien, R. W., *Adv. Colloid Interface Sci.* **16**, 281 (1982).

TABLE I

Electrophoretic mobilities and ζ–potentials for amphoteric latex and silica dispersions as a function of electrolyte concentration.

Amphoteric Latex:

[HNO_3]	aκ	mobility[a]	ζ–potential[b]
.0001 M	3.7	4.5	144[c]
.0002 M	5.3	4.3	111
.0005 M	8.3	4.6	125
.001 M	11.8	4.7	98

Silica:

[HCl]	aκ	mobility	ζ–potential
.0001 M	5.4	-2.4	-42
.0002 M	7.7	-2.3	-37
.0005 M	12.1	-1.7	-27

[a]Mobility units are μm-cm/volt-sec.

[b]ζ–potential units are mV.

[c]The ζ–potential at the mobility maximum, which is 4.31 micron-cm/volt sec.

FIGURE CAPTIONS

Figure 1a: Dielectric constants for an amphoteric latex in 0.2mM HNO_3 at 25°C.
● ϕ = 0.000; ◆ ϕ = 0.016; ▲ ϕ = 0.023; ■ ϕ = 0.032.

Figure 1b: Normalized dielectric difference spectra for an amphoteric latex in 0.2mM HNO_3 at 25°C.
◆ ϕ = 0.016; ▲ ϕ = 0.023; ■ ϕ = 0.032.

Figure 2a: Specific conductivities for an amphoteric latex in 0.2mM HNO_3 at 25°C.
● ϕ = 0.000; ◆ ϕ = 0.016; ▲ ϕ = 0.023; ■ ϕ = 0.032.

Figure 2b: Normalized conductivity difference spectra for an amphoteric latex in 0.2mM HNO_3 at 25°C. ◆ ϕ = 0.016; ▲ ϕ = 0.023; ■ ϕ = 0.032.

Figure 3: Normalized dielectric difference spectra for an amphoteric latex as a function of ionic strength at 25°C. Data points are averages of measurements made at three volume fractions.
● 0.1mM HNO_3; ■ 0.2mM HNO_3; ▲ 0.5mM HNO_3; ◆ 1mM HNO_3; O 0.1mM HCl; □ 0.2mM HCl; △ 0.5mM HCl; ◇ 1mM HCl.

Figure 4: Normalized conductivity difference spectra for an amphoteric latex as a function of ionic strength at 25°C. Data points are averages of measurements made at three volume fractions.
● 0.1mM HNO_3; ■ 0.2mM HNO_3; ▲ 0.5mM HNO_3; ◆ 1mM HNO_3; O 0.1mM HCl; □ 0.2mM HCl; △ 0.5mM HCl; ◇ 1mM HCl.

Figure 5: Normalized dielectric difference spectra for silica as a function of ionic strength at 25°C. Data points are averages of measurements made at four volume fractions.
■ 0.1mM HCl; ▲ 0.2mM HCl; ◆ 0.5mM HCl.

Figure 6: Normalized conductivity difference spectra for silica as a function of ionic strength at 25°C. Data points are averages of measurements made at four volume fractions.
■ 0.1mM HCl; ▲ 0.2mM HCl; ◆ 0.5mM HCl.

Figure 7: Comparison between experiment and theory for an amphoteric latex in HNO_3.
1mM HNO_3: ▲ experiment, —— theory; 0.2mM HNO_3: ■ experiment, - - - theory.

Figure 8: Comparison between experiment and theory for silica in HCl.
0.1mM HCl: ■ experiment, —— theory; 0.2mM HCl: ▲ experiment, ---- theory;
0.5mM HCl: ◆ experiment, – – theory.

Figure 1a

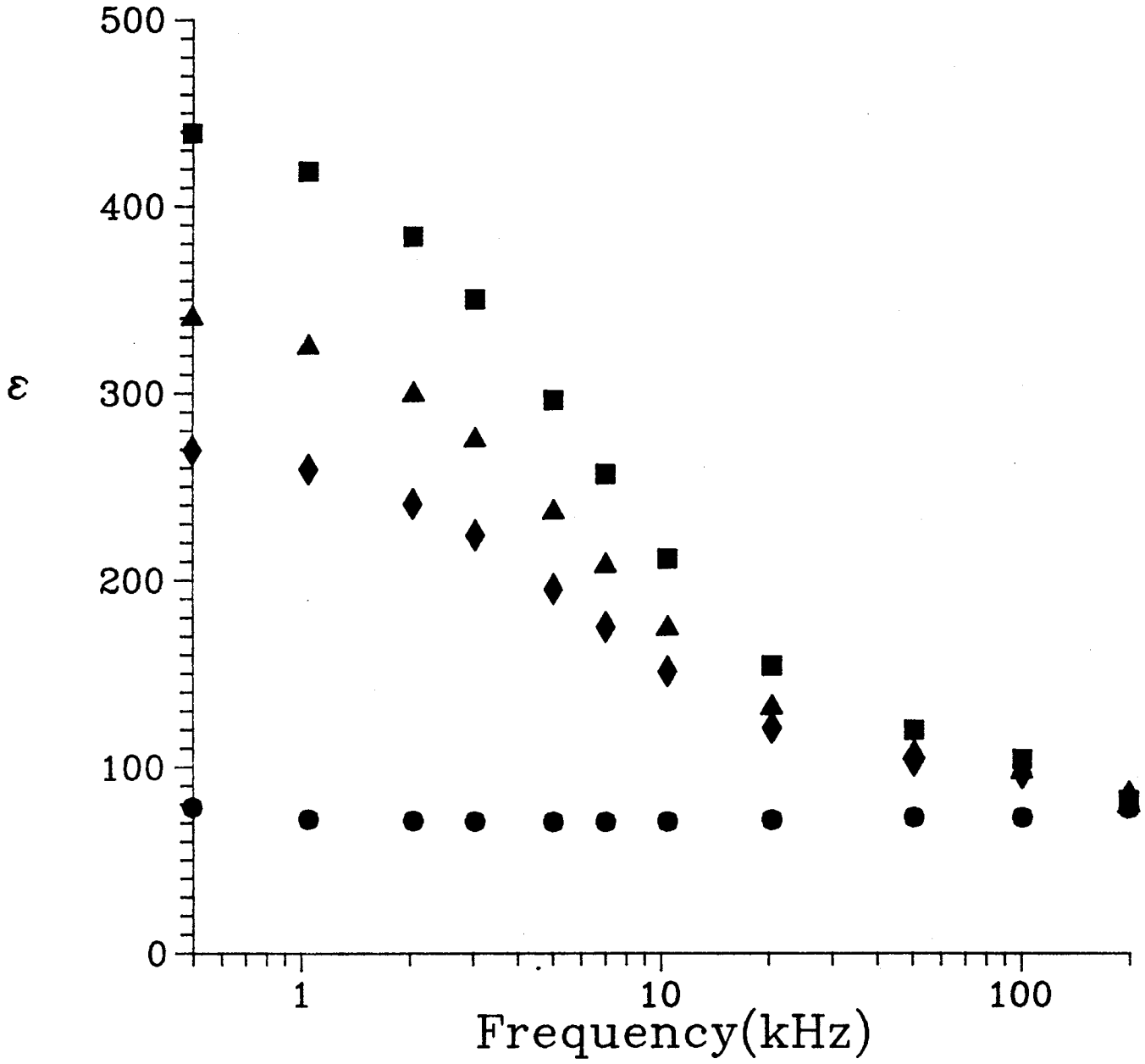

Figure 1b

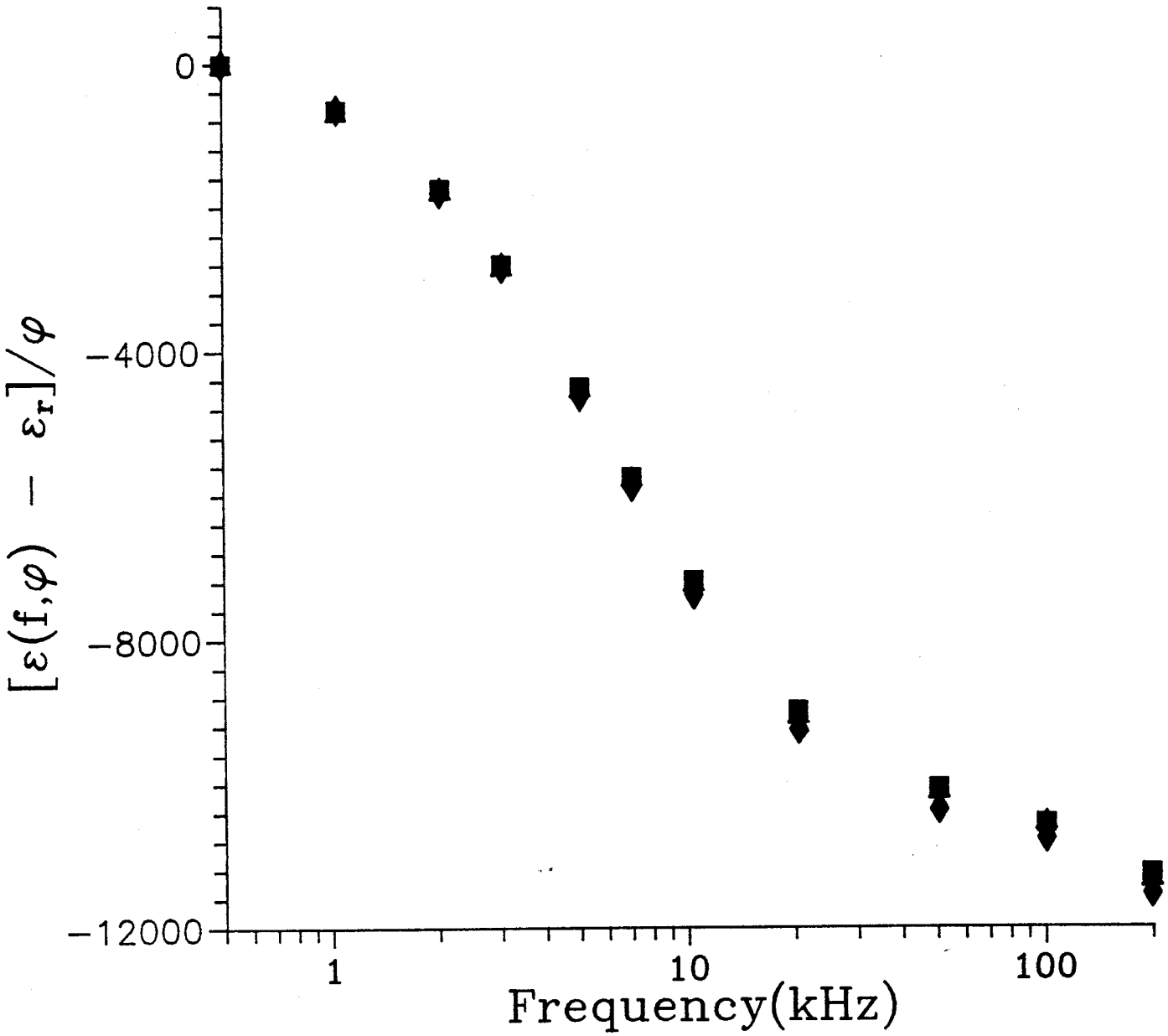

Figure 2a

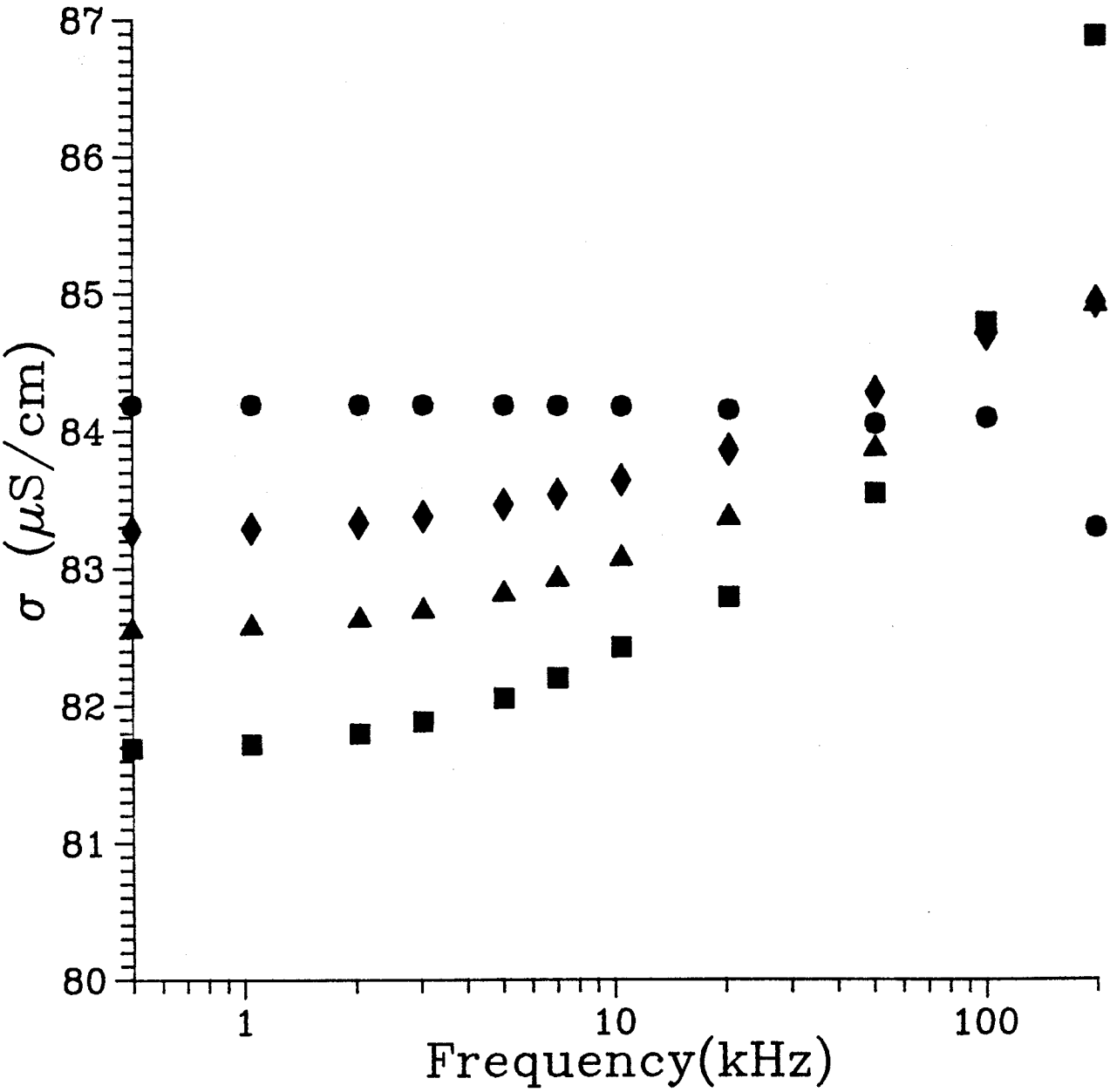

Figure 2b

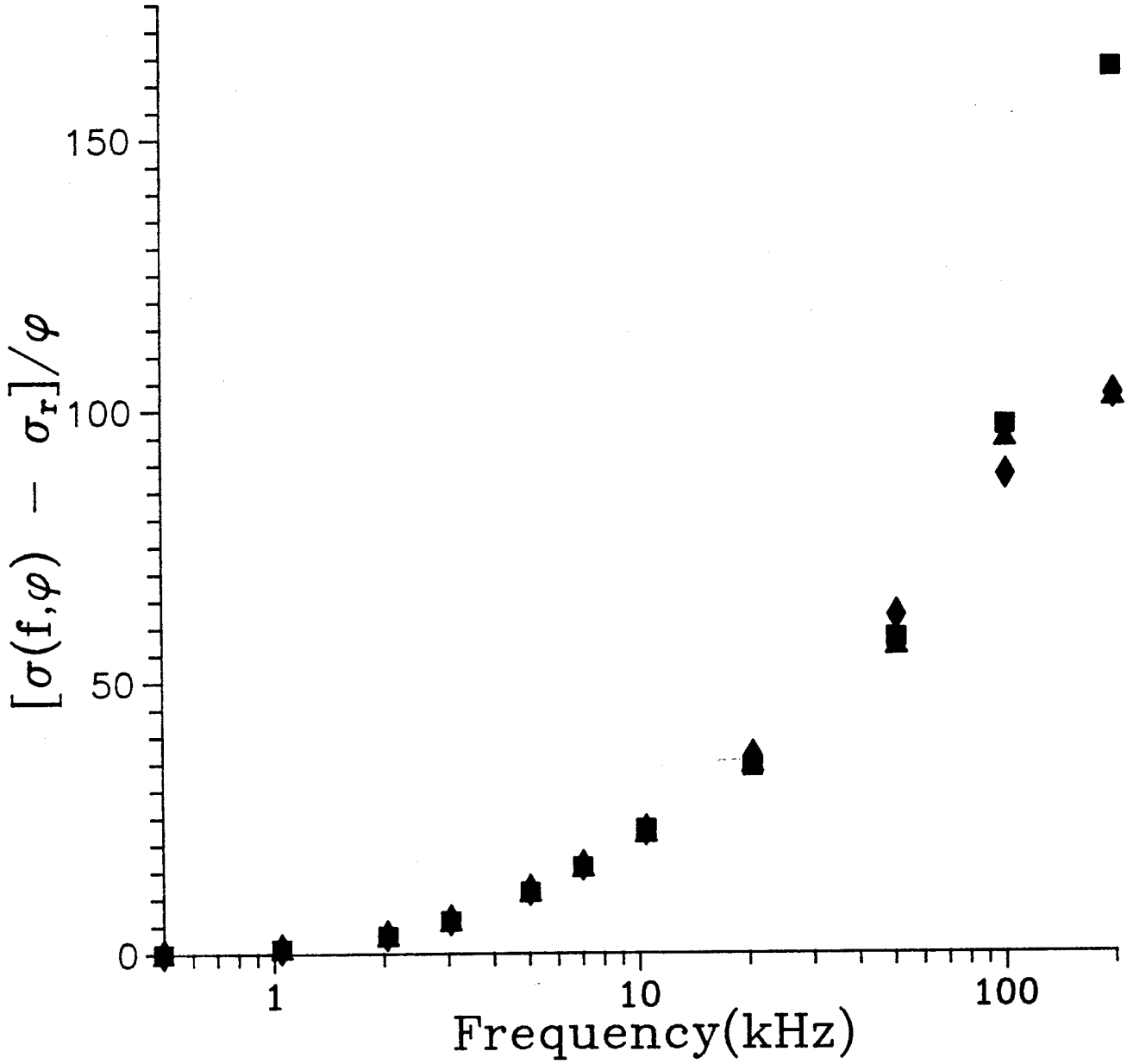
150
100
50
0
$[\sigma(f,\varphi) - \sigma_r]/\varphi$
1
10
100
Frequency(kHz)

Figure 3

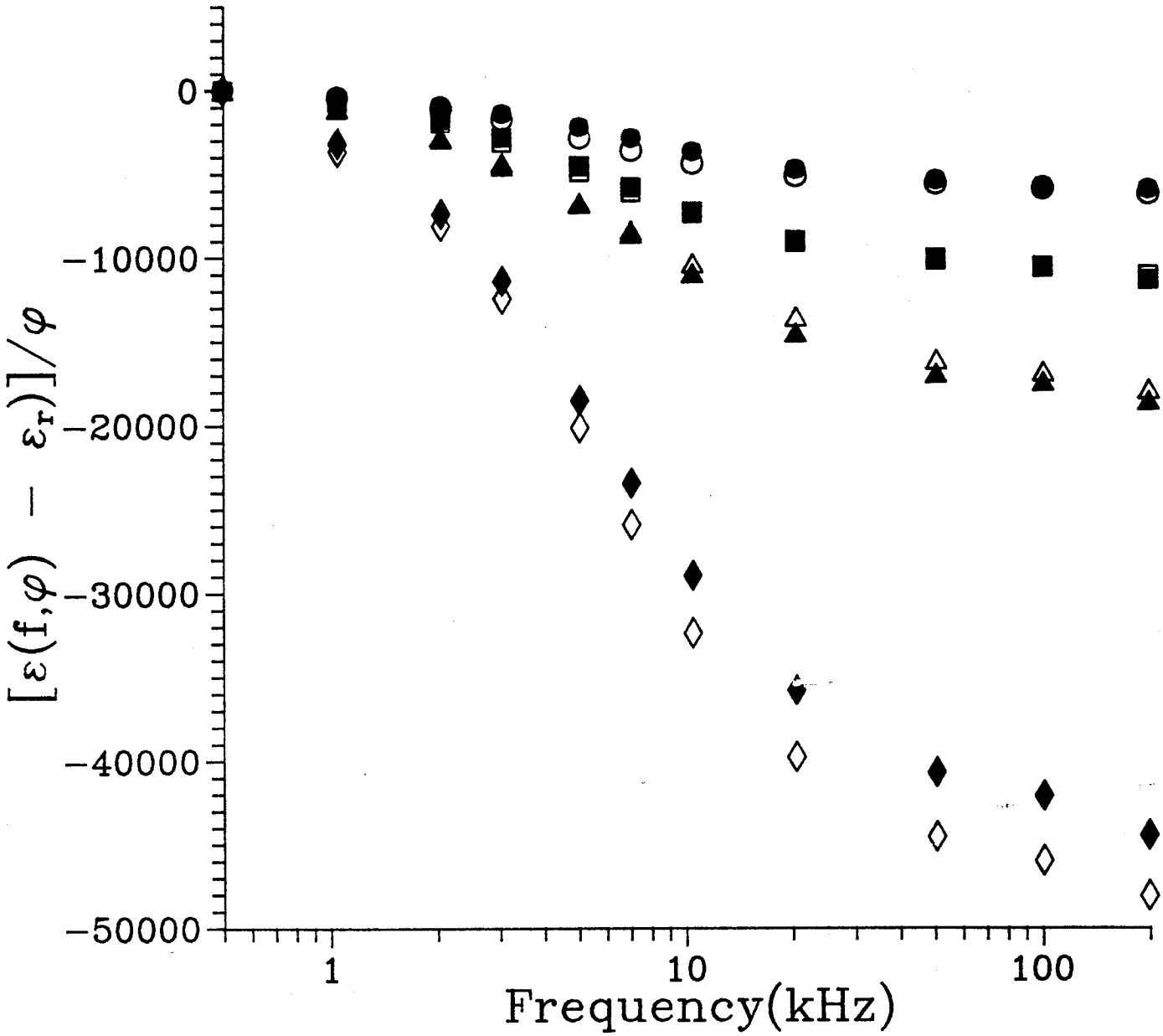
0
−10000
−20000
−30000
−40000
−50000
[ε(f,φ) − εr)]/φ
1
10
100
Frequency(kHz)

Figure 4

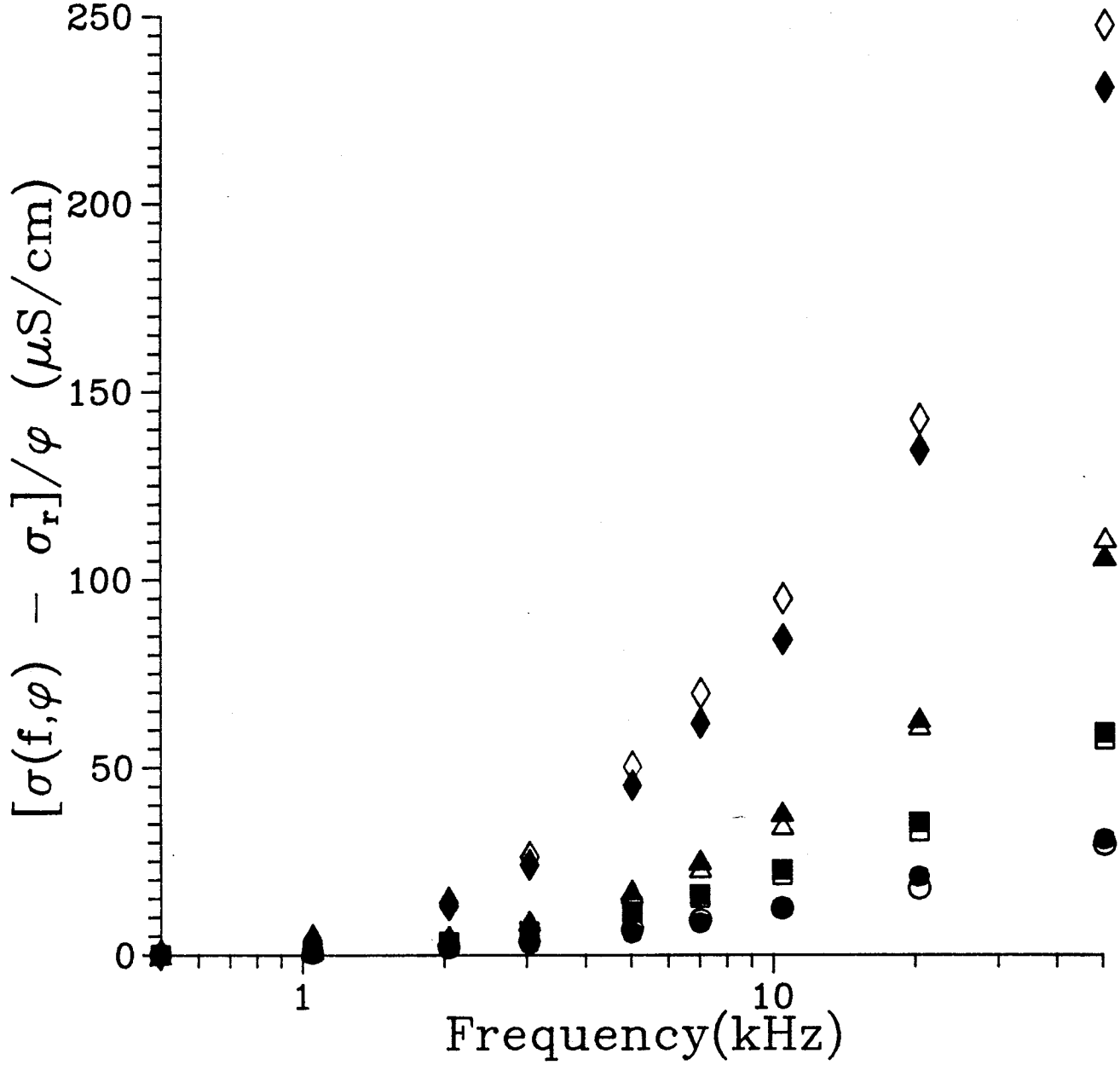
250
200
150
100
50
0
1
10
Frequency(kHz)
$[\sigma(f,\varphi) - \sigma_r]/\varphi$ (μS/cm)

Figure 5

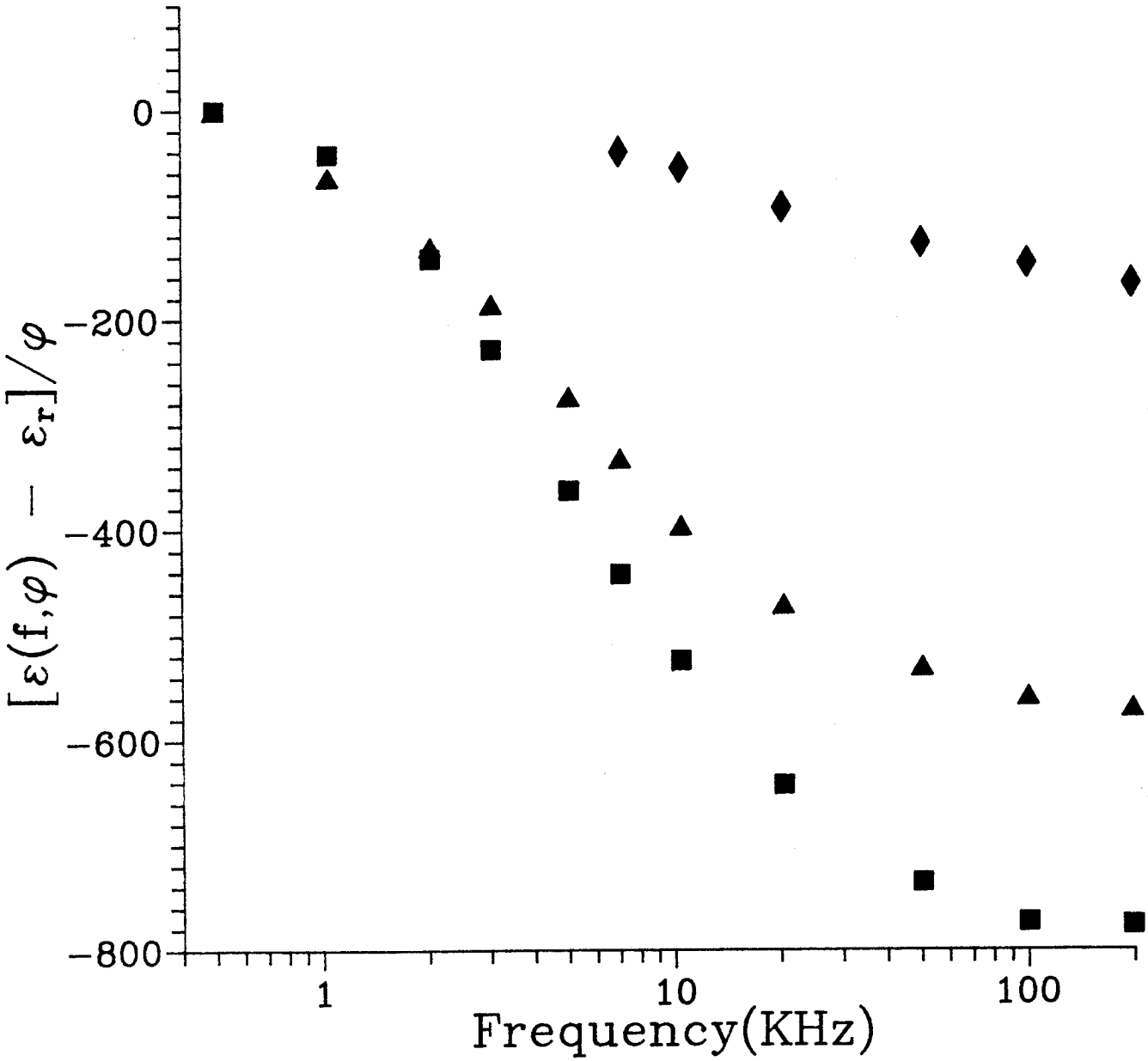

Figure 6

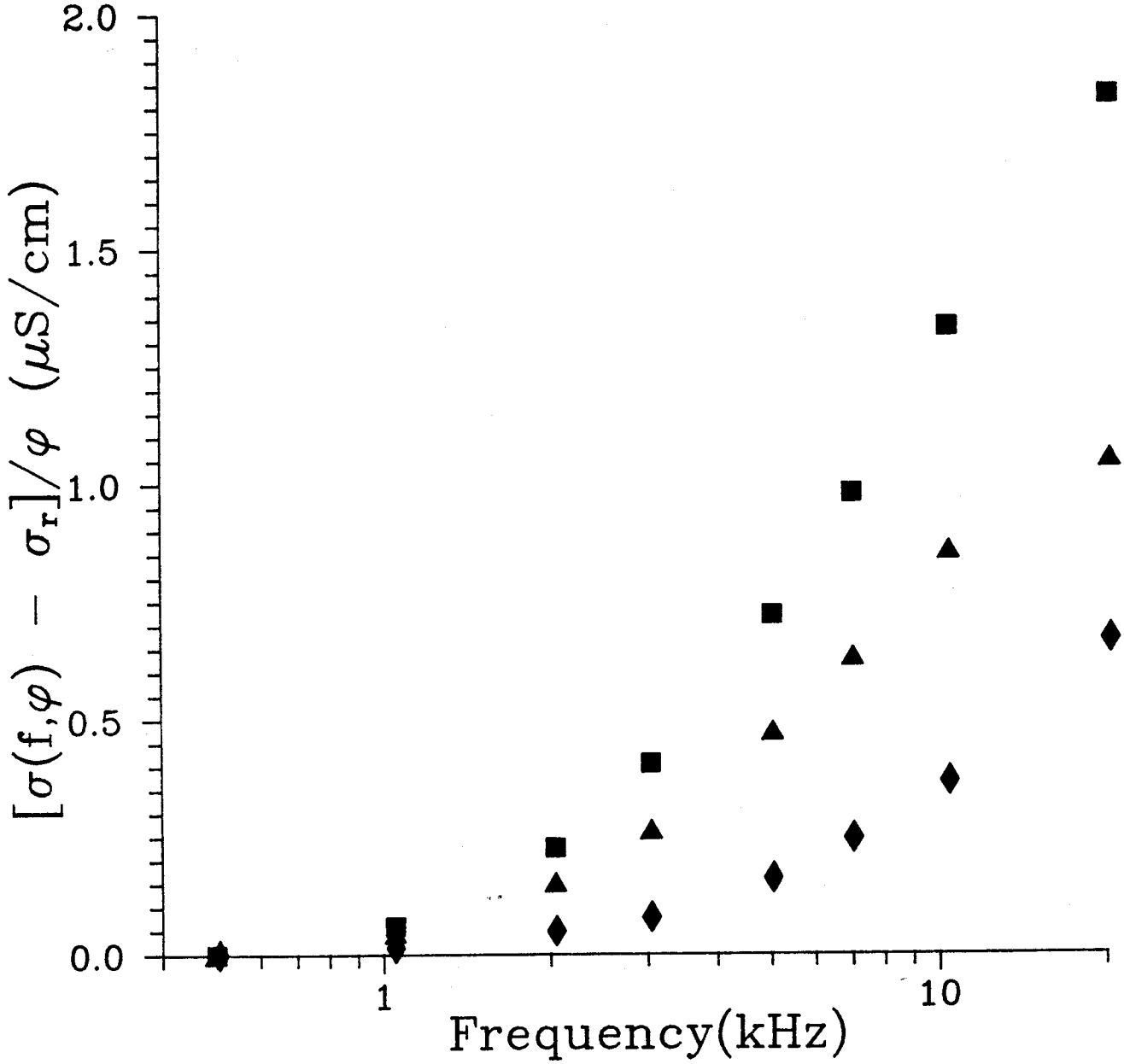
2.0
1.5
1.0
0.5
0.0
$[\sigma(f,\varphi) - \sigma_r]/\varphi$ (μS/cm)
1
10
Frequency(kHz)

Figure 7

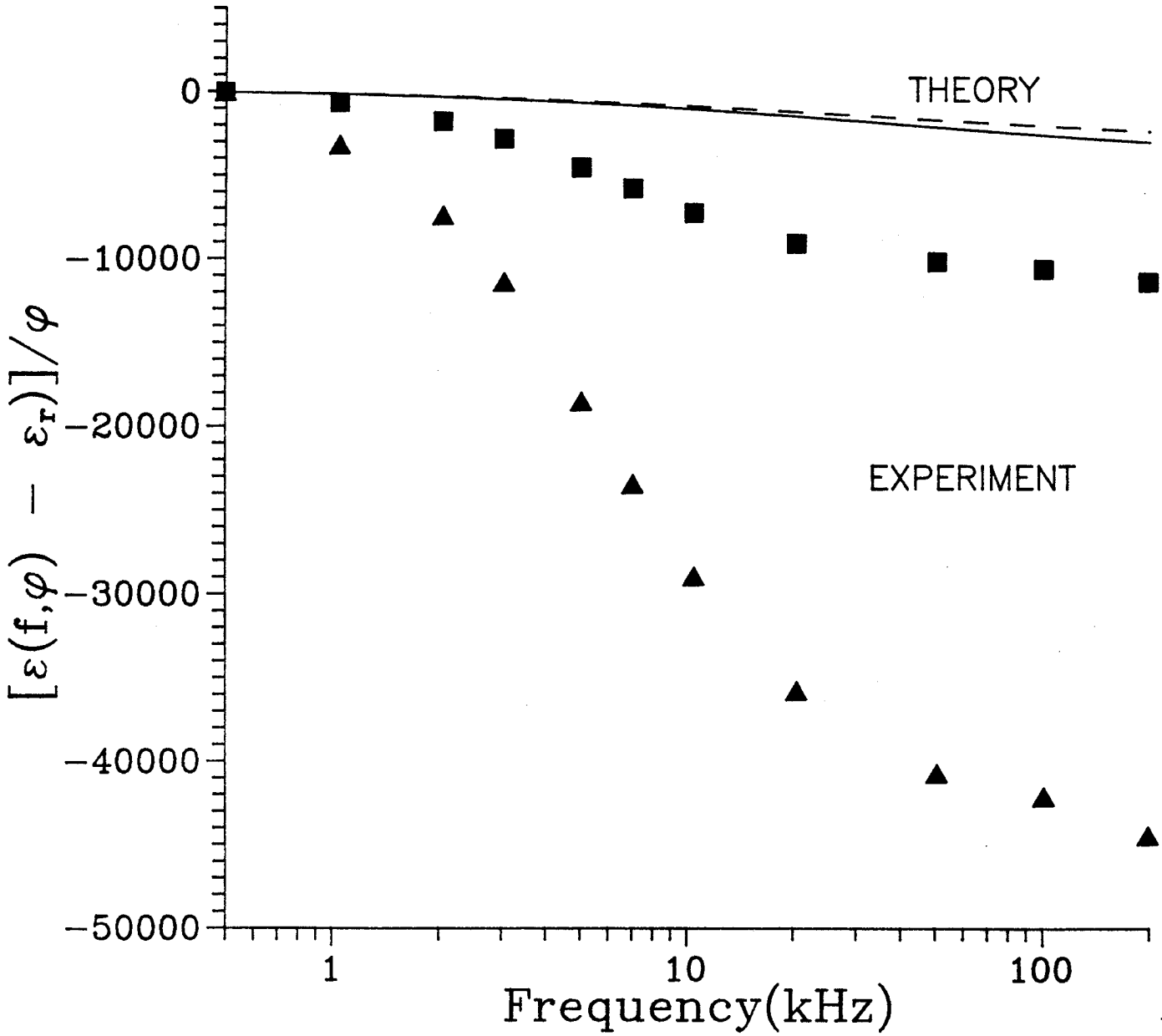
0
−10000
−20000
−30000
−40000
−50000
[ε(f,φ) − εr)]/φ
1
10
100
Frequency(kHz)
THEORY
EXPERIMENT

Figure 8

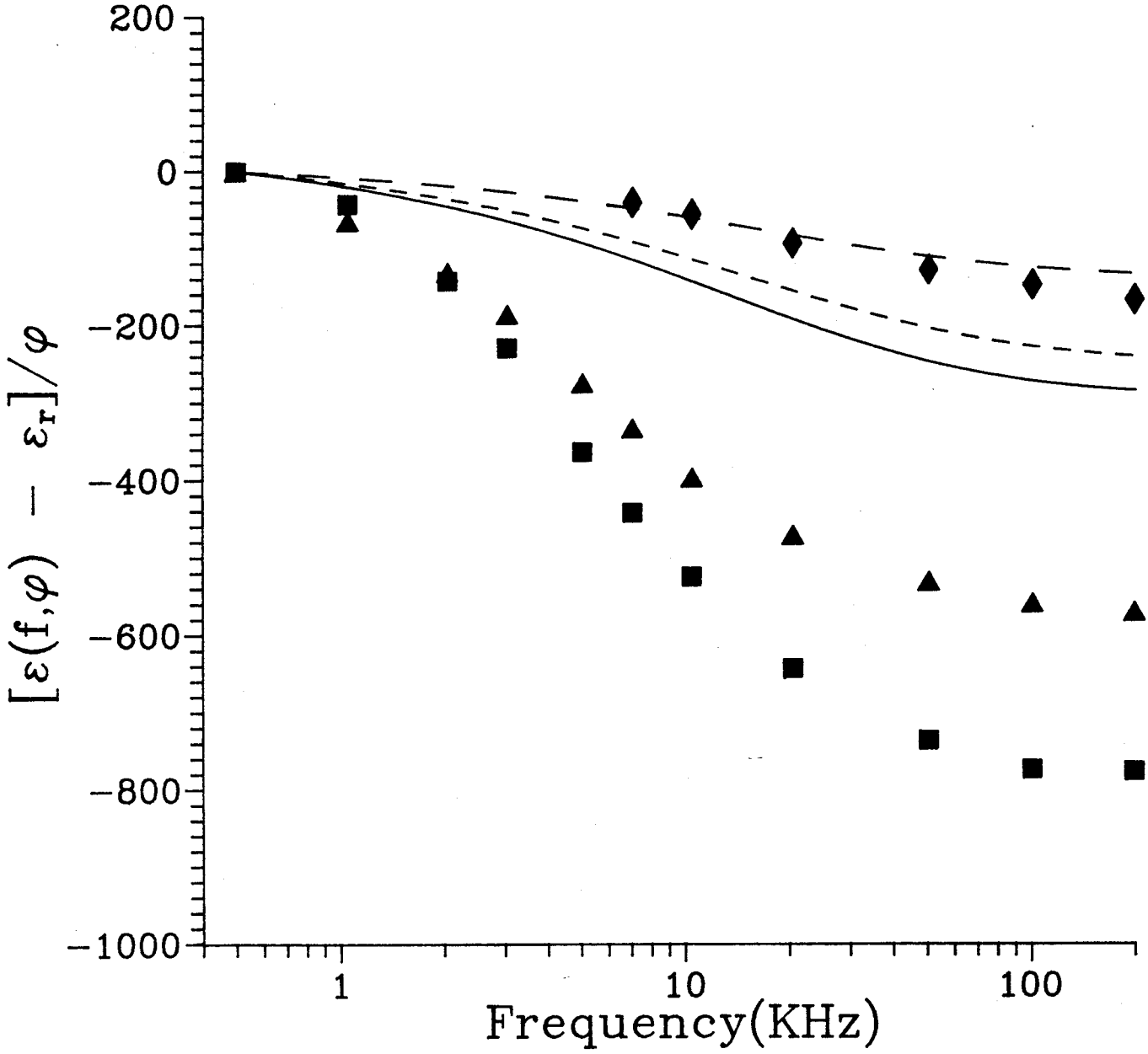

The Dielectric Response of Polystyrene Latexes: Effects of Alterations in the Structure of the Particle Surface

Manuscript #8243K-revised March 28, 1990

To appear in J. Colloid Interface Science

L. A. Rosen and D. A. Saville

Department of Chemical Engineering

Princeton University

Princeton NJ 08544

Abstract

The presence of a "hairy" layer or surface roughness has been hypothesized to explain discrepancies between the electrokinetic theory and experiments with polystyrene latexes by Van der Put and Bijsterbosch [*J. Colloid Interface Sci.* **92**, 499 (1983)]. We tested the ~~hairy layer~~ hypothesis by making electrokinetic measurements on latexes before and after they had been heated above the polystyrene glass transition temperature. This sort of treatment should smooth the particle surface by allowing ~~induce~~ the ~~charged~~ polymer filaments which comprise the layer to collapse onto the particle surface. Low-frequency dielectric measurements reveal that heat-treatment improves the agreement between experiment and theory. For an amphoteric latex, the dielectric constant and conductivity decrease with heat-treatment time, and the characteristic relaxation frequency increases. This is consistent with the hairy surface hypothesis, suggesting that heat-treatment smooths the surface, creating particles which more closely conform to the assumptions of the classical theory. Experiments with an anionic latex further suggest the presence of surface structure, but discrepancies between experiment and theory persist; it appears that factors other than hairiness contribute to these discrepancies. The suspension's dielectric properties are evidently very sensitive to the state of the particle surface, and thus dielectric spectroscopy offers a promising means of studying the structure of colloidal interfaces.

Introduction

Polystyrene latexes produced by surfactant-free emulsion polymerization (1) consist of monodisperse spherical particles stabilized by covalently-bound charge. These dispersions should be excellent model systems for studies of colloid stability and electrokinetic phenomena. Nevertheless, a large body of experimental evidence indicates that latexes do not behave as the standard or "classical" theories predict. For example, results of coagulation studies disagree with the theoretical stability ratio-ionic strength relationships (2,3). The ionic strength dependence of the ζ–potential for certain latex systems exhibits a maximum not predicted by electrokinetic theory (4-6). Conductivity measurements on polystyrene latex porous plugs provide ζ–potentials which are inconsistent with ζ–potentials determined from microelectrophoresis (7,8). Furthermore, the ζ–potentials obtained from microelectrophoresis differ from those inferred from dilute suspension conductivity measurements (8,9).

Pervasive inconsistencies are also apparent in the dielectric properties of polystyrene latexes at low frequencies. Here, the measured dielectric constant can exceed the theoretical prediction by an order of magnitude or more, and the relaxation frequency can be much lower than predicted (10).

The source of the disagreement between experiment and theory is not well understood, although it appears likely that the discrepancies arise from effects associated with the particle surface rather than the diffuse double layer. The classical theories are based on the Gouy-Chapman theory of the equilibrium diffuse layer, as described by the full non-linear Poisson-Boltzmann equation. The available experimental evidence indicates that the Gouy-Chapman theory quantitatively predicts the electrostatic repulsion between two charged mica

surfaces, down to separations of a few nanometers (11,12). Thus it is believed that this theory provides an adequate representation of the diffuse layer.

Studies of electrode and metal oxide surfaces show that there is a region close to the surface where the ionic composition and potential distribution differ from that of the diffuse layer. This region, called the Stern layer, consists of specifically adsorbed ions and solvent molecules (13). In the classical theories, the charge inside the Stern layer is constant and the Stern layer ions are immobile. Accordingly, the layer is static, and fully decoupled from transport processes occuring in the diffuse layer. It was shown recently that accounting for non-equilibrium effects in the Stern layer can significantly affect the predicted electrokinetic behavior of colloidal suspensions (14,15).

A related aspect called into question by recent experiments (6,16) is the smoothness of the polystyrene surface. It has been suggested that the surface may be "hairy" due to the presence of terminally-charged polymer chains which interact electrostatically at low to moderate ionic strengths (6). Should such chains protrude into the Stern layer or the inner diffuse layer, electrokinetic effects will be altered in several ways. The displacement of covalently-bound charge from the surface means that the distribution of fixed charge will differ from that specified in the classical theory which assumes that the fixed charge is located in a region of infinitesimal thickness at the particle surface. Extended chains will shift the location of the shear surface away from the interface, resulting in a decrease in the ζ-potential relative to the value for a smooth surface possessing the same fixed charge. This expansion of the inner double layer should accentuate the importance of the dynamic Stern layer effects (14,15) not accounted for in the classical electrokinetic theory. Interfacial ion transport will be hindered by surface hairs, so that surface ion mobilities will be lower than their corresponding bulk values.

Suppose we adopt the hypothesis that the polystyrene surface is hairy. If this is true, then the surface should be susceptible to heat-treatment above the polystyrene glass transition (16). Under these conditions, the extended chains will be mobile, and may be expected to collapse onto the particle surface. Such alterations in the structure of the interfacial region should be revealed in the electrokinetic behavior, for the reasons discussed above.

We have made low-frequency dielectric spectroscopy and microelectrophoresis measurements on "untreated" and "heat-treated" polystyrene latexes. The untreated latexes exhibit large deviations from the predicted response, but heat-treatment improves agreement with the predictions of the classical theory. With an amphoteric latex, four hours of treatment produces a suspension which behaves approximately as the classical theory predicts. These results are consistent with the hairy surface hypothesis. With an anionic latex, heat-treatment for twelve hours improves the agreement between experiment and theory, but significant discrepancies remain.

The presentation is organized as follows. In the next section, we review the basic features of the classical or standard theory of electrokinetics with which our results will be interpreted. Following this is a description of the experimental protocols. Next we outline the techniques used to depict the results, discuss the use of difference spectra, and explain how experiment and theory will be compared. The results are described next, followed by a set of concluding remarks.

Theoretical Considerations

In what follows, the terminology classical theory or standard electrokinetic model means the set of partial differential equations and associated boundary conditions used to describe the behavior of an isolated spherical particle immersed in a dilute electrolyte (17,18), in the presence of an externally applied electric field. The equations are Poisson's equation for the distribution of electrical potential, the Stokes equations with an electrical body force for the low Reynolds number incompressible fluid motion, and conservation equations for the transport of mass and ionic species. The constitutive relation for the ion transport includes the effects of convection, diffusion, and electromigration. Far away from the surface, the influence of the particle disappears, and the field quantities obtain uniform values. At the surface, the no-slip condition is assumed, the charge is taken to be constant, and the normal flux of ions into the particle is identically zero. Note that this formulation does not take into account effects such as surface charge polarization and Stern layer transport (14,15).

The standard electrokinetic model equations have been solved numerically by O'Brien and White (19) for the single particle electrophoretic mobility and by DeLacey and White (20) to predict the dielectric response of a dilute suspension. These are the most comprehensive treatments available, and are not restricted to thin double layers or small surface potentials. For our suspensions, which consist of small, highly charged particles at low ionic strengths, more approximate models (21-24) are not generally applicable. Accordingly, results from the O'Brien-White and DeLacey-White methodologies will be used in the comparisons between theory and experiment.

Experimental Methods

An amphoteric polystyrene latex, designated as Latex A, was synthesized according to the procedure of Homola and James (25), using the modification discussed by Harding and Healy (26). Based on the synthesis recipe, the predicted isoelectric pH for this latex is approximately 5.4. For our experiments, the latex was in the cationic form.

The anionic latex, Latex B, was synthesized via the method of Goodwin et al. (27). The electrophoretic mobilities of Latex B were uniformly negative, consistent with the hypothesis that the charge arises from the dissociation of surface sulfate groups and possibly some carboxylic acid groups.

The latexes were cleaned by sedimentation/decantation in a Beckman Model L5-65 ultracentrifuge with a Type 21 rotor. The first four cycles consisted of an acid pre-wash (1mM HCl). Subsequent wash cycles employed the electrolyte to be used as the suspension medium; normally ten cycles were required for the conductivity of the supernatant to reach a value within 1% of the wash electrolyte. The untreated Latex A was easily resuspended without sonication. Heat-treated Latex A was more difficult to resuspend, requiring light sonication in a bath-type ultrasonic cleaner (L & R Model T-9B, Sargent Welch). Latex B required sonication both before and after heat-treatment.

Before heat-treatment the latex was diluted to a volume fraction of 0.5% solids, and placed in a citrate glass beverage bottle with a teflon-lined bottle cap. The purpose of the dilution was to minimize aggregation during the high-temperature treatment. Such aggregates would effectively increase the polydispersity, making the dielectric data difficult to interpret. The bottled suspensions were heated to 120 $\pm$ 2 ^{o}C in a Deluxe pressure cooker/canner (Presto Ind., Eau Claire WI) equipped with a dial thermometer (Omega, Stamford CT). At the end of the treatment, the

suspension was allowed to cool slowly to room temperature inside the pressure cooker. The heat-treated suspensions showed no evidence of particle coagulum. We did observe that rapid cooling, e.g. immediate refrigeration, caused a number of large fused aggregates to form.

After heat-treatment, the latex was reconcentrated (2-6% solids by volume) by centrifugation, with additional cycles as needed to bring the conductivity to within 1% of the value for the pure electrolyte. The last cycle always took place between 12 and 24 hours before the dielectric spectroscopy experiments.

Particle size and monodispersity were determined by transmission electron microscopy. The particles appeared uniform and spherical before and after heat-treatment. The magnification was calibrated with latex standards of known diameter (Interfacial Dynamics, Portland OR). The results (Table I) indicate that the mean particle diameter and uniformity were essentially unaffected by the heat-treatment procedure. For Latex B, a few large spherical particles were observed in the electron micrographs following heat-treatment. These appear to have been formed by the coalescence of primary particles above T_g.

Electrophoretic mobilities were measured with a Rank Brothers Mark II instrument, in the four-electrode cell configuration with palladium current electrodes. Mobilities were converted into ζ-potentials using the computer program of O'Brien and White (19).

The dielectric and conductivity spectra were determined using the four-electrode frequency-difference dielectric spectrometer of Myers and Saville (28) operated at a reference frequency of 500 Hz. The instrument operation and calibration procedures are described in detail elsewhere (28,29). Note that the four-electrode cell eliminates complications due to electrode polarization (30) and the electronic drift compensation system provides precise "effective" temperature control, estimated to be better than 0.0001°C (28). The absolute temperature inside

the cell was maintained at 25.0 ± 0.1°C by a temperature control system which employs thin film heaters (Minco, Minneapolis, MN) and a refrigerated air stream (31). The low-frequency conductivity, which is needed in the data analysis (28), was measured using an Altex conductivity bridge (Beckman) operated at 85 Hz.

The normalized difference spectra for each suspension were determined at three or four volume fractions using a successive dilution technique. After measuring the dielectric response at a given volume fraction, a small amount of suspension was withdrawn from the cell and saved for a dry-weight determination, assuming the density of polystyrene to be 1.057. The material removed was replaced with the same volume of pure electrolyte yielding a suspension of lower particle concentration.

Methods of Presenting the Experimental Data

Dielectric and conductivity data are presented in terms of normalized frequency-difference functions (28),

$$[\varepsilon(f,\phi) - \varepsilon_r]/\phi \ , [\sigma(f,\phi) - \sigma_r]/\phi \qquad [1]$$

where ε_r and σ_r are the dielectric constant and conductivity at the reference frequency, i.e. $\varepsilon(f_r,\phi)$ and $\sigma(f_r,\phi)$, and ϕ is the particle volume fraction. By subtracting the signals at the reference frequency, the frequency-difference functions eliminate the frequency-independent contribution of the background electrolyte. The normalized frequency-difference functions are independent of ϕ to the extent that particle-particle interactions are negligible. These functions are directly related to DeLacey and White's (20) functions, which are the $O(\phi)$ coefficients in the density expansions:

$$\varepsilon(f,\phi) = \varepsilon(f,0) + \Delta\varepsilon'(f)\,\phi + \ldots$$

$$\sigma(f,\phi) = \sigma(f,0) + \Delta K^{eff}(f)\,\phi + \ldots \quad . \qquad [2]$$

Here, $\varepsilon(f,0)$ and $\sigma(f,0)$ refer to the dielectric constant and conductivity of the pure electrolyte ($\phi = 0$), which are frequency-independent over the measurement range (18). It follows that

$$[\varepsilon(f,\phi) - \varepsilon_r]/\phi = \Delta\varepsilon'(f) - \Delta\varepsilon'(f_r)$$

$$[\sigma(f,\phi) - \sigma_r]/\phi = \Delta K^{eff}(f) - \Delta K^{eff}(f_r) \ . \qquad [3]$$

The normalized frequency-difference functions employed in this work are equivalent to the frequency-difference of the DeLacey-White functions.

Dielectric relaxation data is sometimes presented in terms of a complex dielectric constant $\varepsilon' + i\varepsilon''$. Here, ε' is the real or "in-phase" part of the dielectric constant; ε'' is the imaginary or "out-of-phase" component, referred to as the dielectric loss. In a perfect dielectric ε'' is zero; nonzero values arise in colloidal systems due to diffusion, which reduces the orientation polarization and therefore the dielectric constant ε' (18). The dielectric loss can be related to the measurable suspension conductivity:

$$\sigma(f,\phi) = \sigma(0,\phi) + \omega \varepsilon_v \varepsilon''(f,\phi). \qquad [4]$$

Here, ω represents the angular frequency in radians/second; $f = \omega/2\pi$. Equation [4] separates the conductivity into a dc component $\sigma(0,\phi)$ and a frequency-dependent term which involves the dielectric loss function. The constant ε_v denotes the vacuum permittivity, 8.854×10^{-12} F/m. At the reference frequency, Eq. [4] can be rewritten:

$$\sigma_r(f_r,\phi) = \sigma(0,\phi) + \omega_r \varepsilon_v \varepsilon_r''(f_r,\phi) . \qquad [5]$$

Subtracting [5] from [4] eliminates the dc conductivity, yielding an expression for the conductivity difference function:

$$\sigma(f,\phi) - \sigma_r(f_r,\phi) = \omega \varepsilon_v \varepsilon''(f,\phi) - \omega_r \varepsilon_v \varepsilon_r''(f_r,\phi) . \qquad [6]$$

Now if the conductivity measured at the reference frequency $\sigma_r(f_r,\phi)$ is equal to the dc conductivity $\sigma(0,\phi)$, then it follows from Eq. [5] that $\varepsilon_r''(f_r,\phi) = 0$. According to Eq. [6],

$$\varepsilon''(f,\phi)/\phi = [\sigma(f,\phi) - \sigma_r(f_r,\phi)]/\omega\,\varepsilon_v\,\phi\ . \qquad [7]$$

Measurements show that the suspension conductivity is essentially constant below 1 kHz, so the assumption $\sigma_r(f_r,\phi) = \sigma(0,\phi)$ is justified. The dielectric loss function exhibits peaks in the vicinity of the characteristic relaxation frequencies, and thus provides a convenient means of viewing changes in the relaxation response.

The frequency-difference functions for each experiment were checked to establish that the data were linear with particle volume fraction. Correlation coefficients from linear regression normally exceeded 0.99. The conductivity-differences above 50 kHz were non-linear in ϕ so we report conductivity data only up to 50 kHz. For each amphoteric suspension, the reported normalized difference functions reflect average values of the successive dilution experiments at three volume fractions. Measurements were made at four volume fractions in experiments with anionic latex. Typically, the standard deviation was 1-5% of the mean. The only exception was with the four hour heat-treated amphoteric latex. In this case, the relative error was larger due to the small magnitude of the signals, as will be discussed below.

Experimental Results

Amphoteric particles (cationic form)

Figure 1 shows the normalized dielectric difference function for Latex A in 1mM HCl as a function of treatment time at 120 °C. The initial one hour treatment produced a remarkable change in the dielectric response in that the magnitude of the high frequency dielectric difference decreased from almost 49,000 for the untreated latex to 17,000. The normalized conductivity function, shown in Fig. 2, underwent a similar depression.

This data must be viewed in conjunction with the electrophoretic mobility, which also exhibited interesting behavior. The mobility (Fig. 3) increased from 5.13 to 6.18 μm-cm/volt-sec after one hour, which substantially exceeds the theoretical maximum predicted by the O'Brien-White solution (19). It is difficult to interpret this data in terms of ζ-potentials, since, according to the theory, there is no ζ-potential which corresponds to the measured mobility. Critical coagulation concentrations (CCC) were also measured for the latexes. For the untreated Latex A, 0.25M < CCC < 0.30M in a KNO_3/HNO_3 solution at pH=1.3. The one hour heat-treated Latex A had lower aggregation stability, with .20M < CCC < .25M at pH=1.3. So, despite the increase in mobility, the heat-treated latex was more susceptible to aggregation.

Additional heat-treatments resulted in further attenuation of the low frequency relaxation signals. Figure 4 shows the behavior of ε''/ϕ as a function of treatment time. Values of the loss function were computed from the measured conductivity differences using Eq. [7]. From Fig. 4, it is evident that the low frequency response (<10 kHz) is supressed by the heat-treatment procedure. At the same time, there is a suggestion that a higher frequency mode (~50 kHz) is present. After four hours of treatment, there is no longer a low-frequency peak, and the principal relaxation occurs above 20 kHz. The small magnitude of the conductivity-

difference signal combined with the inherent limitations of the measurement technique at high frequencies (29,30) made it impossible to resolve the high frequency peak for the four hour data.

Returning to Fig. 1, we see that the magnitude of dielectric-difference after four hours at 120°C is only 2300. The standard deviation associated with the value of $[\varepsilon(f,\phi) - \varepsilon_r]/\phi$ at 200 kHz is about 15% of the mean. This relatively large error is due to the decrease in the dielectric constant of the suspension brought about by four hours of heat-treatment. For a suspension containing 2% particles by volume, the dielectric constant at 500 Hz is only about 125, compared to over 1000 for the untreated latex. This huge decrease in signal means that it is much more difficult to measure the dielectric-difference function (29,30). Nevertheless, we are able to achieve sufficient accuracy to make meaningful comparisons with the electrokinetic theory.

The electrophoretic mobility of the four hour heat-treated particles (Fig. 3) decreased to within the range permitted by the O'Brien-White solution. The measured mobility corresponds to a ζ-potential of 81 mV, which was used as input in the DeLacey-White computer program. The predicted response is shown in Figures 1-2. It is clear that the agreement between experiment and theory has been vastly improved by the heat-treatment procedure. The measured and predicted high frequency magnitudes agree to within the experimental error (15%), and the relaxation frequency is much closer to the value expected from the classical theory. Thus, the electrokinetic theory appears internally consistent when applied to amphoteric particles heat-treated for a sufficiently long period of time.

Based on the mobility measurements, there is considerable uncertainty in the ζ-potential as a function of treatment time. In particular, the ζ-potential for untreated and one hour heat-treated latexes may be higher than the 81 mV estimate for the four hour latex. A sensitivity analysis (28,29) demonstrates that

even after increasing the ζ-potential to 250 mV, the classical theory fails to predict the dielectric data for untreated and one hour heat-treated latexes. Thus, the large discrepancies noted in Figures 1,2, and 4 are not due to ambiguities in the ζ-potential.

Anionic Particles

Following the experiments with Latex A, an anionic latex was studied to see if the sensitivity to heat-treatment was a peculiarity of the amphoteric surface or a more general characteristic of polystyrene latexes. Figures 5-7 summarize the dielectric spectroscopy experiments with the anionic latex; the electrophoretic mobility history is displayed in Fig. 8. It is apparent that Latex B does not respond as rapidly to heat-treatment as Latex A. Four hours of treatment, which dramatically transformed Latex A, results in a modest 40% reduction in the magnitude of the dielectric relaxation for Latex B. Additional heating produces smaller shifts, with very little difference between the eight hour and twelve hour data. Furthermore, the shift to higher relaxation frequencies observed with Latex A apparently does not take place with Latex B. From Fig. 7, the low-frequency peak in ε''/ϕ persists even after twelve hours of treatment, and if any shift occurs it is to slightly *lower* frequencies.

The electrophoretic mobility (Fig. 8) increases by about 15% after heat-treatment to values which approach or exceed the theoretical maximum. The ζ-potential at the maximum is -130 mV. Using this ζ-potential, the theoretical spectra were computed for Latex B (Figs. 5-7). Even after twelve hours of heat-treatment, a significant discrepancy remains between the measured response and the theoretical prediction. It is clear from the behavior of Latex B that heat-treatment is not always sufficient to produce classical or "model" polystyrene particles.

Discussion

The concept of a hairy layer on the polystyrene surface was advanced by Van der Put and Bijsterbosch (6) to explain discrepancies between theory and experiment observed in their electrokinetic data. According to these authors, the surface is covered by a flexible hairy layer consisting of polymer chains terminated by charged groups which derive from the initiator used in the latex synthesis. The thickness of the layer is determined by interactions between the charged end groups, and thus depends on the ionic strength. Van der Put and Bijsterbosch estimated a layer thickness of 1-2 nanometers at low (≤ 1 mM) ionic strength (6). Convection is presumed absent in the hairy layer, however ionic conduction within the layer makes an important contribution to the electrokinetic response (6).

Independent non-electrokinetic evidence for the hairy layer model was reported by Goossens and Zembrod (32). The hydrodynamic radius of latex particles was measured by photon correlation spectroscopy, and was shown to be a sensitive function of pH and ionic strength under conditions where particle-particle interactions were unlikely. The hydrodynamic radius varied by as much as 12 nanometers; at the same time electron microscopy detected no dependence of particle size on pH. The variation in hydrodynamic radius was attributed to changes in the surface layer thickness due to the pH-ionic strength dependence of electrostatic segment-segment interactions (32).

Recently, Chow and Takamura (16) tested the hairy layer hypothesis by heat-treating a carboxylated styrene-acrylamide copolymer latex at 115 °C for 16 hours. Electrophoretic mobilities were measured with a laser doppler apparatus. The results showed that the ζ-potential increased significantly following the heat-treatment. This observation was attributed to a shift in the shear plane due to the creation of a smoother surface, resulting in an increase in the electrokinetic

charge. It was concluded that the surface roughness or hairiness was an important factor in determining ζ-potentials from electrophoretic mobility measurements (16).

The present work shows how another electrokinetic property, the dielectric response, is influenced by the structure of the particle surface. Previous studies with untreated anionic (33,34) and amphoteric (10) latexes identified very large discrepancies between experiment and theory. Based on these results, it appeared that either the electrokinetic theory is flawed, or else the "model" polystyrene suspensions do not conform to the assumptions of the theory. Considering the second possibility, attention is naturally directed to the particle surface. From a structural standpoint, less is known and more is assumed about the surface than either the diffuse layer or the adjoining bulk phases. Our results suggest that the structure of the surface region can be altered, but the particle size remains constant as a result of heat-treatment.

The results of our experiments show that the dielectric response is very sensitive to the state of the particle surface. Indeed, the changes in the dielectric properties with heat-treatment are much more pronounced than the corresponding shifts in the electrophoretic mobility reported in this work or in the previous heat-treatment study (16). The magnitude of the frequency-difference spectra for Latex A decreases continuously with treatment time, reaching values within 15% of the theoretical prediction. The decrease in the magnitude is accompanied by a shift in the relaxation to higher frequencies. The frequency shift indicates that ion transport near the interface is facilitated by the change in surface structure, since scaling arguments predict that the characteristic frequency is directly proportional to the ion diffusivity (18). The apparent increase in the ion diffusivity can be explained in light of the hairy layer model: the collapse of surface hairs decreases

the resistance to surface transport, and this leads to an increase in the ion diffusivity, which is reflected experimentally by the shift to higher frequencies.

The behavior of the Latex A mobility as a function of treatment time (Fig. 3) draws attention to the complex nature of the amphoteric latex surface. The initial increase in mobility to values above the theoretical maximum is similar to the behavior observed by Chow and Takamura (16) for the carboxylated latex. The subsequent decrease for longer times suggests that effects other than surface-smoothing may be operative. One possibility is that the heat-treatment removes some of the fixed charge on the particle by hydrolysis. This possibility will be checked in future studies by determining the titratable charge before and after heat-treatment. The increase in ion mobility apparently brought about by surface smoothing might give rise to increased electroosmotic drag on the particle, which would tend to lower the electrophoretic mobility. It appears likely that a number of surface effects contribute interactively to the electrokinetic response of amphoteric latex.

The experiments with Latex B demonstrate that surface hairiness by itself cannot explain all of the discrepancies between theory and experiment. As with Latex A, the magnitude of the relaxation response decreases with treatment time, however much longer treatments are required to affect the signals. Inspection of Fig. 7 shows that the characteristic frequency, which is lower than the theoretical prediction by about a factor of two, does not shift to higher frequencies even after twelve hours of heat-treatment. The slight shift to lower frequencies may have been caused by the presence of a relatively small number of large particles formed during the heat-treatment; such particles were occasionally observed in the electron micrographs of heat-treated Latex B.

The electrophoretic mobility of Latex B (Fig. 8) is relatively insensitive to the heat-treatment. This is reminiscent of earlier experiments by Ma et al. (35), who

demonstrated that for latex particles of low (< 5 $\mu C/cm^2$) titratable charge density, complete hydrolysis of titratable sulfate groups to the hydroxyl form did not sensibly affect the electrophoretic mobility. The mobilities and ζ–potentials measured for Latex B are considerably higher than those of Ma et al., so if hydrolysis did take place the surface was altered in a manner which enhanced the development of negative charge, presumably by chloride ion adsorption.

Finally, it is noteworthy that the dielectric response decreases concommitant with the small increases in mobility for Latex B. Theory predicts that the magnitude of the dielectric response should increase monotonically with the ζ-potential, so clearly there is some difficulty in using ζ-potentials from microelectrophoresis to predict dielectric relaxation of polystyrene latexes. This finding is consistent with the earlier data of Van der Put and Bijsterbosch (7) and Zukoski and Saville (9), demonstrating once again that the ζ-potential is insufficient to characterize the electrokinetic behavior of polystyrene latexes. The use of surface structural models to account for ion binding and Stern layer transport (14,15) may help explain the discrepancies between theory and experiment in the dielectric spectra.

Conclusions

Dielectric measurements on polystyrene latex suspensions indicate that treatment above T_g alters the structure of the particle surface. The effects of the heat-treatment increase systematically with treatment time. The results for an amphoteric latex are consistent with the view that the surface of these particles is hairy, and that the heat-treatment is able to collapse the surface hairs, creating particles which resemble the smooth spheres assumed in the classical theory. For our anionic latex, the agreement between theory and experiment is greatly

improved, however persistant discrepancies in the relaxation frequency suggest that other physicochemical factors are present. These require elucidation. Our results concur with earlier studies (7-10) which demonstrate that the ζ-potential measured from microelectrophoresis does not adequately characterize the electrokinetic behavior of polystyrene latexes. Dielectric spectroscopy, which provides more information per experiment than traditional electrokinetic methods, also appears to be more sensitive to changes in the structure of the particle surface than microelectrophoresis.

There are, no doubt, many reasons for the non-classical behavior of latex particles. Among these may be ion adsorption of various sorts, surface roughness or porosity, and the presence of polymer filaments that form a hairy surface layer. For example, van den Hul and Vanderhoff (36) found that heat-treatment reduced the porosity of latex particles based on differences between surface areas derived from electron microscopy and the BET method. Certainly the mix of factors will vary according to the synthesis procedure and subsequent treatment of the latex. Our results show that heat-treatment alters electrokinetic properties substantially and in a manner consistent with the presence of a hairy layer on the amphoteric particles studied. Nevertheless, much more work will be necessary to establish the roles of the various mechanisms with a given particle and our results do not rule out other explanations. Indeed, in the case of the anionic particles, non-classical behavior persists in the face of heat-treatment.

Acknowledgments

This work was supported by NASA's Microgravity Science and Applications Division, the Xerox Corp., and a grant from the Shell Foundation. We are indebted to A. B. Eidsath for synthesizing the amphoteric latex and to D. F. Myers for his comments on an earlier version of the manuscript.

References

1. "Emulsion Polymers and Emulsion Polymerization" (D. R. Bassett and A. E. Hamielec, Eds.), ACS Symposium Series Vol. 165, Amer. Chem. Soc., Washington, D.C., 1981.
2. Ottewill, R. H., and Shaw, J. N., *Disc. Far. Soc.* **42**, 154 (1966).
3. Prieve, D. C., and Ruckenstein, E., *J. Colloid Interface Sci.* **73**, 539 (1980).
4. Meijer, A. E. J., van Megen, W. J., and Lyklema, J., *J. Colloid Interface Sci.* **66**, 99 (1978).
5. Midmore, B. R. and Hunter, R. J., *J. Colloid Interface Sci.* **122**, 521 (1988).
6. Van der Put, A. G., and Bijsterbosch, B. H., *J. Colloid Interface Sci.* **92**, 499 (1983).
7. Van der Put, A. G., and Bijsterbosch, B. H., *J. Colloid Interface Sci.* **75**, 512 (1980).
8. O'Brien, R. W., and Perrins, W. T., *J. Colloid Interface Sci.* **99**, 20 (1984).
9. Zukoski, C. F.,IV, and Saville, D. A., *J. Colloid Interface Sci.* **107**, 322 (1985).
10. Myers, D. F., and Saville, D. A., *J. Colloid Interface Sci.* **131**, 460 (1989).
11. Israelachvili, J. N., and Adams, G. E., *J. Chem. Soc. Faraday Trans. I* **74**, 975 (1978).
12. Pashley, R. M., and Israelachvili, J. N., *J. Colloid Interface Sci.* **97**, 446 (1984).
13. Hunter, R. J., "Zeta Potential in Colloid Science", Academic Press, NY, 1981.
14. Zukoski, C. F.,IV, and Saville, D. A., *J. Colloid Interface Sci.* **114**, 32 (1986).
15. Zukoski, C. F.,IV, and Saville, D. A., *J. Colloid Interface Sci.* **114**, 45 (1986).
16. Chow, R. S., and Takamura, K., *J. Colloid Interface Sci.* **125**, 226 (1988).
17. Saville, D. A., *Ann. Rev. Fluid Mechanics* **9**, 321 (1977).
18. Russel, W. B., Saville, D. A., and Schowalter, W. R., "Colloidal Dispersions", Cambridge U. Press, 1989.
19. O'Brien, R. W., and White, L. R., *J. Chem. Soc. Faraday Trans. II* **74**, 1607 (1978).
20. DeLacey, E. H. B., and White, L. R., *J. Chem. Soc. Faraday Trans. II* **77**, 2007 (1981).
21. Schwarz, G., *J. Phys. Chem.* **66**, 2636 (1962).
22. Chew, W. C., and Sen, P. N., *J. Chem. Phys.* **77**, 4683 (1982).
23. Grosse, C., and Foster, K. R., *J. Phys. Chem.* **91**, 3073 (1987).
24. Vogel, E., and Pauly H., *J. Chem. Phys.* **89**, 3823 (1988).

25. Homola, A., and James, R. O., *J. Colloid Interface Sci.* **59**, 123 (1977).
26. Harding, I. H., and Healy, T. W., *J. Colloid Interface Sci.* **89**, 185 (1982).
27. Goodwin, J. W., Hearn, J., Ho, C. C., and Ottewill, R. H., *Colloid Polymer Sci.* **252**, 464 (1974).
28. Myers, D. F., and Saville, D. A., *J. Colloid Interface Sci.* **131**, 448 (1989).
29. Myers, D. F., "Dielectric Spectroscopy of Colloidal Suspensions", Ph.D. Thesis, Princeton University, 1988.
30. Schwan, H. P., in "Physical Techniques in Biological Research", Vol. VI, W. L. Nastuk, Ed., Academic Press, 1963.
31. Rosen, L. A., Ph.D. Thesis, Princeton University, in preparation.
32. Goossens, J. W. S., and Zembrod, A., *Colloid Polymer Sci.* **257**, 437 (1979).
33. Springer, M. M., Korteweg, A., Lyklema, J., *J. Electroanal. Chem.* **153**, 55 (1983).
34. Lim, K.-H., and Franses, E. I., *J. Colloid Interface Sci.* **110**, 201 (1986).
35. Ma, C. M., Micale, F. J., El-Aasser, M. S., and Vanderhoff, J. W., in "Emulsion Polymers and Emulsion Polymerization" (D.R. Bassett and A.E. Hamielec, Eds.), ACS Symposium Series Vol. 165, Amer. Chem. Soc., Washington, D.C., 1981, p. 251.
36. van den Hul, H. J., and Vanderhoff, J. W., in "Polymer Colloids" (R. M. Fitch, Ed.), Plenum Press, New York, 1971, p. 1.

TABLE I

Particle size information for untreated and heat-treated polystyrene latexes

	diameter(nm)	% variation
Latex A, untreated	226	3.0%
Latex A, heat-treated 4 hr.	229	1.5%
Latex B, untreated	416	1.3%
Latex B, heat-treated 4 hr.	417	2.6%
Latex B, heat-treated 12 hr.	421	1.6%

Figure Captions

Figure 1: The effect of heat-treatment on the normalized dielectric-difference spectra of Latex A in 1mM HCl. ● untreated; ■ 1 hour at 120 °C; ▲ 2 hours at 120 °C; ◆ 4 hours at 120 °C; —— prediction from the classical theory, ζ = 81 mV.

Figure 2: The effect of heat-treatment on the normalized conductivity-difference spectra of Latex A in 1mM HCl. ● untreated; ■ 1 hour at 120 °C; ▲ 2 hours at 120 °C; ◆ 4 hours at 120 °C; —— prediction from the classical theory, ζ = 81 mV.

Figure 3: The effect of heat-treatment on the electrophoretic mobility of Latex A in 1 mM HCl. Error bars reflect one standard deviation about the mean. Theoretical maximum according to the O'Brien and White numerical solution (19).

Figure 4: The effect of heat-treatment on the normalized dielectric loss spectra of Latex A in 1mM HCl. ● untreated; ■ 1 hour at 120 °C; ▲ 2 hours at 120 °C; ◆ 4 hours at 120 °C; —— prediction from the classical theory, ζ = 81 mV.

Figure 5: The effect of heat-treatment on the normalized dielectric-difference spectra of Latex B in 1mM KCl. ● untreated; ■ 4 hours at 120 °C; ▲ 8 hours at 120 °C; ◆ 12 hours at 120 °C; —— prediction from the classical theory, ζ = -130 mV.

Figure 6: The effect of heat-treatment on the normalized conductivity-difference spectra of Latex B in 1mM KCl. ● untreated; ■ 4 hours at 120 °C; ▲ 8 hours at 120 °C; ◆ 12 hours at 120 °C; —— prediction from the classical theory, ζ = -130 mV.

Figure 7: The effect of heat-treatment on the normalized dielectric loss spectra of Latex B in 1mM KCl. ● untreated; ■ 4 hours at 120 °C; ▲ 8 hours at 120 °C; ◆ 12 hours at 120 °C; —— prediction from the classical theory, ζ = -130 mV.

Figure 8: The effect of heat-treatment on the electrophoretic mobility of Latex B in 1 mM KCl. Error bars reflect one standard deviation about the mean. Theoretical maximum according to the O'Brien and White numerical solution (19).

Figure 1

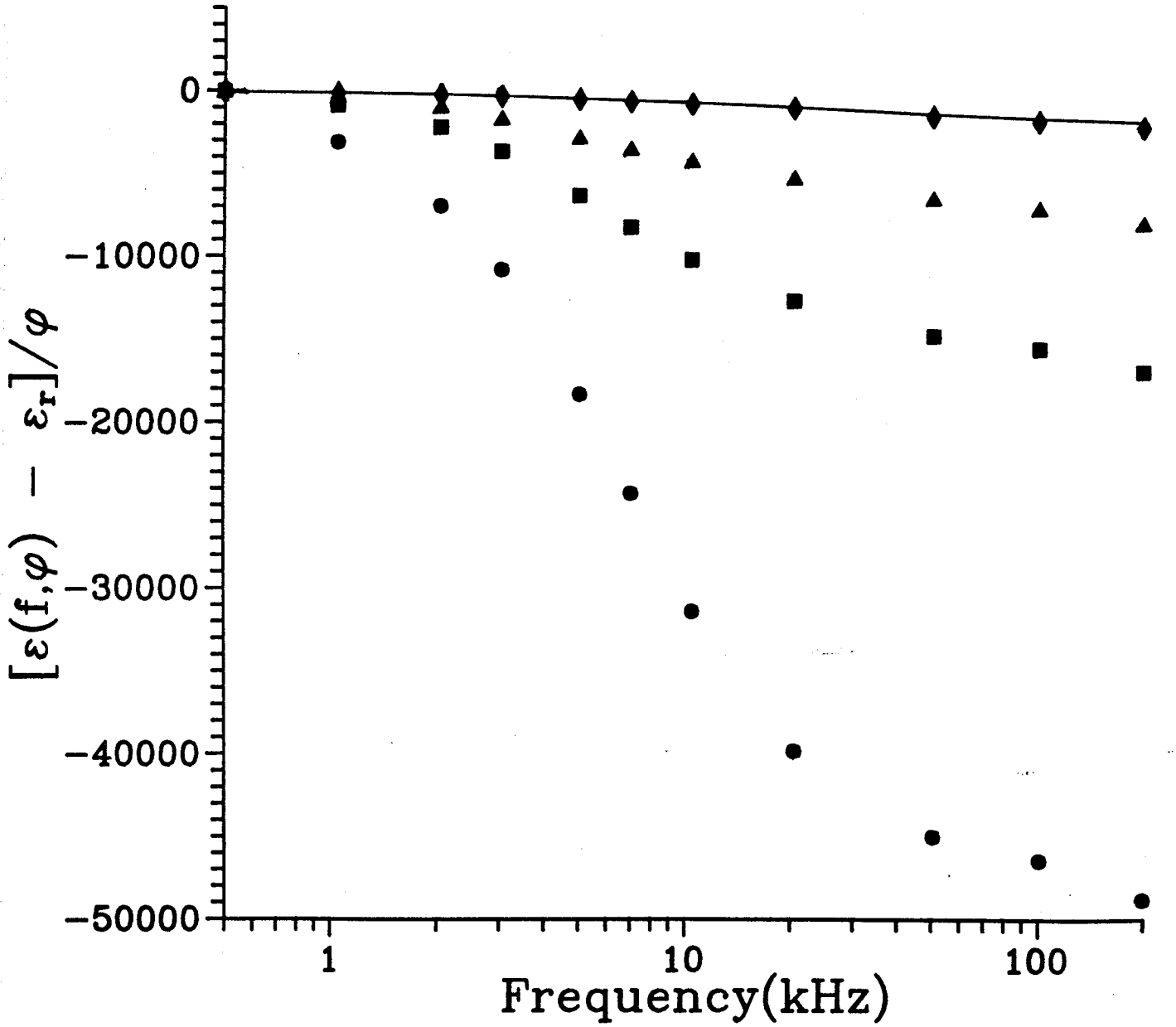
0
−10000
−20000
−30000
−40000
−50000
[ε(f,φ) − εr]/φ
1
10
100
Frequency(kHz)

Figure 2

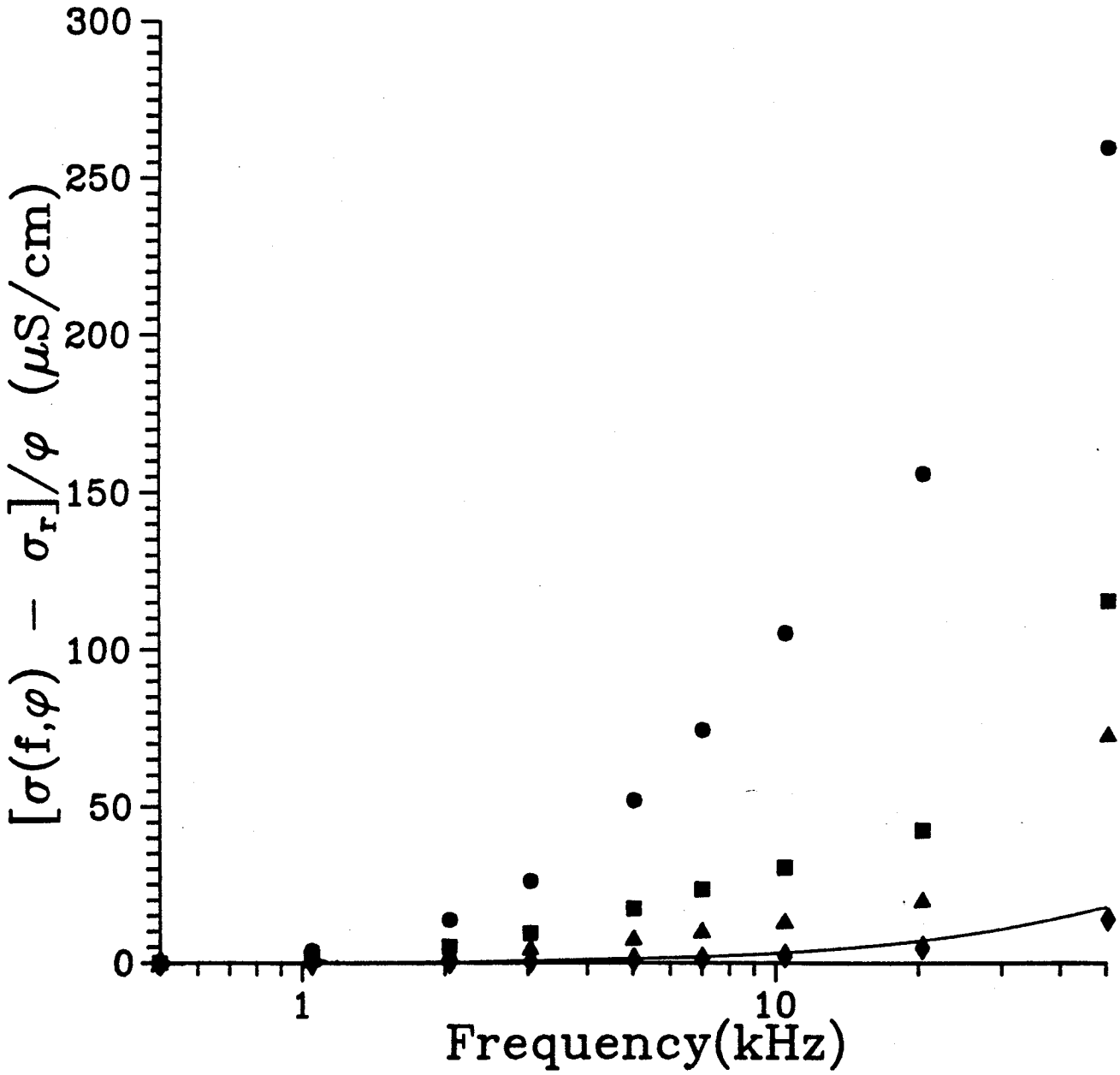
300
250
200
150
100
50
0
$[\sigma(f,\varphi) - \sigma_r]/\varphi$ (μS/cm)
1
10
Frequency(kHz)

Figure 3

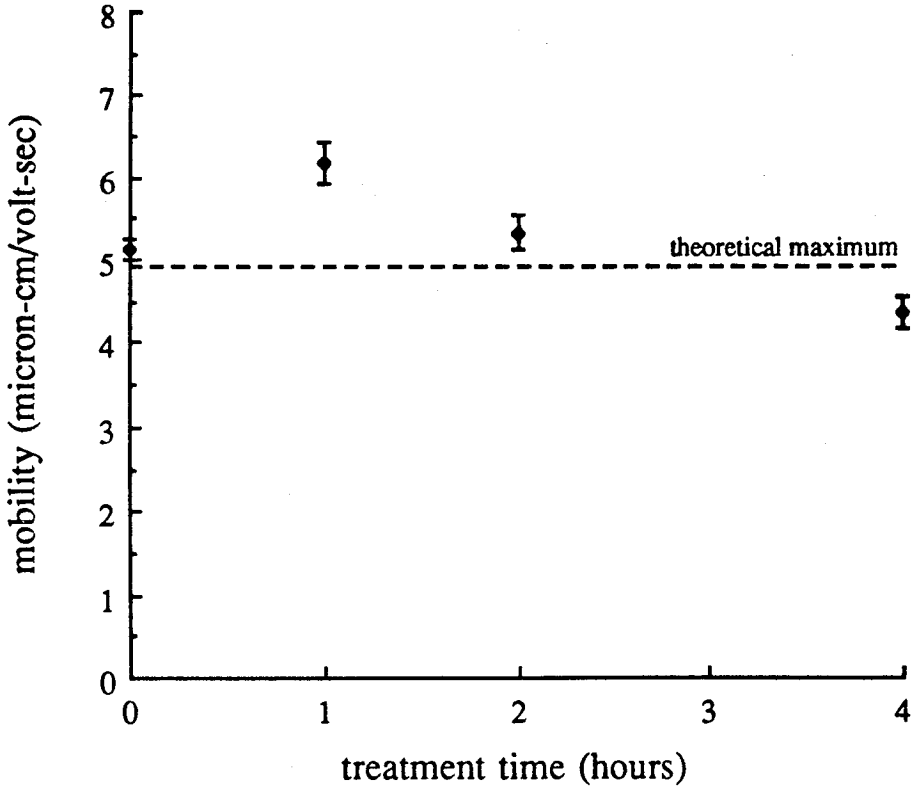
mobility (micron-cm/volt-sec)
8
7
6
5
4
3
2
1
0
theoretical maximum
0
1
2
3
4
treatment time (hours)

Figure 4

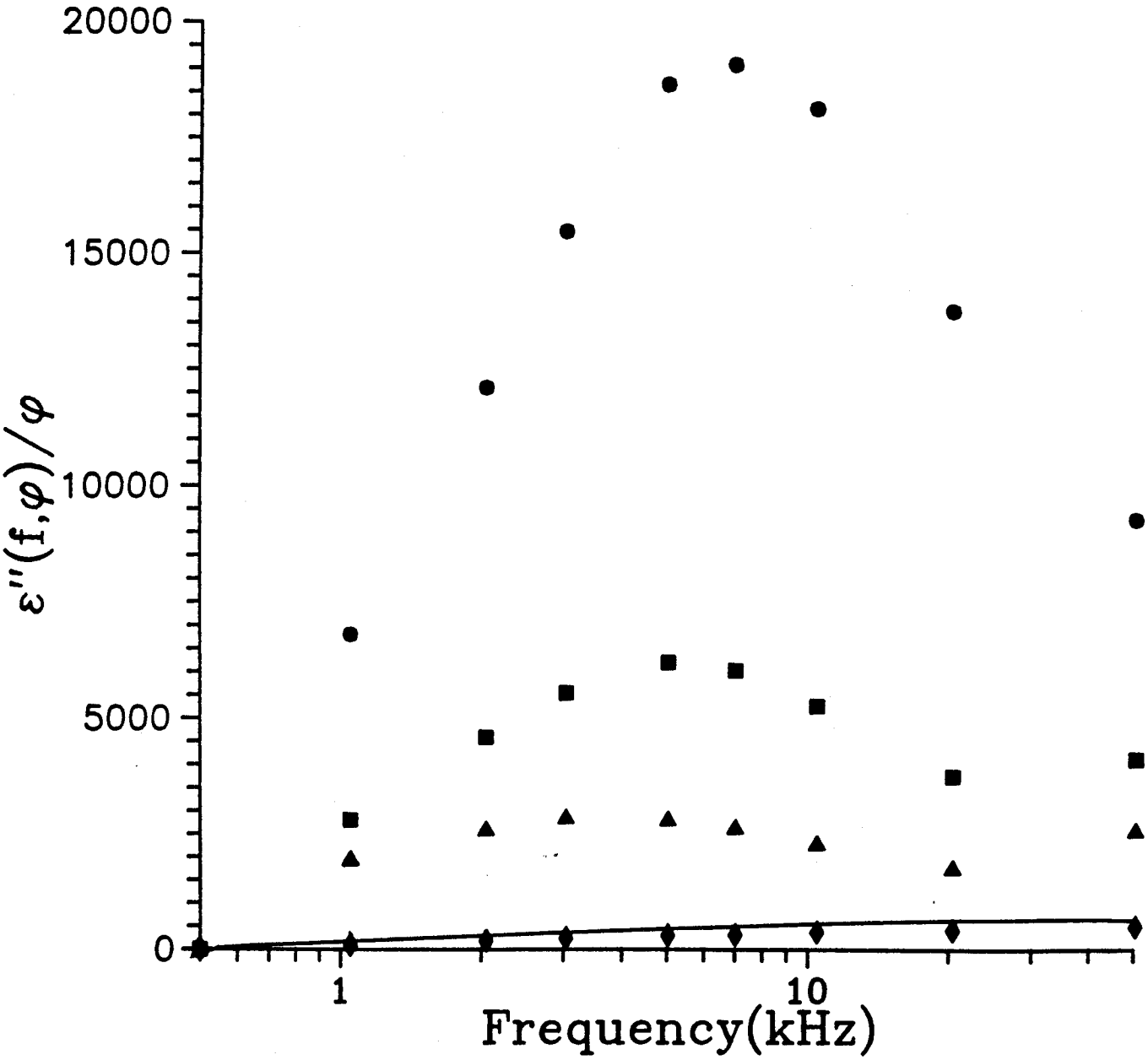

Figure 5

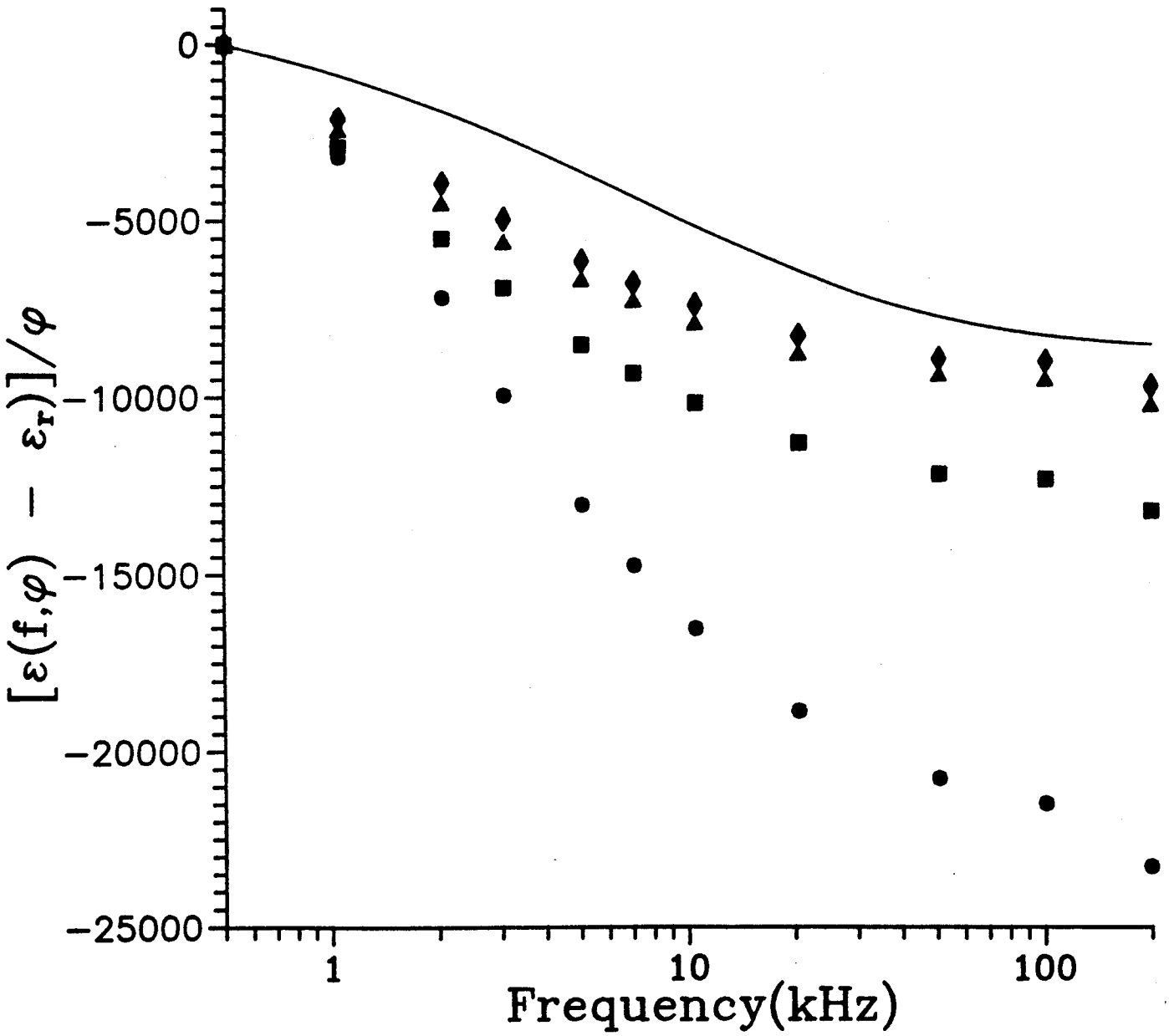

Figure 6

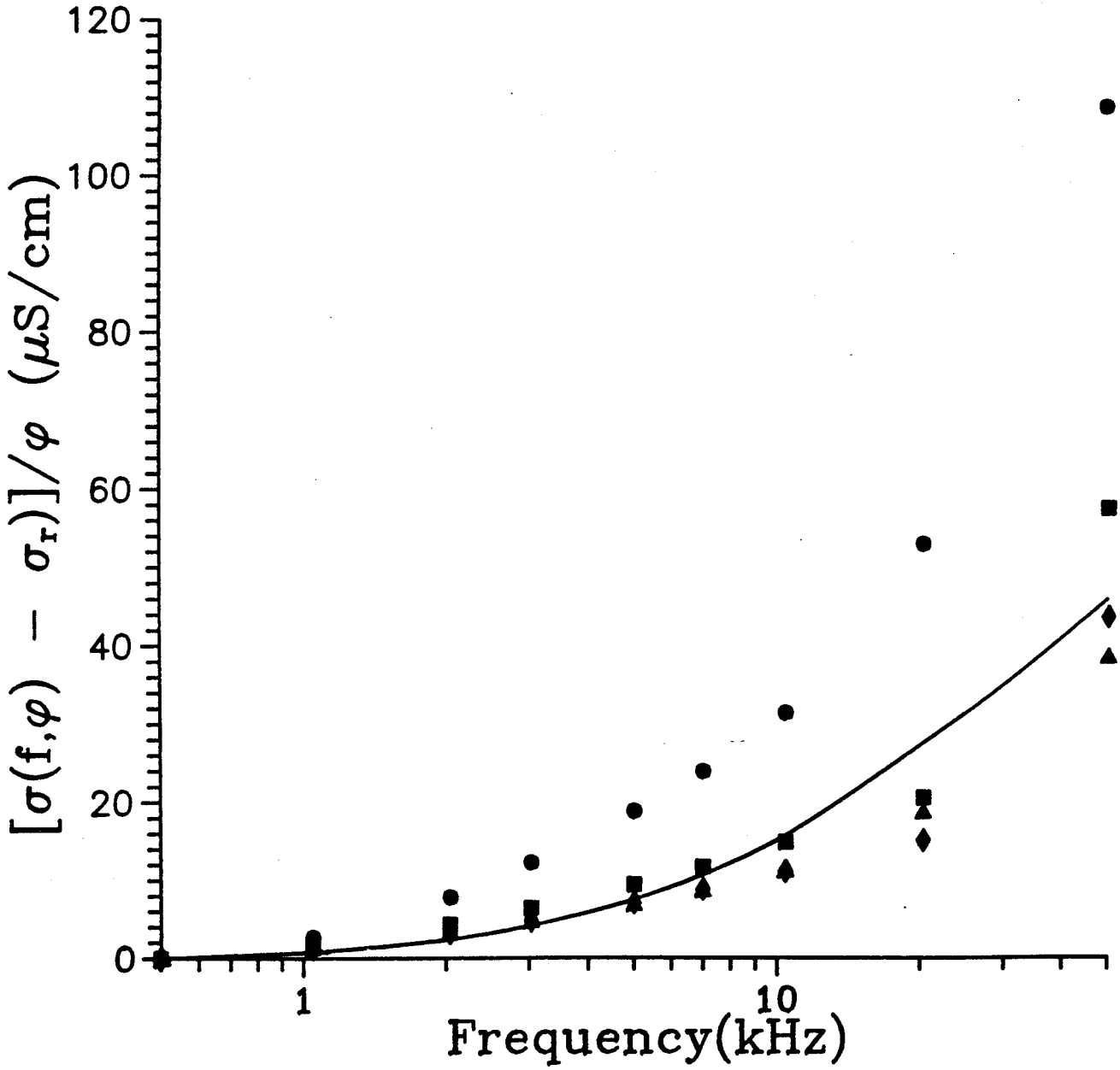

Figure 7

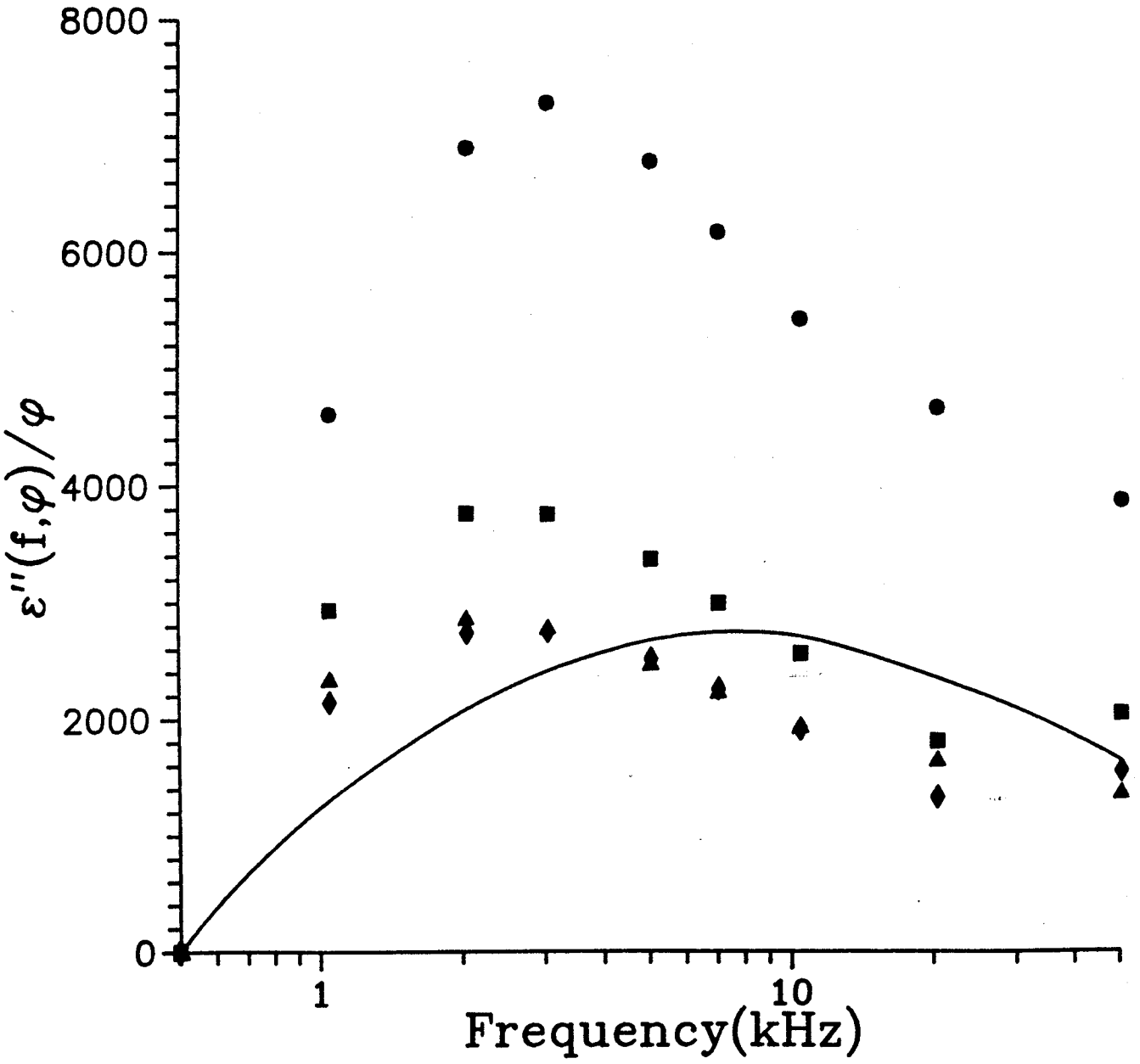

Figure 8

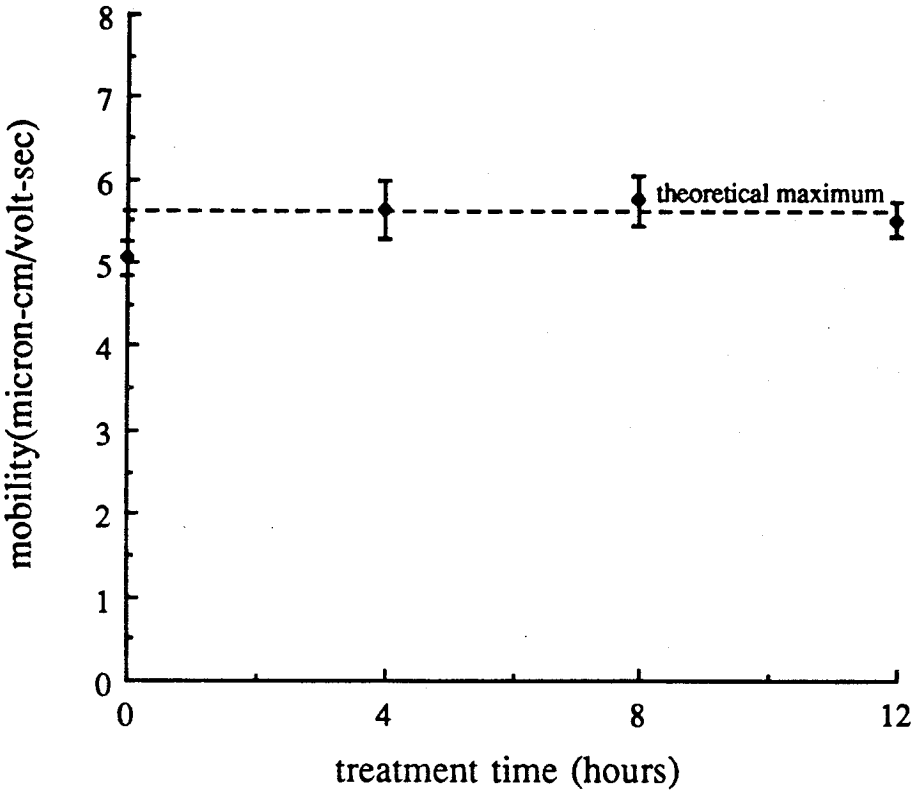
mobility(micron-cm/volt-sec)
8
7
6
5
4
3
2
1
0
theoretical maximum
0
4
8
12
treatment time (hours)

Electrokinetic Properties of Particles in Concentrated Suspensions: Heterogeneous Systems

C. F. ZUKOSKI IV[1] AND D. A. SAVILLE[2]

Department of Chemical Engineering, Princeton University, Princeton, New Jersey 08544

Received August 12, 1988; accepted November 29, 1988

The first paper in the series [*J. Colloid Interface Science* **115**, 422 (1987)] dealt with the electrokinetic behavior of homogeneous suspensions. There it was found that the net particle–particle interaction was negligible for particles undergoing electrophoresis; the particles behaved as electromechanical ghosts. In the current work, attention is focused on heterogeneous systems where a portion of the particles that make up the suspension have electrokinetic properties different from the remainder. Transparent particles (fast ghosts) were prepared by lysis of red blood cells to remove hemoglobin and fixed using glutaraldehyde. To prepare particles with a different mobility (slow ghosts), the fixed ghosts were treated with neuraminidase to remove part of the sialic acid. Tracer particles were prepared in similar ways by omitting the lysis step. The electrical conductivities of suspensions of fixed ghosts and neuraminidase treated fixed ghosts were almost indistinguishable, whereas the electrophoretic mobility of the latter particles was less than half that of the untreated particles. Although the average conductivity of a 50–50 mixture of fast and slow ghosts decreased rapidly with increasing particle concentration, the mobilities of individual constituents did not. To within the experimental accuracy of the measurement, the mobilities of individual constituents varies as $(1 - C)$, C being the volume fraction of particles, irrespective of the electrokinetic makeup of the suspension. This behavior is the same as that encountered with homogeneous systems.

I. INTRODUCTION

Electrokinetic processes are used to characterize all sorts of suspended particles and play important roles in the fractionation of mixtures into relatively pure subpopulations (1, 2). However, despite their importance, few experimental studies exist on heterogeneous mixtures. Most studies deal with homogeneous suspensions where average mobilities are measured by moving boundary or mass transport techniques (3–8). These yield little information about the dynamics of individual constituents.

Modeling of suspension electrokinetics has, in fact, preceded detailed experimental studies. The cell models of Moller, Van Os, and Overbeek (7, 8) and Levine and Neale (9) deal with particle concentration effects in homogeneous suspensions, whereas Reed and Morrison (10) analyzed the motion of spheres with different zeta potentials. Anderson (11) used the two-sphere results of Reed and Morrison (10) to estimate the electrophoretic velocity of a test sphere of one type in a dilute suspension of spheres of different zeta potentials. These studies indicate that particle–particle interactions are relatively weak; detailed experimental work (12) shows that this is true for homogeneous systems.

In our paper on homogeneous suspensions (12), mobilities of individual tracer particles were measured over a wide range of particle concentrations and ionic strengths. This involved the use of red blood cell ghosts and tracer particles with almost identical electrokinetic properties. With these suspensions, the electrical conductivity decreased rapidly with increasing cell concentration, indicating strong

[1] Now at the Department of Chemical Engineering, University of Illinois, Urbana, IL 61801.

[2] To whom correspondence should be addressed.

0021-9797/89 $3.00

electrostatic interactions between particles. Nevertheless, the mobilities of individual particles were relatively insensitive to the presence of neighbors. The speed of translation varied as $(1 - C)$, C being the volume fraction of particles, up to the highest volume fractions achieved. Since this $O(C)$ term arises solely from the backflow necessary to conserve volume in a space filling suspension, particle–particle interactions cancel insofar as electrophoresis is concerned. The particles behave as electromechanical, as well as optical, ghosts. The purpose of the current paper is to report on the behavior of heterogeneous suspensions, i.e., those containing particles of differing mobilities.

For this study we needed suspensions of stable, transparent, colloidal particles with different electrophoretic mobilities, along with tracer particles with the same electrokinetic properties. These can be prepared from suspensions of human red blood cells (RBCs) via osmotic lysis (13), which yields transparent spherical ghosts with electrophoretic mobilities equal to those of the native cells (12). The ghosts and native RBCs were fixed with glutaraldehyde to render them "rigid" and stable to reduction in ionic strength (14). Treatment of fixed cells with Neuraminidase (15) reduces the electrophoretic mobilities of RBCs and ghosts substantially below those of native cells. Heterogeneous suspensions were prepared by mixing untreated (or fast) ghosts with enzyme treated (or slow) ghosts.

Our experiments show that the electrophoretic mobilities of either fast or slow tracers are relatively insensitive to the presence of other particles in the suspension. Tracer mobilities were linear functions of total suspension volume fraction out to the point where a change in rheological behavior occurs. At this volume fraction (approximately 0.45 at the ionic strength used here), the particles appeared to "lock together" and relative movement of fast and slow particles was inhibited.

The remainder of this paper is divided into four sections. Section II deals with the experimental details and Section III with the results. Section IV discusses previous electrokinetic experiments and existing models. Concluding remarks are in Section V.

II. EXPERIMENTAL TECHNIQUES

The ghost preparation procedures used in this work closely follow the protocol laid out by Zukoski and Saville (12). Fresh human blood was drawn by venipuncture into 5-ml Vacutainers (Vacutainer Systems, Rutherford, NJ) and anticoagulated with 2.1 mg disodium EDTA per milliliter of blood.

Ghosts were prepared by an iso-ionic lysis technique described by Billah *et al.* (13). Whole blood was washed three times in 0.15 M PBS (containing 2.54×10^{-2} M Na_2HPO_4, 4.62×10^{-3} M NaH_2PO_4, and 0.120 M NaCl, pH 7.5 ± 0.2) and one time in 0.15 M PBS + $MgCl_2$ (the same 0.15 M PBS buffer described above but containing 2×10^{-3} M/liter $MgCl_2$). Packed cells were resuspended to a volume fraction of 0.25 with 0.15 M PBS + Gly (0.15 M PBS + $MgCl_2$ containing 2 M/liter ethylene glycol). The suspensions were incubated 15 min at room temperature and then 15 min at 0°C. Twenty parts of ice cold 0.15 M PBS + $MgCl_2$ was added rapidly to the chilled suspension for every part of original cell pack volume (final cell volume fraction, 0.04). Lysis was evident by clearing of the turbid appearance. The ghost cells were packed by centrifugation at 16,000g for 20 min in a Beckman L5-65 Preparative Ultra-Centrifuge using a type 21 rotor. The resulting cell pack was washed once in 0.15 M PBS + $MgCl_2$ and the lysis procedure repeated until the desired amount of hemoglobin was removed from the ghosts; four lysis steps were usually required to produce hemoglobin free ghosts.

The ghosts are uniformly spherical and, as reported by Billah *et al.* (13), impermeable to large macromolecules such as dextrans or albumin. Little evidence for ghost fragmentation was observed. As reported earlier (12), the average ghost volume was 120 ± 20 μm^3, and neither average size nor the size distribution was altered by fixation.

All electrokinetic studies reported in this paper were carried out with fixed ghosts and fixed RBCs. Fixation stabilized the suspensions against degradation over time, as well as the action of the enzyme treatment described below, and rendered the cells rigid. Fixation was carried out by washing packed RBCs or ghosts twice in 0.15 *M* PBS and resuspending them to a final volume fraction less than 0.10 in 0.15 *M* PBS containing 1% (w/v) glutaraldehyde (Sigma, electron microscopy grade). The RBC suspensions were checked for hemoglobin release and discarded if any was present. This fixation process, adapted from the work of Vassar *et al.* (14), produced stabilized cells that retained their original shape and size distribution. The fixed RBCs showed no signs of rupture when suspended in deionized water and viewed under the microscope. The fixation process did not alter the size or shape distribution of the ghost cells, and the ghost cells were stable when washed into media of lower ionic strength. However, if the process was reversed, the cells appeared to collapse under the action of the external osmotic pressure. Consequently, fixed ghosts were always washed into lower ionic strength media.

Neuraminidase treatment followed the work of Nordt *et al.* (15). Type V neuraminidase (Sigma) was reported by the manufacturer to have a specific activity of 4.9 units/mg protein using *N*-acetyl neuraminic-lactose as a substrate and 0.5 units/mg protein with bovine submaxillary mucin as a substrate. One unit will liberate 1.0 μmole of *N*-acetyl neuraminic acid per minute at pH 5.0 at 37°C using the indicated substrate. Fixed RBCs and ghosts were washed three times in 0.15 *M* PBS and finally resuspended to a volume fraction of approximately 0.20. Neuraminidase was dissolved in 0.15 *M* PBS and added to suspensions such that the final concentration was 0.27 units per 10^{10} cells. Then the suspensions were incubated for 2.5 h at 37°C, washed two times in 0.5 *M* PBS, and stored at 4°C until use or resuspended in 0.15 *M* PBS containing 1% (w/v) glutaraldehyde. The shape and size distributions of the fixed RBCs and fixed ghosts were not altered by this enzymatic treatment. The enzyme treated cells showed signs of aggregation in 0.15 *M* PBS but were easily redispersed under mild shear. Before and after treatment the mobilities of RBCs and ghosts were the same to within experimental error (5%). Enzyme treatment reduced the RBC and ghost mobilities by almost 70% (Table I). Cells were treated in amounts such that all electrokinetic experiments reported here could be carried out using RBCs and ghosts from the same neuraminidase preparation. Experiments carried out using another enzyme preparation, however, showed similar results.

Electrokinetic studies were carried out using a Rank Mark II Electrophoresis Apparatus (Rank Brothers, Bottisham, England) equipped with silver/silver chloride electrodes and a flat cell. The silver/silver chloride electrodes eliminated electrode polarization, which would occur with platinum or palladium electrodes at the ionic strengths of these experiments. Conductivity measurements were made on suspensions in a flat quartz electrophoresis chamber with an Altex (Beckman) conductivity bridge capable of measuring conductivities at 80 and 1000 Hz. Within this frequency range the conductivity of suspensions did not vary. All measurements were carried out at 25 ± 0.02°C.

To measure mobilities, small amounts of RBC tracers were added to suspensions of ghosts to give a RBC tracer concentration near that used in analytical electrophoresis. Then the electrophoresis chamber was filled with the suspension just prior to making the mobility and conductivity measurements. After the measurement, small volumes of the suspension (0.5–1.0 ml) were removed for subsequent volume fraction determination and replaced with fresh buffer. This process was repeated until the ghost volume fraction reached a low value, typically less than 0.08. The tracer/ghost volume fraction ratio stayed approximately constant during the dilution process.

As discussed earlier (12), the velocity of particles in a dilute system is a sum of the

particle's electrophoretic velocity and the electroosmotic velocity of the fluid in the chamber. The electrophoretic velocity of a particle is relatively independent of position, whereas the electroosmotically driven flow is not. Moreover, if the volume fraction is low, a parabolic flow profile exists. In such situations the mobility can be measured at the stationary plane where the electroosmotic velocity of the fluid is zero. This position depends on chamber geometry and can be found a priori. On the other hand, if the suspension is concentrated, the position of the stationary plane will depend on the constitutive relationship between stress and strain, as well as chamber geometry. Under these circumstances, the stationary plane cannot be found in an a priori fashion. Nevertheless, the electrophoretic mobility can be separated from the effects of bulk flow since the net flow through the chamber is still zero. Integrating the tracer velocity profile across the chamber yields the electrophoretic velocity directly. As discussed by Hunter (16), this technique reduces errors associated with the position of the stationary level even under standard analytical electrophoresis conditions.

In the experiments described here, the velocity of individual tracer particles was measured at 10–15 positions across the chamber, starting close to one wall and making the final measurements close to the opposite wall. However, to avoid excluded-volume effects, positions very close to either wall were avoided. At each depth, between 4 and 10 tracer velocities were measured in alternately opposite directions. The resultant velocity profile was integrated numerically to calculate the average tracer velocity and tracer mobility. Typical field strengths were less than 10 V/cm, but at the elevated volume fractions where the suspensions were highly viscous, field strengths of 20 V/cm were used. Nevertheless, the average tracer velocity always varied linearly with the applied field strength.

The fixed ghost volume fractions were determined from the suspension number concentration and the average volume of the ghost particles. Spherical ghosts prepared by the ethylene glycol lysis technique (13) could be counted and sized accurately using a Particle Data Elzone Celloscope (Particle Data, Elmherst, IL) calibrated with standard latex particles. This electronically determined size distribution was checked against a microscopically determined size distribution (12). To within experimental error, the two gave the same distribution and average size.

In experiments where a 50–50 mixture of fast and slow ghosts was used, dilute suspensions of each were made up and adjusted to the same number concentration. Equal volumes of each suspension were mixed, and the resulting suspension packed by centrifugation. The difference between the concentrations of fast and slow ghosts was less than 1%.

Most of our electrokinetic studies were carried out in 0.045 *M* PBS (0.15 *M* PBS diluted with deionized water). Here the suspensions were washed two times in 0.045 *M* PBS and allowed to stand overnight at 4°C in 0.045 *M* PBS prior to a final washing. This assured equilibration of ionic strength across the membrane.

III. RESULTS

Some preliminary experiments were carried out on homogeneous suspensions of native tracers and ghosts and enzyme treated tracers and ghosts in 0.15 *M* PBS. At this ionic strength, the enzyme treated ghosts (and tracers) have electrophoretic mobilities of -0.56 (μm/s)/(V/cm), which corresponds to a surface potential of approximately -7.0 mV. These suspensions were very viscous and non-Newtonian. This suggests that the enzyme treated cells were colloidally unstable under these conditions and coagulation caused the anomalous results. All the results reported here are for systems where the electrolyte was 0.045 *M* PBS and the particles were stable.

Figures 1 and 2 show conductivities for homogeneous suspensions in 0.045 *M* PBS. Conductivities for homogeneous suspensions of fast and slow ghosts coincide, to within ex-

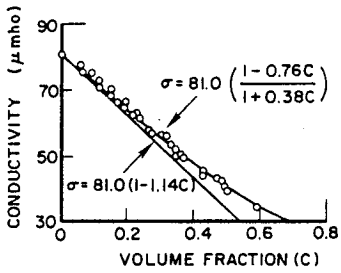

FIG. 1. The conductivity of suspensions of fixed untreated ghosts as a function of suspension volume fraction. The background electrolyte is 0.045 *M* PBS (pH 7.4).

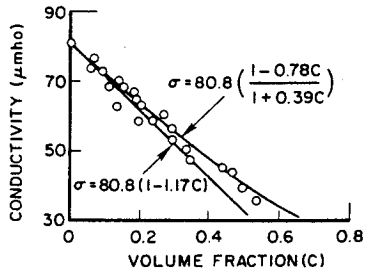

FIG. 2. The conductivity of suspensions of fixed enzyme treated ghosts as a function of suspension volume fraction. The background electrolyte is 0.045 *M* PBS (pH 7.4).

perimental uncertainty at volume fractions as large as 0.6, suggesting that enzyme treatment does not significantly alter membrane properties at this ionic strength. Due to the high ionic strength and low surface charge in these suspensions, changes in the surface charge have a negligible effect on the bulk conductivity. The deviation of the limiting slope from the value of -1.5 given by Maxwell's equation may be due to membrane or double-layer conductance. Figure 3 shows the electrophoretic mobility of fast tracers in suspensions of fast ghosts, along with the mobility of slow tracers in slow ghosts. The tracer mobility varies linearly with ghost volume fraction, independent of enzyme treatment. For these suspensions, the electrophoretic increments derived by linear regression are -0.97 for suspensions of fast tracers in fast ghosts and -1.00 for suspensions of slow ghosts.[3]

Figure 4 depicts the mobility–volume fraction relationships for fast tracers in suspensions of slow ghosts and slow tracers in suspensions of fast ghosts. There is a linear volume fraction dependence of fast tracer electrophoretic mobilities in slow ghost suspensions, and the electrophoretic increment is, to within experimental error, the same as the electrophoretic increment for fast tracers suspended in fast ghosts. Similarly, the mobility of slow tracer particles in suspensions of fast ghosts is linearly dependent on ghost volume fraction out to a volume fraction of 0.4. The electrophoretic increment for the linear portion of the curve is -1.15; within experimental uncertainty, this equals the electrophoretic increment for slow tracers in slow ghost suspensions.

Above a volume fraction of 0.4 the suspensions become substantially non-Newtonian and the electrophoretic mobility of the slow tracers in the fast ghosts increases. At the highest volume fraction studied (0.59), the velocity profile had a blunt shape at the cham-

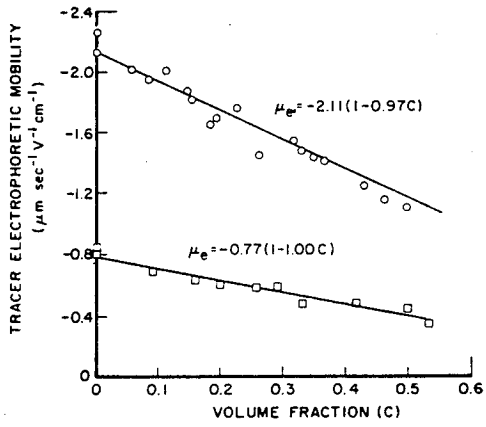

FIG. 3. The electrophoretic mobility of fixed untreated RBC tracers in suspensions of fixed untreated ghosts (○) and the electrophoretic mobility of fixed enzyme treated tracers in suspensions of fixed enzyme treated ghosts (□) as a function of suspension volume fraction. The background electrolyte is 0.045 *M* PBS (pH 7.4).

[3] The electrophoretic increment, $\Delta\mu$, is defined through an expansion of the particle's mobility, μ_e, in total suspension volume fraction C, as $\mu_e = \mu_e^0(1 + \Delta\mu C + \cdots)$, where μ_e^0 is the mobility as $C \to 0$.

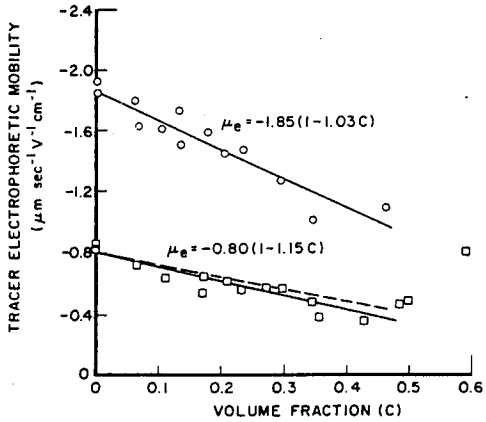

FIG. 4. The electrophoretic mobility of fixed untreated RBC (fast) tracers in suspensions of fixed enzyme treated (slow) ghosts (○) and the electrophoretic mobility of fixed enzyme treated (slow) tracers in suspensions of fixed untreated ghosts (□) as a function of suspension volume fraction. The dashed line represents a mobility that varies as $(1 - C)$. The background electrolyte is 0.045 *M* PBS (pH 7.4).

ber center and the suspension displayed some elasticity. Here the slow tracer mobility equaled that expected for fast tracers in fast ghost suspensions. This suggests that the slow tracer particles were locked in place and carried along with the fast ghosts. It should also be noted that the mobility intercept for fast tracers shown in Fig. 4 is lower than those reported in Figs. 3 or 5. For this batch of fast tracers, the mobilities decreased as a result of fixation and, consequently, these tracers were used only in the experiments shown in Fig. 4.

Figure 5 shows electrophoretic mobilities for fast and slow tracer particles plotted as a function of volume fraction for a 50–50 mixture of fast and slow ghosts. Up to volume fractions of 0.35, the mobilities of both fast and slow tracer particles are linearly dependent on total suspension volume fraction. Moreover, the electrophoretic increments for both the slow and the fast tracer particles are, to within experimental error, the same as for fast tracers suspended in fast ghosts and slow tracers suspended in slow ghosts.

At volume fractions greater than 0.36, a large amount of time dependent structure was observed to build up in the heterogeneous suspensions. This structure took the form of wavy alternating dark and light bands perpendicular to the direction of particle motion and moving with the particles. At a volume fraction of 0.40, the structure was so intense as to make measurements irreproducible. Here the tracer particles gradually slowed down at the center of the chamber until the entire system moved in plug flow. Reversing the field caused the structure to break down over a period of 8 to 10 s until the tracers appeared suspended in a uniformly grainy background. Suspension structure reformed moving in the opposite direction within approximately 30 s. During this time, the tracer particles would slow down and form a flat velocity profile. In the volume fraction range from 0.36 to 0.30, structure became less evident, and tracer velocities were independent of the length of time the electric field had been applied. No structure was observed at volume fractions less than 0.30. It should be noted that with homogeneous suspensions, little or no structure was observed at volume fractions as large as 0.59. At this volume fraction, a small amount of elasticity was observed, but after a short time (10–15 s) the tracer velocities were independent of time. The data presented in

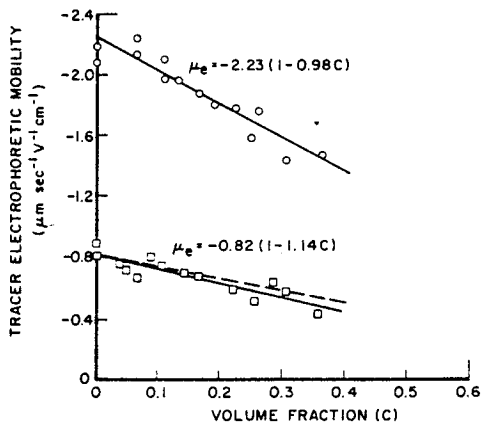

FIG. 5. The mobility of fixed untreated RBC (fast) tracers (○) and fixed enzyme treated tracers (□) in suspensions of a 50–50 mixture of fixed untreated and fixed enzyme treated ghosts. The dashed line represents a mobility that varies as $(1 - C)$. The background electrolyte is 0.045 *M* PBS (pH 7.4).

Fig. 5 were taken on suspensions only where steady mobilities were observed. The inability to gather meaningful tracer velocity profiles above volume fractions of 0.4 in 50–50 mixtures of slow and fast ghosts suggests that a mechanism similar to the "locking-up" observed for slow tracers in suspensions of fast ghosts was present.

The electrophoretic data presented in Figs. 3–5 are rather surprising. If the suspension volume fraction is kept below a certain value, the electrophoretic mobilities of the tracer particles are almost independent of the electrokinetic properties of the other particles which make up the bulk of the suspension volume fraction and depend only on the overall particle concentration.

III. DISCUSSION

Previous studies have established sialic acid as the main charge determining moiety on the red blood surface (17) and treatment of RBCs with neuraminidase is known to release virtually all external membrane-bound sialic acid (15). In 0.15 *M* NaCl (pH 7.2), the electrophoretic mobility of fresh neuraminidase treated RBCs is virtually zero, suggesting a complete removal of the red cell's electrokinetic charge. Subsequent glutaraldehyde fixation of RBCs that had been treated with neuraminidase to reduce the mobility almost to zero increases cell electrophoretic mobilities to -0.45 ± 0.09 $(\mu m/s)/(V/cm)$ (14). The source of this increase in mobility is not known; however, the increase is stable over time. Fixation of native RBCs and native RBC ghosts with glutaraldehyde raises the cell mobility from -1.08 ± 0.05 $(\mu m/s)/(V/cm)$ to -1.26 ± 0.07 $(\mu m/s)/(V/cm)$ in 0.15 *M* NaCl, pH 7.2. Again this increase is of unknown origin and is stable with time (15). Table I gives the electrophoretic mobilities at infinite dilution of the native and enzyme treated particles used in this study. According to the table, neuraminidase treatment reduced the mobilities of the RBCs and ghosts by almost 70%.

For the studies at hand, particles of substantially different mobility were required, and the enzyme treatment described here provided these particles. At the ionic strengths used here, fixed RBCs and fixed ghosts had the same electrophoretic mobilities as did the enzyme

TABLE I

Electrokinetic Properties

Sample[a]	$\Delta\sigma$[b]	α[c]	μ_e^0[d] (μm/s)(V/cm)	ζ[e] (mV)
Untreated RBC/ghosts in 0.15 *M* PBS	−1.26	0.110	−1.26 ± 0.06	−16.2
Enzyme-treated RBC/ghosts in 0.15 *M* PBS	−1.90	—	−0.56 ± 0.08	−7.0
Untreated RBC/ghosts in 0.045 *M* PBS	−1.14	0.170	−2.20 ± 0.08	−29.0
Enzyme-treated RBC/ghosts in 0.045 *M* PBS	−1.17	0.170	−0.80 ± 0.06	−10.5

[a] Note that all the cells were fixed with glutaraldehyde.

[b] The conductivity increment, $\Delta\sigma$, was calculated from the limiting slope of the conductivity–volume fraction relationship for suspensions of ghosts alone.

[c] The relative conductivity of the particles in suspension, α, is calculated from $\Delta\sigma$ and is valid only for the ghost particles and does not necessarily hold for the tracer RBC (12).

[d] The electrophoretic mobility, μ_e^0, measured at infinite particle dilution, was the same for RBC tracers and ghosts for both untreated and enzyme treated samples.

[e] The electrokinetic surface potential, ζ, as calculated from the Smoluchowski formula.

treated fixed RBCs and enzyme treated fixed ghosts. Moreover, the enzyme treatment did not substantially alter the distribution of electrophoretic mobilities, which remained roughly Gaussian with a standard deviation of ±5% (17). Thus, enzyme treated RBCs faithfully duplicated the behavior of the enzyme treated ghost particles.

The electrokinetic behavior of the homogeneous suspensions used in this work was similar to that found in the earlier study (12). Figure 3 shows that the mobilities are linear in the volume fraction of particles and the electrophoretic increment is, to within experimental error, −1.0. This sort of behavior can be attributed to the irrotational nature of the velocity field of identical particles undergoing electrophoresis when the diffuse layer is thin, as it is here. The argument hinges on the fact that the electrostatic and hydrodynamic interactions between a pair of particles cancel and goes as follows.

The velocity of a pair of identical spheres undergoing electrophoresis can be calculated using the method of reflections. Starting with the velocity of an isolated sphere, the velocity of the other sphere is calculated, ignoring its effect on the velocity of the first. Then the velocity of the first sphere is corrected for the presence of the second, after which the velocity of the second is recalculated using the corrected velocity of the first sphere. When repeated *ad infinitum,* this yields the velocity of either sphere in the presence of the other.

First we note that a single particle translating through an infinite fluid produces a certain velocity field, $\mathbf{u}(\mathbf{r})$, in the surrounding fluid. A second particle placed in this fluid will respond to the viscous and electrical forces. The velocity of the second particle differs from what it would be if it were all alone due to the shear flow and alteration in the electric field produced by the first particle. The velocity of a single particle placed in a shear flow can be found from Faxen's law (18) as

$$\mathbf{U} = \mathbf{U}_0 + \mathbf{u}(\mathbf{r}) + \nabla^2\mathbf{u}(\mathbf{r}). \qquad [1]$$

Here $\mathbf{U}_0$ represents the electrophoretic velocity of the second sphere, i.e., the product of the mobility and the local field at the particle's location, viz.,

$$\mathbf{U}_0 = \mu_e^0(\mathbf{E} + \delta\mathbf{E}). \qquad [2]$$

$\mathbf{E}$ is the undisturbed field, $\delta\mathbf{E}$ is the disturbance to the uniform field, and μ_e^0 is the electrophoretic mobility of the isolated particle. Note that Faxen's law does not account for the effect of the second particle on the velocity of the first and, at this stage, Eq. [1] simply represents the uncorrected velocity of the second particle in the presence of the first. To complete the first stage of the calculation we need the velocity field and the deformation to the electric field produced by the first particle. For a single particle undergoing electrophoresis, it is easily shown that when the diffuse layer is thin the velocity field around it is irrotational and given by

$$\mathbf{u}(\mathbf{r}) = -\mu_e^0 \tfrac{1}{2} r^{-3}[\mathbf{I} - 3r^{-2}\mathbf{rr}]\cdot\mathbf{E}. \qquad [3]$$

Here $\mathbf{r}$ is the position vector scaled on the particle radius and $\mathbf{I}$ is the unit tensor. The disturbance to the electric field produced by the first sphere is

$$\delta\mathbf{E}(\mathbf{r}) = \tfrac{1}{2} r^{-3}[\mathbf{I} - 3r^{-2}\mathbf{rr}]\cdot\mathbf{E}. \qquad [4]$$

Combining Eqs. [1]–[4] shows that in the first approximation the second particle moves at the speed it would if the first particle were absent. At the next stage in the process we calculate the correction to the velocity of the first particle due to the presence of the second; it too vanishes. Continuing the process shows that the two identical spheres move as if they were all alone, regardless of their orientation with respect to the field. This is the result found by Reed and Morrison (10) by means of a more detailed calculation. To calculate the velocity of a test particle in a space filling suspension requires an accounting for: (i) the backflow due to the motion of all other particles and (ii) the alteration in the strength of the field due to the particles. The former calculation is straightforward for systems where the particles are distributed at random around the test particles (18) and yields

$$\mu_e = \mu_e^0(1 - C) \qquad [5]$$

for the mobility. It may also be noted that the argument given above holds for concentrated suspensions where, due to the irrotational nature of the velocity and electric field, the hydrodynamic and electrostatic effects cancel up to particle concentrations where the diffuse layers overlap.

The theory of electrophoresis in a dilute, homogeneous system was worked out by Anderson (11) by adapting Batchelor's results for sedimentation (18). However, the fact that the structure of the mean field is altered by the particles in a space filling suspension is absent from Eq. [5] and, according to Anderson (19), accounting for this effect with nonconducting particles adds $-\frac{1}{2}\mu_e^0 C$ to the equation. Nevertheless, the experimental results clearly show that the electrophoretic increment for homogeneous suspensions is close to -1, not $-\frac{3}{2}$, although the reason for this discrepancy is unknown. It could be due to the slightly polydisperse, slightly nonspherical nature of the particles. Or there might be a subtle error in the theory. In any event, the problem deserves further study.

The results from experiments where the mobility of the tracer differs from that of the suspension particles were shown in Fig. 4. Here the electrophoretic increments derived from linear regression of the experimental data are -1.03 and -1.15 for fast tracers in slow ghosts and slow tracers in fast ghosts, respectively. These are not significantly different from -1, as the dashed line in the figure clearly indicates. With fast or slow tracers in slow or fast ghosts, the distribution of neighbors around the tracer is nonuniform and the increment should differ from -1. Evidently the effect of the nonuniformity is weak.

The situation with heterogeneous suspensions shown in Fig. 5 is even more interesting. Here the increments are, to within the accuracy of the measurement, -1 for either sort of tracer in 50–50 mixtures of fast and slow ghosts. To compare this result with a theory of the sort embodied in Eq. [5] requires knowledge of particle distribution around the test particle.[4] The methodology has been worked out for sedimentation in dilute systems (20–22) and adapted for electrophoresis (23). For binary systems the result is

$$\mu_{e,i} = \mu_{e,i}^0[1 - C - 0.13\nu_{j,i}C_j] \qquad [6]$$

to $O(C)$. Here the i, j subscripts identify the particle type and

$$\nu_{j,i} = 1 - \mu_{e,j}^0/\mu_{e,i}^0. \qquad [7]$$

The numerical coefficient 0.13 depends on the pair distribution, and its value is extremely sensitive to the details of the particle–particle interaction at close separations. Thus, the numerical value reported here may be revised when more accurate calculations are available. Upon using the results from Table I we have

$$\mu_{e,f} = \mu_{e,f}^0[1 - 1.04C] \qquad [8]$$

and

$$\mu_{e,s} = \mu_{e,s}^0[1 - 0.89C] \qquad [9]$$

for fast and slow particles in 50–50 mixtures of the two. The theory indicates, as expected, that fast particles are slowed somewhat by interactions with slower neighbors (Eq. [8]). Similarly, slow particles are helped along by interactions with faster neighbors (Eq. [9]) compared with their behavior in homogeneous systems. Nevertheless, the effect is weak and not very different from the experimental results in Fig. 5. Finally, it should be noted that these calculations are for dilute systems, and multiparticle interactions have been ignored.

V. CONCLUSIONS

The experimental work reported here on heterogeneous systems shows that particle–particle interactions in suspensions are surprisingly weak insofar as electrophoretic processes are concerned. With homogeneous systems it can be shown that electrostatic and hydrodynamic interactions cancel so the ab-

[4] Anderson's calculation for heterogeneous systems (11) is applicable only when the spheres around the test particle are "well stirred."

sence of particle–particle interactions is readily understood, even in concentrated systems. However, with heterogeneous systems interactions do not cancel, and the distribution of particles around a test particle is no longer uniform in a dilute system. However, although stronger interactions might have been anticipated, the redistribution of particles has a rather weak effect on electrophoretic mobility.

ACKNOWLEDGMENTS

This work was supported by the NASA Microgravity Science and Applications Division and grants from the Xerox Corporation and the Shell Foundation. Our discussions with Dr. G. V. F. Seaman regarding the preparation and use of red blood cells and ghosts were particularly helpful.

REFERENCES

1. Hannig, K., Separation of cells and particles by continuous flow electrophoresis, *in* "Techniques of Biomedical and Biophysical Morphology" (D. Glick and R. M. Rosenbaum, Eds.), Wiley, New York, 1972.
2. Pruzik, Z., *J. Chromatogr.* **91,** 867 (1974).
3. Long, R. P., and Ross, S., *J. Colloid Interface Sci.* **20,** 438 (1965).
4. Long, R. P., and Ross, S., *J. Colloid Interface Sci.* **26,** 434 (1968).
5. Hoyer, H. W., Mysels, K. J., and Stigter, D., *J. Phys. Chem.* **58,** 385 (1954).
6. Stigter, D., and Mysels, K. J., *J. Phys. Chem.* **59,** 45 (1955).
7. Moller, W. J. H. M., Van Os, G. A. J., and Overbeek, J. Th.G., *Trans. Faraday Soc.* **57,** 312 (1961).
8. Moller, W. J. H. M., Van Os, G. A. J., and Overbeek, J. Th.G., *Trans. Faraday Soc.* **57,** 325 (1961).
9. Levine, S., and Neale, G. H., *J. Colloid Interface Sci.* **47,** 520 (1974).
10. Reed, L. D., and Morrison, F. A., *J. Colloid Interface Sci.* **54,** 117 (1976).
11. Anderson, J. L., *J. Colloid Interface Sci.* **82,** 248 (1981).
12. Zukoski, C. F., and Saville, D. A., *J. Colloid Interface Sci.* **115,** 422 (1987).
13. Billah, M. M., Fineman, J. B., Coleman, R., and Mitchell, R. H., *Biochim. Biophys. Acta* **433,** 54 (1976).
14. Vassar, P. S., Hurd, J. M., Brooks, D. E., Hagenberger, B., and Seaman, G. V. F., *J. Cell Biol.* **53,** 809 (1972).
15. Nordt, F. J., Knox, R. J., and Seaman, G. V. F., *J. Cell Physiol.* **97,** 209 (1978).
16. Hunter, R. J., "Zeta Potential in Colloid Science." Academic Press, New York, 1981.
17. Seaman, G. V. F., Electrokinetic behavior of red cells, *in* "The Red Blood Cell II" (D. M. Surgenor, Ed.), pp. 1136–1230. Academic Press, New York, 1975.
18. Batchelor, G. K., *J. Fluid Mech.* **52,** 245 (1972).
19. Anderson, J., Personal communication, 1985.
20. Haber, S., and Hetsroni, G., *J. Colloid Interface Sci.* **79,** 56 (1981).
21. Batchelor, G. K., *J. Fluid Mech.* **119,** 379 (1982).
22. Batchelor, G. K., and Wen, C. S., *J. Fluid Mech.* **124,** 495 (1982).
23. Zukoski, C. F., IV, "Studies of Electrokinetic Behavior in Suspensions." Ph.D. dissertation, Princeton University, 1984.

Particle migration in suspensions by thermocapillary or electrophoretic motion

By A. ACRIVOS, D. J. JEFFREY AND D. A. SAVILLE

Reprinted from
Volume 212 of the Journal of Fluid Mechanics
dedicated to Professor G. K. Batchelor on his 70th Birthday

Printed in Great Britain

J. Fluid Mech. (1990), *vol.* 212, *pp.* 95–110
Printed in Great Britain

Particle migration in suspensions by thermocapillary or electrophoretic motion

By A. ACRIVOS,[1] D. J. JEFFREY[2] AND D. A. SAVILLE[3]

[1] The Levich Institute, Steinman 202, City College of New York, New York, NY 10031, USA

[2] Department of Applied Mathematics, University of Western Ontario, London, Ontario, Canada N6A 5B9

[3] Department of Chemical Engineering, Princeton University, Princeton, NJ 08544, USA

(Received 24 August 1989)

Two problems of similar mathematical structure are studied: the thermocapillary motion of bubbles and the electrophoresis of colloidal particles. The thermocapillary motion induced in a cloud of bubbles by a uniform temperature gradient is investigated under the assumptions that the bubbles are all the same size, that the surface tension is high enough to keep the bubbles spherical, and that the bubbles are non-conducting. In the electrophoresis problem, the particles, identical spheres having a uniform zeta potential, are suspended in an electrolyte under conditions that make the diffuse charge cloud around each particle small when compared with the particle radius. For both problems, it is shown that in a cloud of n particles surrounded by an infinite expanse of fluid, the velocity of each sphere under creeping flow conditions is equal to the velocity of an isolated particle, unchanged by interactions between the particles. However, when the cloud fills a container, conservation of mass shows that this result cannot continue to hold, and the average translational velocity must be calculated subject to a constraint on the mass flux. The computation requires 'renormalization', but it is shown that the renormalization procedure is ambiguous in both problems. An extension of Jeffrey's (1974) second group expansion, together with the constraint of conservation of mass, removes the ambiguity. Finally, it is shown that the average thermocapillary or electrophoretic translational velocity of a particle in the cloud is related to the effective conductivity of the cloud over the whole range of particle volume fractions, provided that the particles are identical, non-conducting and, for the thermocapillary problem, inviscid.

1. Introduction

If a temperature gradient is applied to a viscous fluid containing bubbles, the bubbles move towards the hotter fluid, owing to the dependence of surface tension on temperature. Similarly, if an electric field is applied to an electrolytic solution containing charged particles, the particles move in directions dictated by their charge. Under conditions described below, the problems of thermocapillary motion and electrophoresis are mathematically similar, the governing equations being the same except for one boundary condition. We wish to calculate the average velocity of a particle in a cloud (we shall understand the word 'particle' to encompass bubbles as well) when the cloud is placed in a uniform gradient of temperature or electric potential and the particle concentration is low. The problem has several features in common with that of calculating the average settling velocity of a particle in a

sedimenting cloud, a problem that was the subject of a paper by Professor Batchelor (Batchelor 1972) that gave a strong stimulus to research on the mechanics of suspensions. Its significance lay not just in its calculation of a sedimentation velocity, but equally in the way it addressed wider themes, such as the use of statistical methods to calculate average properties of suspensions and the solution of a subtle technical problem, namely how to express the average properties of a suspension of particles in terms of convergent integrals. The success of this and later work on the mechanics of suspensions, together with parallel progress on other flow systems containing small lengthscales, lead Batchelor (1976) to identify a new branch of specialization in fluid mechanics: microhydrodynamics.

One of the technical difficulties that must be solved during a calculation of the bulk properties of a suspension is the appearance of non-convergent integrals in various formal expressions for the quantities of interest, such as the average sedimentation velocity of the particles or the effective viscosity of a suspension. Earlier workers had already noted and tackled this difficulty (Burgers 1942; Pyun & Fixman 1964; see also references in Jeffrey 1977), and so its widespread occurrence was known when Batchelor (1972) published his method for overcoming it. Because of this, the new method, later called renormalization, was quickly applied to other problems (for example, Batchelor & Green 1972; Jeffrey 1973; Chen & Acrivos 1978). In addition, the method attracted a great deal of examination for its own sake, and was later refined and extended in many different ways (Jeffrey 1974; Willis & Acton 1976; McCoy & Beran 1976; Goddard 1977; O'Brien 1979; Felderhof, Ford & Cohen 1982).

Several concerns can be identified in the papers that reanalysed Batchelor's method of renormalization. The first was whether renormalization was of physical or mathematical significance. It must be remembered that both Rayleigh (1892) and Einstein (1906) had evaluated non-convergent sums or integrals in the course of deriving firmly established results, and consequently non-convergence seemed to some to be a purely mathematical issue and to others a detail requiring just some additional physical justification. Thus the first notable feature of the new approach was its stress on the *necessity* of renormalization. In this regard, an important benefit of tackling the sedimentation problem first (rather than, say, the viscosity problem) was the fact that the integrals were always infinite, and a discussion of 'physically significant' evaluations was impossible.

A second concern, closely related to the first, was a desire to simplify a key step in the original analysis which entailed looking 'for a quantity whose mean is known exactly from some overall condition or constraint in the specification of the problem and whose value at $\boldsymbol{x}_0$ [the position of a test particle – notation similar to Batchelor's is defined in §3] has the same long-range dependence on the presence of a sphere at $\boldsymbol{x}_0+\boldsymbol{r}$ as the velocity of the test sphere; and, once found, the difference between $\bar{\boldsymbol{U}}$ [the sedimentation velocity] and the mean of this quantity can be expressed as an integral...which can be legitimately...evaluated explicitly.' This description and the finding of renormalizing quantities were not easy to grasp, and even rereading Batchelor (1972) today, one is struck by the difficulty of some of the ideas; who, for example, would find it obvious to choose the divergence of the deviatoric stress for use in Batchelor's equation (3.10)?

In fact, a discussion of the physical differences between a cloud of particles that fills a container and one that is surrounded by clear fluid appears as early as the second paragraph of Batchelor (1972), and this is the essence of a physical interpretation. Nevertheless, renormalization was presented as a means of removing a convergence problem which had a physical interpretation, rather than as a means

of accounting for backflow that had a mathematical formulation. Similarly, although it was clearly expected that the renormalizing quantity would be physically related to the integrand being renormalized, it was not until Jeffrey (1974) that a methodology was introduced that enforced this requirement systematically. The inadequacy of the purely mathematical interpretation was clearly displayed when a problem was discovered in which several choices of the renormalizing quantity appeared to be possible (Chen & Acrivos 1978), a problem we discuss below.

Another reason why Batchelor's method was re-examined stemmed from issues connected with the distinction between the value of the external field applied to the suspension and the mean value of that field within the suspension. Ever since the investigation of effective viscosity by Einstein (1906), the possible difference between the applied field – in other words, the field 'at infinity' – and the mean field had been a point of debate. Investigators studying the electrostatic and elastostatic properties of dispersions of particles could formulate problems in which the suspension was surrounded by clear fluid or matrix, and thereby they could separate the applied and the mean fields. For sedimentation, however, the very nature of the problem made it necessary to deal with a space-filling suspension from the outset, leaving these issues unresolved. They were addressed in subsequent work (cited above) and the results obtained by Batchelor verified; and although the original method has now been filled out in completeness and rigour, it has yet to be replaced by an approach that is simpler or more direct, at any rate for problems to which it is suited.

Batchelor's 1972 paper stimulated work in other ways as well. It drew attention to the difference between the sedimentation of a random dispersion of freely moving spheres, the sedimentation of a periodic array of spheres and the flow through a random array of fixed spheres. The last case is a 'strong interaction' problem that cannot be solved by Batchelor's method, and the efforts to understand this and find an alternative method lead to the averaged-equation approach (Childress 1972; Saffman 1973; Howells 1974; Hinch 1977). It is interesting to note that the new approach had first to explain Batchelor's method in its own terms (Hinch 1977). Finally, it is instructive to list the topics not treated in the original paper which received attention in later years. For example, the paper contains comments on the importance of particle motions for the probability distribution for the particle positions, even though in the actual calculation, specific distributions were simply assumed. This lead was taken up by many later papers, and the motions of pairs of particles under the influence of hydrodynamic and non-hydrodynamic forces have been explored in detail. Other extensions to the original investigation include the addition of non-hydrodynamic effects, such as Brownian motion, the effects of unequal sizes and of inhomogeneous conditions.

It is a tribute to Batchelor's idea that a new problem should be discovered that leads us to re-examine the basis of his method. This problem, which concerns the thermocapillary motion or electrophoresis of particles, brings a new element into the analysis and adds another example of a well-known difficulty. The new element concerns the 'applied field'. Specifically, when Jeffrey (1974) presented a general treatment of Batchelor's renormalization, all the problems known at that time could be summarized symbolically in terms of a quantity $\boldsymbol{S}$ to be averaged and a quantity $\boldsymbol{H}$ – the applied field – whose average was known. In the thermocapillary and electrophoretic problems, however, there are two quantities whose averages are specified and which determine the velocities of the particles, because both the applied field (electric or thermal) and the volume flux across any boundary spanning the suspension are known and can be used as renormalizing quantities. The well-known

difficulty is the possibility, first discovered by Chen & Acrivos (1978), that a study of two-particle interactions may not be sufficient to prove which of several choices gives the correct renormalization strategy.

The study of thermocapillary phenomena has taken on new significance with the development of the space shuttle and the opportunities for experimenting and manufacturing under near-weightless conditions. For example, unwanted gas bubbles in a mixture are usually removed by buoyancy forces, but this force is not available in an orbiting laboratory. In fact, even on Earth a viscous fluid can retain bubbles for a significant length of time if the bubbles are small enough, and under near-weightless conditions forces other than buoyancy must be found to move bubbles, which is why thermocapillary forces are of interest. The motion of a single bubble was studied by Young, Goldstein & Block (1959) and the motion of two bubbles by Meyyappan, Wilcox & Subramanian (1983), Meyyappan & Subramanian (1984), Anderson (1985*a*) and Feuillebois (1989). All of these two-bubble papers noted the remarkable result that two equi-sized bubbles move with the same velocity as one bubble; Meyyappan *et al.* (1983) showed this numerically for the case of axisymmetric motion and Feuillebois proved it analytically, while Meyyappan & Subramanian and Anderson showed that, for bubbles at any angle to the applied temperature gradient, the result was true to the order to which they carried out their approximations. The study of electrophoretic phenomena, on the other hand, has important applications in areas concerned with the fractionation of mixtures of proteins or biological cell populations. Recall that electrophoresis has a venerable history, beginning with the work of Smoluchowski in the early part of this century; see Hunter (1981) for an extensive discussion of particle electrophoresis. But, for our purpose, the work of Reed & Morrison (1976) is especially noteworthy in that they showed that two identical spheres with thin double layers would move with the same velocity in an electric field as one sphere (the Smoluchowski velocity), irrespective of their separation and orientation in the electric field.

In what follows, we shall extend the studies referred to above and explore their consequences for the averaging of thermocapillary and electrophoretic velocities in clouds of particles. The presentation is organized as follows. For the sake of simplicity, we first concentrate on the thermocapillary problem and then show how the electrophoresis problem can be addressed using the same mathematics. Thus, in §2 thermocapillary motion is discussed in detail and we show how particles in a cloud translate with the same velocity that one bubble would have if it were all alone. Thermocapillary motion of a space-filling cloud and the effect of backflow are then taken up in §3 where the renormalization ambiguity is set forth in detail. Next, the formal series for the many-body interactions is developed in §4, where we discover how to reduce the integral based on three-body interactions to one based on two-body interactions. Once the thermocapillary problem has been discussed, it is a simple matter to show how the analysis can be adapted for electrophoresis. This is done in §5 where we show that particles in a cloud of identical spheres move at the same velocity as an isolated sphere. In §6, we derive a surprising result which relates uniquely the average thermocapillary or electrophoretic velocity of a test particle to the effective conductivity of the suspension over the whole range of the particle concentration c. The paper concludes with a discussion in §7.

2. Equations of motion

Consider, first, a bubble in an infinite expanse of fluid of viscosity μ and density ρ, in which a uniform, constant temperature gradient $\boldsymbol{H}$ far from the bubble is

imposed. Let the surface tension of the interface between the bubble and the fluid be γ. and assume that γ decreases linearly with temperature T, and that the surface tension is high enough to keep the bubble spherical (of radius a). Then, as shown by Young *et al.* (1959), the bubble moves with a velocity

$$\boldsymbol{U}_{\mathrm{YGB}} = -a\frac{\mathrm{d}\gamma}{\mathrm{d}T}\frac{\boldsymbol{H}}{2\mu},$$

under the assumptions of low Reynolds number

$$R = \rho a U_{\mathrm{YGB}}/\mu,$$

and small Marangoni number

$$Ma = \frac{aU_{\mathrm{YGB}}}{\alpha} = -H\frac{\mathrm{d}\gamma}{\mathrm{d}T}\frac{a^2}{2\mu\alpha},$$

where α is the thermal diffusivity of the fluid.

We can use these results to non-dimensionalize the equations governing the temperature and velocity fields in this limit. Distances are scaled using the bubble radius a, the temperature is scaled using aH and the bubble centre is placed at the origin. We shall denote the dimensionless temperature gradient by $\boldsymbol{h} = \boldsymbol{H}/H$. The temperature field T is then determined by

$$\nabla^2 T = 0, \tag{2.1}$$

together with the boundary conditions

$$\nabla T \to \boldsymbol{h} \quad \text{as} \quad |\boldsymbol{x}| \to \infty, \tag{2.2}$$

and

$$\boldsymbol{n}\cdot\nabla T = 0 \quad \text{on} \quad |\boldsymbol{x}| = 1. \tag{2.3}$$

The velocity and pressure fields are scaled with the Young–Goldstein–Block velocity, giving

$$-\nabla p + \nabla^2 \boldsymbol{u} = 0, \tag{2.4}$$

and

$$\nabla\cdot\boldsymbol{u} = 0, \tag{2.5}$$

together with the boundary conditions

$$\boldsymbol{u} \to 0 \quad \text{as} \quad |\boldsymbol{x}| \to \infty, \tag{2.6}$$

$$\boldsymbol{u}\cdot\boldsymbol{n} = U\boldsymbol{h}\cdot\boldsymbol{n} \quad \text{on} \quad |\boldsymbol{x}| = 1, \tag{2.7}$$

and

$$\boldsymbol{\sigma}\cdot\boldsymbol{n} - \boldsymbol{n}\boldsymbol{n}\cdot\boldsymbol{\sigma}\cdot\boldsymbol{n} = 2\nabla T \quad \text{on}\, |\boldsymbol{x}| = 1. \tag{2.8}$$

In (2.7) the unknown velocity of the bubble is written as $U\boldsymbol{h}$, but since we have scaled velocities with the known solution. U will equal 1 for the single-bubble problem. The boundary condition (2.8) has been simplified from its usual form using (2.3). The solution to these equations. for $|\boldsymbol{x}| \geqslant 1$, is

$$T = \boldsymbol{h}\cdot\boldsymbol{x} - \tfrac{1}{2}\boldsymbol{h}\cdot\nabla|\boldsymbol{x}|^{-1}, \tag{2.9}$$

and

$$\boldsymbol{u} = -\tfrac{1}{4}\boldsymbol{h}\cdot\nabla^2\boldsymbol{J}, \tag{2.10}$$

where $\boldsymbol{J}$ is the Green function for the Stokes equations:

$$\boldsymbol{J}(\boldsymbol{x}) = \boldsymbol{I}/|\boldsymbol{x}| + \boldsymbol{x}\boldsymbol{x}/|\boldsymbol{x}|^3.$$

The solution can be interpreted as follows. From (2.9) we see that the response of the bubble to the temperature gradient is equivalent to adding a thermal dipole at the bubble centre. Also. a bubble held fixed in a temperature gradient exerts a force on

the fluid (Subramanian 1985), but our problem requires the bubble to be force free, and therefore it translates with whatever velocity is needed to create a cancelling force. The difference between the two flow fields is a Stokes quadrupole, which is represented by (2.10).

We now wish to consider the problem of n interacting bubbles, all of the same size, in an infinite expanse of fluid. We shall suppose that the centre of bubble p is at $\boldsymbol{r}_p$ and let $\boldsymbol{x}_p$ be a vector from the centre of that bubble to an arbitrary point $\boldsymbol{x}$, so that $\boldsymbol{x} = \boldsymbol{r}_p + \boldsymbol{x}_p$. Boundary conditions must now be applied on each surface $|\boldsymbol{x}_p| = 1$. We shall denote the velocity of bubble p by $\boldsymbol{U}_p$. The case of two bubbles (centres at $\boldsymbol{r}_1$ and $\boldsymbol{r}_2$) was studied by Anderson (1985*a*) using the method of reflections, and he found that the velocities were given by

$$\boldsymbol{U}_1 = \boldsymbol{U}_2 = \boldsymbol{h} + O(|\boldsymbol{x}_1 - \boldsymbol{x}_2|^{-8}).$$

In other words, the velocity of one sphere was unaltered by the presence of a second to the indicated order of the approximation. We begin by extending Anderson's analysis to three spheres and arrive at the equivalent result. In order to do so, we first rewrite some of his intermediate expressions in a more compact form. Anderson found that in addition to (2.9) and (2.10) he needed the velocity and temperature fields around a bubble in a quadratic temperature field, obtained from the ambient field T by evaluating $\boldsymbol{\nabla\nabla} T$ at the point $\boldsymbol{r}_p$. In dimensional variables, we can write

$$T = (\boldsymbol{\nabla\nabla} T)_p : (\boldsymbol{xx} + \tfrac{1}{9}\boldsymbol{\nabla\nabla}|\boldsymbol{x}|^{-1}), \tag{2.11}$$

$$\boldsymbol{u} = \frac{-\mathrm{d}\gamma}{\mathrm{d}T}\frac{1}{6\mu}(\boldsymbol{\nabla\nabla} T)_p : \boldsymbol{\nabla}(1 + \tfrac{1}{6}\nabla^2)\boldsymbol{J}. \tag{2.12}$$

As with the constant-temperature-gradient case, we can interpret these results using multipoles. A bubble responds to a linear temperature gradient by generating a quadrupole thermal disturbance and a stresslet (Stokes dipole) velocity disturbance. It should be noted that the stresslet flow field decays only as $|\boldsymbol{x}|^{-2}$ whereas the flow field (2.10) decays as $|\boldsymbol{x}|^{-3}$, which is why it cannot be neglected in interaction calculations.

We now consider three bubbles with centres at $\boldsymbol{r}_1, \boldsymbol{r}_2$ and $\boldsymbol{r}_3$. Starting with the bubble $\boldsymbol{r}_1$ in the temperature gradient $\boldsymbol{h}$, we find the disturbance temperature field at bubble $\boldsymbol{r}_2$ from (2.9). Letting $\boldsymbol{r}_{21} = \boldsymbol{r}_2 - \boldsymbol{r}_1$, we find

$$\boldsymbol{\nabla} T_{21} = \tfrac{1}{2}\boldsymbol{h} \cdot (3\boldsymbol{r}_{21}\boldsymbol{r}_{21}/|\boldsymbol{r}_{21}|^5 - \boldsymbol{I}/|\boldsymbol{r}_{21}|^3).$$

This ambient temperature gradient induces a thermal dipole in sphere $\boldsymbol{r}_2$ and gives it an additional velocity equal to $\boldsymbol{\nabla} T_{21}$. However, the velocity field (2.10) around sphere $\boldsymbol{r}_1$ creates an ambient velocity field at bubble $\boldsymbol{r}_2$ equal to

$$\boldsymbol{u}_{21} = -\tfrac{1}{2}\boldsymbol{h} \cdot (3\boldsymbol{r}_{21}\boldsymbol{r}_{21}/|\boldsymbol{r}_{21}|^5 - \boldsymbol{I}/|\boldsymbol{r}_{21}|^3).$$

Thus the total change in the velocity of bubble $\boldsymbol{r}_2$ is $\boldsymbol{\nabla} T_{21} + \boldsymbol{u}_{21} = 0$. We now continue the method of reflections to sphere $\boldsymbol{r}_3$.

The velocity of bubble $\boldsymbol{r}_3$ will consist of contributions from the disturbances arising from the applied temperature gradient being reflected from bubble $\boldsymbol{r}_1$ and from $\boldsymbol{r}_2$ together with the disturbances being reflected from bubble $\boldsymbol{r}_1$ to $\boldsymbol{r}_2$ and then on to $\boldsymbol{r}_3$. The last effect is the one we are interested in. We saw above that bubble $\boldsymbol{r}_1$ induces a thermal dipole in bubble $\boldsymbol{r}_2$. This will produce a change in the ambient gradient near $\boldsymbol{r}_3$ equal to

$$\tfrac{1}{2}\boldsymbol{\nabla} T_{21} \cdot (3\boldsymbol{r}_{32}\boldsymbol{r}_{32}/|\boldsymbol{r}_{32}|^5 - \boldsymbol{I}/|\boldsymbol{r}_{32}|^3).$$

Bubble $\boldsymbol{r}_3$ will therefore pick up a velocity equal to this. Also there is a relative velocity between bubble $\boldsymbol{r}_2$ and the ambient flow at $\boldsymbol{r}_2$ equal to ∇T_{21}, and this will cause a velocity disturbance at $\boldsymbol{r}_3$. The ambient velocity at $\boldsymbol{r}_3$ will be changed by

$$-\tfrac{1}{2}\nabla T_{21}\cdot(3\boldsymbol{r}_{32}\boldsymbol{r}_{32}/|\boldsymbol{r}_{32}|^5-\boldsymbol{I}/|\boldsymbol{r}_{32}|^3),$$

which cancels the temperature-gradient contribution. Finally we must consider the perturbations due to the Stokes dipole field given in (2.12). There are two contributions to this, of which the first comes from the second derivative of the temperature field (2.9) and the other from the rate-of-strain field obtained from the flow field (2.10). It has been shown by Anderson that these also cancel.

We have seen then that two and three spheres move in an applied temperature gradient with velocities unchanged from the single-sphere case. We now wish to extend this to n spheres. Returning to (2.10), we can rewrite it using standard identities as

$$\boldsymbol{u}=\tfrac{1}{2}\boldsymbol{h}\cdot\nabla\nabla|\boldsymbol{x}|^{-1}=\nabla(\tfrac{1}{2}\boldsymbol{h}\cdot\nabla|\boldsymbol{x}|^{-1}). \tag{2.13}$$

From this, we see that if we write (2.9) for the temperature field as

$$T=\boldsymbol{h}\cdot\boldsymbol{x}+\phi,$$

we can rewrite (2.10) as $\boldsymbol{u}=-\nabla\phi$. We now postulate that the last two expressions hold true for the flow around n spherical bubbles, and replace (2.1)–(2.8) with the equations

$$T=\boldsymbol{h}\cdot\boldsymbol{x}+\phi, \tag{2.14}$$

and

$$\boldsymbol{u}=-\nabla\phi, \tag{2.15}$$

where

$$\nabla^2\phi=0, \tag{2.16}$$

together with the boundary conditions

$$\nabla\phi\to 0 \quad \text{as} \quad |\boldsymbol{x}|\to\infty, \tag{2.17}$$

$$\boldsymbol{n}\cdot\nabla\phi=-\boldsymbol{h}\cdot\boldsymbol{n} \quad \text{on} \quad |\boldsymbol{x}_p|=1. \tag{2.18}$$

The velocity field (2.15) will automatically satisfy the Stokes equations with the pressure equal to zero. In addition, the kinematic condition on the spheres' surfaces, that sphere p moves with velocity $\boldsymbol{U}_p$, is

$$\boldsymbol{u}\cdot\boldsymbol{n}=\boldsymbol{U}_p\cdot\boldsymbol{n}=-\boldsymbol{n}\cdot\nabla\phi=\boldsymbol{h}\cdot\boldsymbol{n} \quad \text{on} \quad |\boldsymbol{x}_p|=1, \tag{2.19}$$

meaning $\boldsymbol{U}_p=\boldsymbol{h}$ for all p. The boundary condition left to verify is the stress boundary condition

$$-\boldsymbol{n}\cdot(\nabla\nabla\phi)+\boldsymbol{n}\boldsymbol{n}\cdot(\nabla\nabla\phi)\cdot\boldsymbol{n}=\boldsymbol{h}+\nabla\phi \quad \text{on} \quad |\boldsymbol{x}_p|=1 \tag{2.20}$$

To prove this we use an expansion of ϕ about $\boldsymbol{r}_p$, the centre of sphere p. To introduce this expansion we consider first the special case of just two spheres. The method of twin multipole expansions calculates ϕ for this case by expressing it as a superposition of multipole expansions (Jeffrey 1973). The expression for ϕ is valid everywhere outside the spheres, but it is expressed in more than one coordinate system (Jeffrey 1973, equation 5.2). The coefficients in the expansion are found by transforming it entirely into the coordinate system of one sphere using addition theorems for spherical harmonics (Jeffrey 1973, equation 5.3) and applying boundary conditions. Here, although our aim is not to calculate coefficients, but rather to verify (2.20), we can still use the transformation idea extended to n spheres. Now ϕ will be a superposition of n multipole series in decaying harmonics, with each series centred on

one of the n spheres. But each multipole series can be transferred to the centre of sphere p, where it will become a series of growing harmonics, just as can be seen in the two-sphere case. Thus ϕ can be expanded about $\boldsymbol{r}_p$ in an expansion of growing and decaying harmonics valid in a spherical shell centred at $\boldsymbol{r}_p$ whose inner surface is $|\boldsymbol{x}_p| = 1$ and whose outer surface touches the surface of the nearest neighbour to $\boldsymbol{r}_p$.

Let us denote a general decaying harmonic of order $-n-1$ by ϕ_{-n-1}. Then $|\boldsymbol{x}|^{2n+1}\phi_{-n-1}$ will be a growing harmonic of order n. We now write the expansion of ϕ about $\boldsymbol{r}_p$ as

$$\phi = -\tfrac{1}{2}\boldsymbol{h}\cdot\boldsymbol{\nabla}|\boldsymbol{x}_p|^{-1} + \sum_n [(n+1)|\boldsymbol{x}_p|^{2n+1} + n]\phi_{-n-1}. \tag{2.21}$$

In this form, (2.18) is automatically satisfied. Using the identity

$$\boldsymbol{x}_p\cdot\boldsymbol{\nabla}\phi_{-n-1} = (-n-1)\,\phi_{-n-1}, \tag{2.22}$$

together with the fact that $\boldsymbol{x}_p = \boldsymbol{n}$ on $|\boldsymbol{x}_p| = 1$, one obtains, on $|\boldsymbol{x}_p| = 1$,

$$\boldsymbol{\nabla}\phi = -\tfrac{3}{2}\boldsymbol{n}\boldsymbol{h}\cdot\boldsymbol{n} + \tfrac{1}{2}\boldsymbol{h} + \sum_n (2n+1)(n+1)\,\boldsymbol{n}\phi_{-n-1} + (2n+1)\,\boldsymbol{\nabla}\phi_{-n-1},$$

$$\boldsymbol{n}\cdot(\boldsymbol{\nabla}\boldsymbol{\nabla}\phi) = \tfrac{9}{2}\boldsymbol{n}\boldsymbol{h}\cdot\boldsymbol{n} - \tfrac{3}{2}\boldsymbol{h} + \sum_n (2n+1)(n+1)(n-1)\,\boldsymbol{n}\phi_{-n-1} - (2n+1)\,\boldsymbol{\nabla}\phi_{-n-1},$$

and

$$\boldsymbol{n}\boldsymbol{n}\cdot(\boldsymbol{\nabla}\boldsymbol{\nabla}\phi)\cdot\boldsymbol{n} = 3\boldsymbol{n}\boldsymbol{h}\cdot\boldsymbol{n} + \sum_n (2n+1)(n+1)\,n\boldsymbol{n}\phi_{-n-1},$$

whence one can easily verify that (2.20) holds. Thus the general result is proved. Incidentally, since ϕ is harmonic, (2.15) satisfies the full Navier–Stokes equations, with the pressure given by Bernouilli's equation, as long as the Marangoni number remains small. This exact solution to the thermocapillary problem was also noted earlier for the single bubble case by Crespo & Manuel (1983) and Balasubramaniam & Chai (1987).

3. The average velocity of a bubble in a cloud

Since the velocity of a bubble is unaltered by the presence of other bubbles, it might seem that there is no averaging problem to perform. Thus the first renormalization strategy would be to suppose that $\bar{\boldsymbol{U}} = \boldsymbol{U}_{\mathrm{YGB}}$. This is unsatisfactory, however, as can be shown by a physical argument. If the cloud of bubbles fills a closed container, conservation of volume (the fluid is incompressible) shows that the velocity must change, for if we take a surface through the suspensions perpendicular to the applied temperature gradient, the rate at which volume is displaced by the bubbles equals $c\boldsymbol{U}_{\mathrm{YGB}}$, where c is the volume concentration of the bubbles. Since the net flux across the surface must be zero, there must be a net backflow of fluid reducing the velocity of the bubbles by a factor $(1-c)$.

A second argument in support of renormalization comes from noting that the exact cancellation of the two velocity perturbations only occurs for non-conducting bubbles of the same size, because, as Anderson (1985*a*) showed, if the bubbles (or drops) have any conductivity, or if they differ in size, there is a familiar $1/|\boldsymbol{x}|^3$ non-convergent interaction between them. Thus, for the more general conducting-drop problem, we must renormalize, and then if we take the limit of zero conductivity, we are led to a renormalized integral, not the result $\bar{\boldsymbol{U}} = \boldsymbol{U}_{\mathrm{YGB}}$. However, although these arguments help to settle the question of whether or not renormalization is needed, we must still decide on the renormalization procedure. Recall that from the overall

specification of the problem we have constraints on $\boldsymbol{u}(\boldsymbol{r})$, the velocity at the origin due to a bubble at $\boldsymbol{r}$, and $\nabla T(\boldsymbol{r})$, the temperature gradient at the origin. They are

$$\int \boldsymbol{u} P(\boldsymbol{r})\,\mathrm{d}\boldsymbol{r} = 0 \quad \text{and} \quad \int (\nabla T - \bar{\boldsymbol{H}}) P(\boldsymbol{r})\,\mathrm{d}\boldsymbol{r} = 0.$$

Both of these are non-convergent integrals that cannot be evaluated. From the results above, however, it can be shown that the two integrands have the same dependence on r when the bubbles do not overlap the origin ($r > 1$), but they are different when the bubbles overlap the origin. Therefore the integral

$$\int ([\boldsymbol{U}(r) - \boldsymbol{U}_{\mathrm{YGB}}] P(\boldsymbol{r}|0) - [\lambda_1 \boldsymbol{u} + \lambda_2 (\nabla T - \bar{\boldsymbol{H}})] P(\boldsymbol{r}))\,\mathrm{d}\boldsymbol{r}$$

will be convergent for any value of λ_1, provided $\lambda_1 = \lambda_2$, since both terms in brackets will then be zero for $r > 2$. The expression evaluates to $-\frac{3}{2}\lambda_1 c \bar{\boldsymbol{H}}$ and therefore the mean velocity of the particles in the suspension is

$$(1 - \tfrac{3}{2}\lambda_1 c)\, \boldsymbol{U}_{\mathrm{YGB}}$$

if the particles are non-conducting. Anderson's result is obtained by setting $\lambda_1 = 1$. In fact, even when the particles are conducting or have different sizes, there still exists an indeterminacy, because λ_1 and λ_2 must satisfy only one equation, namely that the non-convergent terms in the two sets of brackets cancel. Analogous considerations hold for particles undergoing electrophoresis (Anderson 1986).

Chen & Acrivos (1978) discovered a similar indeterminate situation, by finding several possible convergent two-body integrals. As here, the integral could apparently be put in a convergent form without renormalization and two renormalized integrals were found. Since these authors were able to resolve the indeterminacy by considering three-body interactions, where only one choice gave a convergent integral, we now extend the group expansion approach of Jeffrey (1974) to include the extra field present, in order to investigate the properties of the expansion and resolve the indeterminacy.

4. Formal series for three-body interactions

In order to write down the integral for three-body interactions, we must add to the notation in Jeffrey (1974) the fact that the velocity of a bubble in the laboratory frame now depends upon two applied fields, viz. the ambient temperature gradient and the ambient velocity. We begin by considering a test bubble at the origin surrounded by n others, the whole cloud being immersed in a temperature gradient $\bar{\boldsymbol{H}}$ and an ambient velocity $\bar{\boldsymbol{u}}$. At the end of the calculation, we shall set $\bar{\boldsymbol{u}}$ to zero, but we have seen in the method-of-reflections solution above that we must consider changes in the ambient flow. We shall write $\boldsymbol{U}(\mathscr{C}_n; \bar{\boldsymbol{H}}; \bar{\boldsymbol{u}})$ as the general notation for the velocity of the test bubble, $\mathscr{C}_n$ being the set of position vectors $\boldsymbol{r}_p$ of the other bubbles. We define incremental velocities in the manner of Jeffrey (1974). Thus $\boldsymbol{U}_0(;\bar{\boldsymbol{H}};\bar{\boldsymbol{u}})$ is the velocity of a single sphere in an ambient temperature gradient $\bar{\boldsymbol{H}}$ and a velocity field $\bar{\boldsymbol{u}}$. With suitable non-dimensionalization we know

$$\boldsymbol{U}_0(;\bar{\boldsymbol{H}};\bar{\boldsymbol{u}}) = \bar{\boldsymbol{H}} + \bar{\boldsymbol{u}}.$$

We next consider the test bubble at the origin with a second bubble (a first neighbour) at $\boldsymbol{r}_1$. The velocity of the test bubble is now $\boldsymbol{U}(\boldsymbol{r}_1;\bar{\boldsymbol{H}};\bar{\boldsymbol{u}})$. From this we define the increment $\boldsymbol{U}_1$ due to the second sphere as

$$\boldsymbol{U}_1(\boldsymbol{r}_1;\bar{\boldsymbol{H}};\bar{\boldsymbol{u}}) = \boldsymbol{U}(\boldsymbol{r}_1;\bar{\boldsymbol{H}};\bar{\boldsymbol{u}}) - \boldsymbol{U}_0(;\bar{\boldsymbol{H}};\bar{\boldsymbol{u}}).$$

Now since two bubbles respond to an ambient velocity $\bar{\boldsymbol{u}}$ by each increasing its velocity by the same speed $\bar{\boldsymbol{u}}$, it follows that U_1 is independent of $\bar{\boldsymbol{u}}$. Therefore

$$U_1(\boldsymbol{r}_1;\bar{\boldsymbol{H}};\bar{\boldsymbol{u}}) = U_1(\boldsymbol{r}_1;\bar{\boldsymbol{H}};0) = U(\boldsymbol{r}_1;\bar{\boldsymbol{H}};0) - U_0(;\bar{\boldsymbol{H}};0).$$

In addition we have seen that two bubbles move at the same speed as one, so in this problem $U_1 = 0$, but in general this would not be so.

The continuation to a third bubble (neighbours at $\boldsymbol{r}_1$ and $\boldsymbol{r}_2$) uses the obvious notation

$$U_2(\boldsymbol{r}_1\boldsymbol{r}_2;\bar{\boldsymbol{H}};\bar{\boldsymbol{u}}) = U(\boldsymbol{r}_1\boldsymbol{r}_2;\bar{\boldsymbol{H}};\bar{\boldsymbol{u}}) - U_1(\boldsymbol{r}_1;\bar{\boldsymbol{H}};\bar{\boldsymbol{u}}) - U_1(\boldsymbol{r}_2;\bar{\boldsymbol{H}};\bar{\boldsymbol{u}}) - U_0(;\bar{\boldsymbol{H}};\bar{\boldsymbol{u}}).$$

Again we see that U_2 is independent of $\bar{\boldsymbol{u}}$ and, for our bubble problem, is actually identically zero.

The first group expansion is the generalization of the non-renormalized integral. It consists simply of averaging the velocity increments just defined:

$$\bar{U} = U_0 + \int U_1(\boldsymbol{r}_1;\bar{\boldsymbol{H}};\bar{\boldsymbol{u}})\,P(\boldsymbol{r}_1|0)\,\mathrm{d}\boldsymbol{r}_1 + \iint U_2 P(\boldsymbol{r}_1\boldsymbol{r}_2|0)\,\mathrm{d}\boldsymbol{r}_1\,\mathrm{d}\boldsymbol{r}_2 + \ldots.$$

Since $U_1 = U_2 = 0$, etc. we again arrive at the unphysical result $\bar{U} = U_0 = U_{\mathrm{YGB}}$. This is different from the previously known case of Chen & Acrivos (1978) in which the expansion broke down visibly at the three-body term by giving a non-convergent integral.

The second group expansion corresponds to generalizing the renormalized integral. To introduce the notation required to write this down, we shall ignore for the moment the fact that $U_1 = U_2 = 0$. It is not true in the more general case of drops with non-zero conductivity, and we need to write down the general asymptotic relations which hold when the spheres are far apart in order to obtain the second expansion. The latter is obtained by rewriting the method-of-reflections results above in a general notation. To do this we need a notation for fields near the origin produced by distant spheres. Consider first a sphere by itself at $\boldsymbol{r}_1$. The temperature gradient at the origin is $\boldsymbol{H}(\boldsymbol{r}_1;\bar{\boldsymbol{H}})$, meaning the field produced by a sphere at $\boldsymbol{r}_1$ immersed in an ambient gradient $\bar{\boldsymbol{H}}$. When there are no spheres present, the field at the origin is just the applied field $\bar{\boldsymbol{H}}$, so we can define an increment in $\boldsymbol{H}$ to be $\boldsymbol{H}_1(\boldsymbol{r}_1;\bar{\boldsymbol{H}}) = \boldsymbol{H}(\boldsymbol{r}_1;\bar{\boldsymbol{H}}) - \bar{\boldsymbol{H}}$. This is the field $\frac{1}{2}\nabla(1/|\boldsymbol{x}|)$ given in (2.9). The velocity field at the origin is $\boldsymbol{u}(\boldsymbol{r}_1;\bar{\boldsymbol{H}};\bar{\boldsymbol{u}})$, meaning a sphere at $\boldsymbol{r}_1$ moving because of the field $\bar{\boldsymbol{H}}$ and ambient flow $\bar{\boldsymbol{u}}$. Again there will be a velocity increment:

$$\boldsymbol{u}_1(\boldsymbol{r}_1;\bar{\boldsymbol{H}};\bar{\boldsymbol{u}}) = \boldsymbol{u}(\boldsymbol{r}_1;\bar{\boldsymbol{H}};\bar{\boldsymbol{u}}) - \bar{\boldsymbol{u}}.$$

This will be independent of $\bar{\boldsymbol{u}}$, so

$$\boldsymbol{u}_1(\boldsymbol{r}_1;\bar{\boldsymbol{H}};\bar{\boldsymbol{u}}) = \boldsymbol{u}_1(\boldsymbol{r}_1;\bar{\boldsymbol{H}};0).$$

The two-body integral of the second group expansion is now the obvious generalization of Jeffrey (1974):

$$\int\{U_1(\boldsymbol{r}_1;\bar{\boldsymbol{H}};\bar{\boldsymbol{u}})\,P(\boldsymbol{r}_1|0) - U_0(;\boldsymbol{H}_1(\boldsymbol{r}_1;\bar{\boldsymbol{H}});\boldsymbol{u}_1(\boldsymbol{r}_1;\bar{\boldsymbol{H}};0))\,P(\boldsymbol{r}_1)\}\,\mathrm{d}\boldsymbol{r}_1.$$

This is the integral evaluated by Anderson. Since U_1 is zero, it reduces to a one-particle integral and gives the result

$$\bar{U} = (1-\tfrac{3}{2}c)\,U_{\mathrm{YGB}}.$$

We now need to consider two spheres far from the test sphere. We can extend our notation in the obvious way. $\boldsymbol{H}_2(\boldsymbol{r}_1\boldsymbol{r}_2;\bar{\boldsymbol{H}})$ is the increment at the origin due to spheres at $\boldsymbol{r}_1$ and $\boldsymbol{r}_2$, while $\boldsymbol{u}_2(\boldsymbol{r}_1\boldsymbol{r}_2;\bar{\boldsymbol{H}};\bar{\boldsymbol{u}})$ is the increment in the fluid velocity at the origin.

We shall not repeat the elaborate asymptotic arguments needed to establish the three-body term in the second (renormalized) expansion, but write it down as the obvious extension of Jeffrey (1974). It is

$$\int\{U_2(\boldsymbol{r}_1\boldsymbol{r}_2;\bar{\boldsymbol{H}};\bar{\boldsymbol{u}})P(\boldsymbol{r}_1\boldsymbol{r}_2|0)-\boldsymbol{U}_1(\boldsymbol{r}_1;\boldsymbol{H}_1(\boldsymbol{r}_2;\bar{\boldsymbol{H}});\boldsymbol{u}_1(\boldsymbol{r}_2;\bar{\boldsymbol{H}};0))P(\boldsymbol{r}_1|0)P(\boldsymbol{r}_2)$$
$$-\boldsymbol{U}_0(;\boldsymbol{H}_2(\boldsymbol{r}_1\boldsymbol{r}_2;\bar{\boldsymbol{H}});\boldsymbol{u}_2(\boldsymbol{r}_1\boldsymbol{r}_2;\bar{\boldsymbol{H}};0))P(\boldsymbol{r}_1\boldsymbol{r}_2)$$
$$+\boldsymbol{U}_0(;\boldsymbol{H}_1(\boldsymbol{r}_1;\boldsymbol{H}_1(\boldsymbol{r}_2;\bar{\boldsymbol{H}}));\boldsymbol{u}_1(\boldsymbol{r}_1;\boldsymbol{H}_1(\boldsymbol{r}_2;\bar{\boldsymbol{H}});0))P(\boldsymbol{r}_1)P(\boldsymbol{r}_2)\}\,\mathrm{d}\boldsymbol{r}_1\,\mathrm{d}\boldsymbol{r}_2.$$

We can now integrate over $\boldsymbol{r}_1$ and $\boldsymbol{r}_2$ and obtain the $O(c^2)$ term. First we simplify. We know that $\boldsymbol{U}_2=\boldsymbol{U}_1=0$. So we need consider only the last two terms.

Since $\boldsymbol{u}=-\nabla\phi$ outside the particles, the third term $\boldsymbol{U}_0(;\boldsymbol{H}_2;\boldsymbol{u}_2)$ will be zero unless one of the particles overlaps the origin, and in that case $\boldsymbol{u}_2=0$ because the velocity of two bubbles equals the velocity of one particle. Therefore the third term is non-zero only if $|\boldsymbol{r}_1|\leqslant 1$, when we have

$$-\boldsymbol{U}_0(;\boldsymbol{H}_2;\boldsymbol{u}_2)P(\boldsymbol{r}_1\boldsymbol{r}_2)=-\boldsymbol{H}_2(\boldsymbol{r}_1\boldsymbol{r}_2;\bar{\boldsymbol{H}})P(\boldsymbol{r}_2|\boldsymbol{r}_1)P(\boldsymbol{r}_1).$$

Now we perform the integration by fixing $\boldsymbol{r}_2-\boldsymbol{r}_1=\boldsymbol{s}$ and integrating first over $\boldsymbol{r}_1$ followed by integration over $\boldsymbol{s}$. The integral over $\boldsymbol{r}_1$ is just the volume integral of $\boldsymbol{H}_2$ over the spherical bubble, which equals the thermal dipole strength of the bubble $\boldsymbol{S}_1$. The integral becomes

$$\iint\boldsymbol{H}_2(\boldsymbol{r}_1\boldsymbol{r}_2;\bar{\boldsymbol{H}})P(\boldsymbol{r}_1\boldsymbol{r}_2)\,\mathrm{d}\boldsymbol{r}_1\,\mathrm{d}\boldsymbol{r}_2=\int\boldsymbol{S}_1(\boldsymbol{r}_2;\bar{\boldsymbol{H}})P(\boldsymbol{r}_2|\boldsymbol{r}_1)\,\mathrm{d}\boldsymbol{r}_2.$$

Finally the last term in the three-body integral can be treated the same way to become

$$\int\boldsymbol{S}_0(;\boldsymbol{H}_1(\boldsymbol{r}_2;\bar{\boldsymbol{H}}))P(\boldsymbol{r}_2)\,\mathrm{d}\boldsymbol{r}_2.$$

Hence the three-body velocity problem reduces to the two-body heat conduction problem. In §6, we shall show that this is part of a more general result.

5. The electrophoresis problem

To show that much of the analysis and all of the conclusions derived thus far for thermocapillarity apply equally well to charged spheres moving through an electrolyte in an electric field we first recall that a single, non-conducting sphere moves in a uniform electric field $\boldsymbol{E}$ at the Smoluchowski velocity

$$\boldsymbol{U}_s=\frac{\epsilon\epsilon_0\zeta}{\mu}\boldsymbol{E} \tag{5.1}$$

as long as the double layer is thin (cf. Hunter 1981). Here ϵ is the dielectric constant of the suspending fluid, ϵ_0 is the permittivity of free space, ζ is the electrostatic potential at the surface of the particle (the zeta potential), and μ is as before the viscosity of the suspending electrolyte. Equation (5.1) applies when the particle motion is slow and the diffuse charge thickness (the Debye length κ^{-1}) is small compared with the particle radius a. Viewed on the lengthscale of the particle, fluid appears to slip past the surface at a speed known as the electro-osmotic slip velocity. However, when the details within the thin region adjacent to the surface are resolved by, for example, singular perturbation methods, the no-slip condition holds and the velocity in the diffuse region joins smoothly to that outside. Inside the diffuse layer the Stokes equations must be modified by adding a term to account for the electrostatic body force on the fluid due to the action of the field on the space charge.

For thin double layers and non-conducting particles, however, we can avoid analysing events within the diffuse layer in a consistent fashion by replacing the no-slip condition by

$$\boldsymbol{U} = \boldsymbol{u} - \frac{\epsilon\epsilon_0\zeta}{\mu}\nabla\psi \tag{5.2}$$

and using the Stokes equations without the extra body force. Here $\boldsymbol{U}$ denotes the particle velocity, $\boldsymbol{u}$ is the fluid velocity, and $-\nabla\psi$ is the local value of the electric field (Anderson 1985*b*; Russel, Saville & Schowalter 1989).

The electric field is governed by solutions of Laplace's equation with the normal gradient equal to zero at a particle surface (non-conducting particles). Inside each particle, Laplace's equation applies and the two fields are continuous at the interface. The potential gradient is constant, i.e. $-\nabla\psi \to E\boldsymbol{h}$, far from the particle, while the velocity and pressure fields follow from solutions of Stokes equations with the velocity vanishing far from the particle. The boundary condition at the particle surface, (5.2), shows that the normal velocity of fluid and particle match at the surface.

Now, the electrophoresis problem can be restated in a form analogous to that used in §2 for thermocapillary motion. First, scale the potential on $(-aE)$ and recover (2.1)–(2.3) to describe the dimensionless potential outside the sphere. Next scale the velocity on the Smoluchowski velocity, $\epsilon\epsilon_0\zeta E/\mu$, to obtain (2.4) and (2.5). The boundary condition (2.6) still holds but in place of (2.7) and (2.8) we use the dimensionless form of (5.2), namely

$$\boldsymbol{U} = \boldsymbol{u} + \nabla T. \tag{5.3}$$

It follows immediately that the dimensionless potential and velocity are given by (2.9) and (2.10).

With these results for a single sphere in hand we can investigate the electrophoresis of two identical spheres. Here, as long as the separation exceeds the Debye thickness, the spheres move at the Smoluchowski velocity irrespective of their separation and orientation (Reed & Morrison 1976). This result also holds for n identical spheres (Zukoski 1984), as can be seen using the arguments given at the end of §2 if (2.8) is replaced by

$$U_p\boldsymbol{h} = \boldsymbol{u} + \nabla T \quad \text{on} \quad |\boldsymbol{x}_p| = 1. \tag{5.4}$$

It follows that $U_p = 1$ and the expansion for ϕ in the harmonic series noted earlier holds. Accordingly, we have the somewhat surprising result that each particle in a cloud of spheres undergoing electrophoresis moves at the same velocity.

6. Equivalence of the migration velocity and the effective conductivity

It was shown in §4 that the integral giving the three-body correction to the thermocapillary or the electrophoretic migration velocity can be reduced to the integral giving the two-body correction to the effective conductivity of the suspension. Here we shall derive a remarkable result that the migration velocity can be obtained simply from the effective thermal conductivity of the suspension of non-conducting particles for all particle concentrations. Specifically, taking the gradient of (2.14), we observe that

$$\nabla T = \boldsymbol{h} + \nabla\phi, \tag{6.1}$$

and averaging this over the volume of the suspension V, we obtain

$$\frac{1}{V}\int_V \nabla T \,\mathrm{d}V = \boldsymbol{h}. \tag{6.2}$$

Splitting the domain of integration into V_f, the part of V occupied by fluid, and V_p, the part occupied by particles, we arrive at

$$\boldsymbol{h} = (1-c)\,\boldsymbol{h} + \frac{1}{V}\int_{V_f} \nabla\phi \,\mathrm{d}V + \frac{1}{V}\int_{V_p} \nabla T \,\mathrm{d}V. \tag{6.3}$$

In the notation of Jeffrey (1973), the last integral is simply equal to $-c\bar{\boldsymbol{S}}$, the average thermal dipole strength of the particles.

Before we can average (2.15) we must remember that this is for particles in an infinite fluid, whereas in a container a backflow $\boldsymbol{U}_B$ will exist which must be included in the equation. Thus (2.15) is replaced by

$$\boldsymbol{u}(\boldsymbol{x}) = -\nabla\phi + \boldsymbol{U}_B, \quad \text{when } \boldsymbol{x} \text{ is outside a particle,} \tag{6.4a}$$

$$\boldsymbol{u}(\boldsymbol{x}) = \bar{\boldsymbol{U}} = \boldsymbol{h} + \boldsymbol{U}_B, \quad \text{when } \boldsymbol{x} \text{ is inside a particle.} \tag{6.4b}$$

Averaging this equation, we obtain

$$\bar{\boldsymbol{u}} = 0 = -\frac{1}{V}\int_{V_f} \nabla\phi \,\mathrm{d}V + (1-c)\,\boldsymbol{U}_B + c\bar{\boldsymbol{U}}. \tag{6.5}$$

Using (6.3) to eliminate the unknown integral from (6.5) and then using (6.4*b*) to eliminate $\boldsymbol{U}_B$ from (6.5), we obtain

$$\bar{\boldsymbol{U}} = \boldsymbol{h} + c\bar{\boldsymbol{S}} = \boldsymbol{K}^* \cdot \boldsymbol{h},$$

where $\boldsymbol{K}^*$ is the effective conductivity of the medium. It should be noted that this result holds for any particle concentration, and allows us to use not only the existing direct calculations of $\boldsymbol{K}^*$ but also bounds on the effective conductivity, such as the Hashin–Shtrikman bounds (Hashin & Shtrikman 1962) or more recently developed expressions (Torquato 1987). For example, using the results for an isotropic well-mixed suspension given in Jeffrey (1973), we obtain

$$\bar{\boldsymbol{U}} = (1 - \tfrac{3}{2}c + 0.59c^2 + \ldots)\,\boldsymbol{h}$$

for the same suspension.

7. Discussion

The problems of electrophoresis and thermocapillarity provide an interesting challenge to the established methods for calculating the average properties of suspensions. Although it is possible to take refuge in the more general cases of conducting particles or particles of different sizes to distinguish between the alternatives here (in conjunction with the three-body problem), this is an unsatisfying solution from a general point of view since there is no guarantee that such generalizations will always be possible. Moreover, special cases are usually chosen for study because they are simpler than the general problem, so it is disappointing to have to return to a general situation in order to address the special case. One argument used successfully in the past to choose between alternative schemes consisted of appealing to higher approximations. Thus, conflicting convergent integral expressions for the two-body interaction were resolved by extending the analysis to three-body schemes. It seemed from the case of Chen & Acrivos (1978) that the second group expansion of Jeffrey (1974) would always be able to distinguish between different possible treatments of the two-body problem by jumping to the three-body problem (another example of generalizing the problem). The particle

problems studied here, however, show that this is not so, because the entire series for the first and second group expansions can be searched without finding an integral that converges in one case but not the other. Thus if we do not wish to leave the confines of the non-conducting particle problem, there is only the argument based on conservation of mass to choose between the mathematically possible alternatives.

Experimental tests of the theory for the thermocapillary or electrophoretic velocity of particles in a suspension are extremely difficult. To begin with, problems arise because of buoyancy and polydispersity. In addition most systems become opaque well before the particle number density is large enough to influence the average translational velocity and this makes it hard to measure the speed of individual particles. Nevertheless, Zukoski & Saville (1987, 1989) were able to prepare neutrally buoyant, transparent suspensions by removing the hemoglobin from red blood cells. A variety of particle shapes could be formed. Then tracer particles with the same electrokinetic properties as the red-blood-cell ghosts could be tracked microscopically over a wide range of particle concentrations. Zukoski & Saville measured the electrophoretic mobility of individual particles and the effective conductivity of the suspension over volume fractions ranging between 0 and 0.8. The effective conductivity was found to follow the Maxwell relation for slightly conducting particles while the mobility varied as $(1-c)$ up to the highest volume fractions. The reasons for the difference between their results and the theory developed here are unclear. It may be due to the slight conductivity of the particles, but further work is obviously necessary.

Andreas Acrivos acknowledges the support of the National Science Foundation under Grant No. CTS-8803048, David Jeffrey the support of the Natural Science and Engineering Research Council of Canada, and Dudley Saville the support of the NASA Microgravity Sciences Program under its Grant No. NAG 8-597. The authors thank Dr E. J. Hinch and Professor R. S. Subramanian for comments on an earlier draft of this paper.

Postscript

The references in the text acknowledge formally the influence Professor Batchelor had on this work, but, less formally, the interplay between physical and mathematical arguments discussed in this paper brings to the mind of one of us (D.J.J.) an exchange that took place during a seminar at Cambridge in the mid 1970s.

SPEAKER (justifying elaborate mathematical argument): The trouble with a physical argument is that you may not get all the terms.

GKB: No, that is the trouble with a *bad* physical argument.

SEVERAL VOICES: How do you tell a good physical argument from a bad one?

GBK: That's easy: you *think*.

REFERENCES

ANDERSON, J. L. 1985*a* Droplet interactions in thermocapillary motion. *Intl J. Multiphase Flow* **11**, 813–824.

ANDERSON, J. L. 1985*b* Effect of a non-uniform zeta potential on particle movement in electric fields. *J. Colloid Interface Sci.* **105**, 45–54.

ANDERSON, J. L. 1986 Transport mechanisms of biological colloids. *Ann. NY Acad. Sci.* **469**, 166–177.

BALASUBRAMANIAM, R. & CHAI, AN-TI 1987 Thermocapillary migration of droplets: an exact solution for small Marangoni numbers. *J. Colloid Interface Sci.* **119**, 531–538.

BATCHELOR, G. K. 1972 Sedimentation in a dilute dispersion of spheres. *J. Fluid Mech.* **52**. 245–268.

BATCHELOR, G. K. 1976 Developments in microhydrodynamics. In *Theoretical and Applied Mechanics* (ed. WT Koiter). pp. 33–55. North-Holland.

BATCHELOR, G. K. & GREEN, J. T. 1972 The determination of the bulk stress in a suspension of spherical particles to order c^2. *J. Fluid Mech.* **56**. 401–427.

BURGERS, J. M. 1942 On the influence of the concentration of a suspension upon the sedimentation velocity. *Proc. Kon. Nederl. Akad. Wet.* **44**. 1045. 1177; and **45**. 9. 126.

CHEN, H. S. & ACRIVOS, A. 1978 The effective elastic moduli of composite materials containing spherical inclusions at non-dilute concentrations. *Intl J. Solids Structures* **14**. 349–364.

CHILDRESS, S. 1972 Viscous flow past a random array of spheres. *J. Chem. Phys.* **56**. 2527.

CRESPO, A. & MANUEL, F. 1983 Bubble motion under reduced gravity. In *Proc. 4th European Symp. on Materials Science under Microgravity. Madrid. Spain: ESA SP-191.*

EINSTEIN, A. 1906 Eine neue Bestimmung der Molekuldimension. *Ann. Phys.* **19**. 289.

FELDERHOF, B. U., FORD, G. W. & COHEN, E. D. G. 1982 Cluster expansion for the dielectric constant of a polarizable suspension. *J. Statist. Phys.* **28**. 135–164.

FEUILLEBOIS, F. 1989 Thermocapillary migration of two equal bubbles parallel to their line of centres. *J. Colloid Interface Sci.* **131**. 267–274.

GODDARD, J. D. 1977 Advances in the rheology of particulate dispersions. In *Continuum Models of Discrete Systems* (ed. J. W. Provan). pp. 605–634. University of Waterloo Press.

HASHIN, Z. & SHTRIKMAN, S. 1963 A variational approach to the theory of the effective magnetic permeability of multiphase materials. *J. Appl. Phys.* **33**. 1514–1517.

HINCH, E. J. 1977 An averaged-equation approach to particle interactions in a fluid suspension. *J. Fluid Mech.* **83**. 695–720.

HOWELLS, I. D. 1974 Drag due to motion of a Newtonian fluid through a sparse random array of small fixed rigid objects. *J. Fluid Mech.* **64**. 449–475.

HUNTER, R. J. 1981 *Zeta Potential in Colloid Science.* Academic.

JEFFREY, D. J. 1973 Conduction through a random suspension of spheres. *Proc. R. Soc. Lond.* A **335**. 355–367.

JEFFREY, D. J. 1974 Group expansions for the bulk properties of a statistically homogeneous, random suspension. *Proc. R. Soc. Lond.* A **338**. 503–516.

JEFFREY, D. J. 1977 The physical significance of non-convergent integrals in expressions for effective transport properties. In *Continuum Models of Discrete Systems* (ed. J. W. Provan). pp. 653–674. University of Waterloo Press.

MCCOY, J. J. & BERAN, M. 1976 Effective thermal conductivity of a random suspension of spheres. *Intl J. Engng Sci.* **14**. 7–18.

MEYYAPPAN, M. & SUBRAMANIAN, R. S. 1984 The thermocapillary motion of two bubbles oriented arbitrarily relative to a thermal gradient. *J. Colloid Interface Sci.* **97**. 291–294.

MEYYAPPAN, M., WILCOX, W. R. & SUBRAMANIAN, R. S. 1983 The slow axisymmetric motion of two bubbles in a thermal gradient. *J. Colloid Interface Sci.* **94**. 243–257.

O'BRIEN, R. W. 1979 A method for the calculation of the effective transport properties of suspensions of interacting particles. *J. Fluid Mech.* **91**. 17–39.

PYUN, C. W. & FIXMAN, M. 1964 Frictional coefficient of polymer molecules in solution. *J. Chem. Phys.* **41**. 937.

RAYLEIGH, LORD 1892 On the influence of obstacles arranged in rectangular order on the properties of the medium. *Phil. Mag.* **34**. 481.

REED, L. D. & MORRISON, F. A. 1976 Hydrodynamic interaction in electrophoresis. *J. Colloid Interface Sci.* **54**. 117–133.

RUSSEL, W. B., SAVILLE, D. A. & SCHOWALTER, W. R. 1989 *Colloidal Dispersions.* Cambridge University Press.

SAFFMAN, P. G. 1973 Settling speed of free and fixed suspensions. *Stud. Appl. Maths* **52**. 115–127.

SUBRAMANIAN, R. S. 1985 The Stokes force on a droplet in an unbounded fluid medium due to capillary effects. *J. Fluid Mech.* **153**. 389–400.

TORQUATO, S. 1987 Thermal conductivity of disordered heterogeneous media from the microstructure. *Rev. Chem. Engng* **4**. 151–204.

WILLIS, J. R. & ACTON, J. R. 1976 Overall elastic moduli of a dilute suspension of spheres. *Q. J. Mech. Appl. Maths* **29**. 163–177.

YOUNG, N. O., GOLDSTEIN, J. S. & BLOCK, M. J. 1959 The motion of bubbles in a vertical temperature gradient. *J. Fluid Mech.* **6**. 350–356.

ZUKOSKI, C. F. 1984 Studies of electrokinetic phenomena in suspensions. Ph.D. thesis, Princeton University.

ZUKOSKI, C. F. & SAVILLE, D. A. 1987 Electrokinetic properties of particles in concentrated suspensions. *J. Colloid Interface Sci.* **115**. 422–436.

ZUKOSKI, C. F. & SAVILLE, D. A. 1989 Electrokinetic properties of particles in concentrated suspensions: heterogeneous systems. *J. Colloid Interface Sci.* **132**. 220–229.